

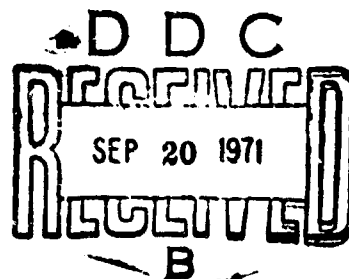
FAILURE MECHANISM OF ATTITUDE CONTROL SYSTEM VALVE IN CHLORINE PENTAFLUORIDE SERVICE

W. D. English
H. D. Samuel, Jr.

McDONNELL DOUGLAS ASTRONAUTICS COMPANY

July 1971

Approved for public release;
distribution unlimited



Air Force Materials Laboratory
Air Force Systems Command
Wright-Patterson Air Force Base, Ohio 45433

Reproduced by
NATIONAL TECHNICAL
INFORMATION SERVICE
Springfield, Va. 2215

209

UNCLASSIFIED

Security Classification
1101

DOCUMENT CONTROL DATA - R&D

(Security classification of title, body of abstract and indexing annotation must be entered when the overall report is classified)

1. ORIGINATING ACTIVITY (Corporate author) McDonnell Douglas Astronautics Company Huntington Beach, California		2a. REPORT SECURITY CLASSIFICATION UNCLASSIFIED	
		2b. GROUP ---	
3. REPORT TITLE Failure Mechanism of Attitude Control System Valve in Chlorine Pentafluoride Service			
4. DESCRIPTIVE NOTES (Type of report and inclusive dates) Final Technical Report July 1970-March 1971			
5. AUTHOR(S) (Last name, first name, initial) English, W. David Samuel, Hubert D., Jr.			
6. REPORT DATE July 1971	7a. TOTAL NO. OF PAGES 202	7b. NO. OF REFS 40	
8a. CONTRACT OR GRANT NO. F33615-70-C-1760	9a. ORIGINATOR'S REPORT NUMBER(S) MDC-G2275		
b. PROJECT NO.			
c.	9b. OTHER REPORT NUMBER(S) (Any other numbers that may be assigned this report)		
d.	---		
10. AVAILABILITY/LIMITATION NOTICES Approved for public release; distribution unlimited			
11. SUPPLEMENTARY NOTES		12. SPONSORING MILITARY ACTIVITY Air Force Material Laboratory Air Force Systems Command Wright-Patterson Air Force Base, Ohio	
13. ABSTRACT As part of a continuing Air Force effort to develop component technology for high-energy propulsion systems, an attitude control system (ACS) valve was developed elsewhere for use with high-energy, storable liquid propellants. This valve performed successfully in most propellants tested; however, it failed by developing excessive leakage when operated in chlorine pentafluoride. The design and operation of the ACS valve were analyzed for modes of possible failure. The modes studied included overstressing of the closures by closing loads; adhesive wear of the closure surfaces/corrosion of the closures by CPF, and hydrofluoric acid/abrasive wear; corrosive wear; and impact-initiated chemomechanical reactions. Some new equations which relate valve wear to operating and material parameters were developed during the analysis. Tests of some materials were conducted to supply data for certain of the analyses, to test the equations used, and to evaluate some candidate materials. For all of the normal modes of possible failure investigated, it was demonstrated conclusively that the valve is adequately designed to withstand any expected level of load or attack. Subsequent to the initiation of this program at MDAC, the Air Force demonstrated that contamination by water was the probable cause for the failures observed. MDAC has shown by analysis and test that impact-initiated chemomechanical reaction of adsorbed water with CPF on the closure surfaces will result in failure of the type observed. Tests of alternative closure materials were conducted. However, the material currently used for closures tungsten carbide-5% cobalt cermet was ranked higher than the alternative materials tested.			

DD FORM 1473
1 JAN 64

201

UNCLASSIFIED

Security Classification

NOTICE

When Government drawings, specifications, or other data are used for any purpose other than in connection with a definitely related Government procurement operation, the United States Government thereby incurs no responsibility nor any obligation whatsoever; and the fact that the Government may have formulated, furnished, or in any way supplied the said drawings, specifications, or other data, is not to be regarded by implication or otherwise as in any manner licensing the holder or any other person or corporation, or conveying any rights or permission to manufacture, use, or sell any patented invention that may in any way be related thereto.

DATE	DATE SECTION	<input checked="" type="checkbox"/>
UC	DIFF SECTION	<input type="checkbox"/>
RESOURCES		<input type="checkbox"/>
LOCATION		
DISTRIBUTION/AVAILABILITY CODES		
Dist.	Avail.	and/or Special
A		

Copies of this report should not be returned unless return is required by security considerations, contractual obligations, or notice on a specific document.

UNCLASSIFIED
Security Classification

14. KEY WORDS	LINK A		LINK B		LINK C	
	ROLE	WT	ROLE	WT	ROLE	WT
Adhesive wear						
Attitude control						
Chlorine pentafluoride						
Contamination						
Corrosive wear						
Friction testing						
Impact testing						
Interhalogen oxidizer						
Leakage						
Long life technology						
Material selection						
Nickel						
Passivation						
Tungsten carbide						
Valves						

INSTRUCTIONS

1. **ORIGINATING ACTIVITY:** Enter the name and address of the contractor, subcontractor, grantee, Department of Defense activity or other organization (*corporate author*) issuing the report.

2a. **REPORT SECURITY CLASSIFICATION:** Enter the overall security classification of the report. Indicate whether "Restricted Data" is included. Marking is to be in accordance with appropriate security regulations.

2b. **GROUP:** Automatic downgrading is specified in DoD Directive 5200.10 and Armed Forces Industrial Manual. Enter the group number. Also, when applicable, show that optional markings have been used for Group 3 and Group 4 as authorized.

3. **REPORT TITLE:** Enter the complete report title in all capital letters. Titles in all cases should be unclassified. If a meaningful title cannot be selected without classification, show title classification in all capitals in parenthesis immediately following the title.

4. **DESCRIPTIVE NOTES:** If appropriate, enter the type of report, e.g., interim, progress, summary, annual, or final. Give the inclusive dates when a specific reporting period is covered.

5. **AUTHOR(S):** Enter the name(s) of author(s) as shown on or in the report. Enter last name, first name, middle initial. If military, show rank and branch of service. The name of the principal author is an absolute minimum requirement.

6. **REPORT DATE:** Enter the date of the report as day, month, year; or month, year. If more than one date appears on the report, use date of publication.

7a. **TOTAL NUMBER OF PAGES:** The total page count should follow normal pagination procedures, i.e., enter the number of pages containing information.

7b. **NUMBER OF REFERENCES:** Enter the total number of references cited in the report.

8a. **CONTRACT OR GRANT NUMBER:** If appropriate, enter the applicable number of the contract or grant under which the report was written.

8b, 8c, & 8d. **PROJECT NUMBER:** Enter the appropriate military department identification, such as project number, subproject number, system numbers, task number, etc.

9a. **ORIGINATOR'S REPORT NUMBER(S):** Enter the official report number by which the document will be identified and controlled by the originating activity. This number must be unique to this report.

9b. **OTHER REPORT NUMBER(S):** If the report has been assigned any other report numbers (*either by the originator or by the sponsor*), also enter this number(s).

10. **AVAILABILITY/LIMITATION NOTICES:** Enter any limitations on further dissemination of the report, other than those

imposed by security classification, using standard statements such as:

- (1) "Qualified requesters may obtain copies of this report from DDC."
- (2) "Foreign announcement and dissemination of this report by DDC is not authorized."
- (3) "U. S. Government agencies may obtain copies of this report directly from DDC. Other qualified DDC users shall request through _____."
- (4) "U. S. military agencies may obtain copies of this report directly from DDC. Other qualified users shall request through _____."
- (5) "All distribution of this report is controlled. Qualified DDC users shall request through _____."

If the report has been furnished to the Office of Technical Services, Department of Commerce, for sale to the public, indicate this fact and enter the price, if known.

11. **SUPPLEMENTARY NOTES:** Use for additional explanatory notes.

12. **SPONSORING MILITARY ACTIVITY:** Enter the name of the departmental project office or laboratory sponsoring (paying for) the research and development. Include address.

13. **ABSTRACT:** Enter an abstract giving a brief and factual summary of the document indicative of the report, even though it may also appear elsewhere in the body of the technical report. If additional space is required, a continuation sheet shall be attached.

It is highly desirable that the abstract of classified reports be unclassified. Each paragraph of the abstract shall end with an indication of the military security classification of the information in the paragraph, represented as (TS), (S), (C), or (U).

There is no limitation on the length of the abstract. However, the suggested length is from 150 to 225 words.

14. **KEY WORDS:** Key words are technically meaningful terms or short phrases that characterize a report and may be used as index entries for cataloging the report. Key words must be selected so that no security classification is required. Identifiers, such as equipment model designation, trace name, military project code name, geographic location, may be used as key words but will be followed by an indication of technical context. The assignment of links, rules, and weights is optional.

AFML-TR-71-94

**FAILURE MECHANISM OF ATTITUDE CONTROL SYSTEM
VALVE IN CHLORINE PENTAFLUORIDE SERVICE**

**W. D. English
H. D. Samuel, Jr.**

McDONNELL DOUGLAS ASTRONAUTICS COMPANY

**Approved for public release;
distribution unlimited**

ABSTRACT

This final technical report describes the work conducted for the U. S. Air Force on Contract F33615-70-C-1760.

As part of a continuing Air Force effort to develop component technology for high-energy propulsion systems, an attitude control system (ACS) valve was developed elsewhere for use with high-energy, storable liquid propellants. This valve performed successfully in most propellants tested; however, it failed by developing excessive leakage when operated in chlorine pentafluoride (CPF).

The design and operation of the ACS valve were analyzed for modes of possible failure. The modes studied included overstressing of the closures by closing loads; adhesive wear of the closure surfaces; corrosion of the closures by CPF and hydrofluoric acid; abrasive wear; corrosive wear; and impact-initiated chemomechanical reactions. Some new equations which relate valve wear to operating and material parameters were developed during the analysis. Tests of some materials were conducted to supply data for certain of the analyses, to test the equations used, and to evaluate some candidate materials.

For all the normal modes of possible failure investigated, it was demonstrated conclusively that the valve is adequately designed to withstand any expected level of load or attack.

Subsequent to the initiation of this program at McDonnell Douglas Astronautics Company (MDAC), the Air Force demonstrated that contamination by water was the probable cause for the failures observed in early testing. MDAC has shown by analysis and test that impact-initiated chemomechanical reaction of adsorbed water with CPF on the closure surfaces will result in failure of the type observed.

Tests of alternative closure materials were conducted. However, the material currently used for closures—tungsten carbide-6 percent cobalt cermet—was ranked higher than the alternative materials tested.

FOREWORD

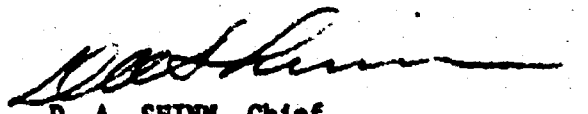
This report was prepared by the Advance Propulsion Department, Research and Development Directorate, Advance Systems and Technology, McDonnell Douglas Astronautics Company under Air Force Contract F33615-70-C-1760. The work was administered under the direction of the Air Force Materials Laboratory, Air Force Systems Command, Wright-Patterson Air Force Base, Ohio 45433, by Fred H. Meyer, Jr., Project Engineer.

This report covers analytical work done to define the mechanism of failure of valve closures when operated in chlorine pentafluoride (CPF), the test work conducted to verify the analyses, and proof testing of candidate substitute closure materials.

McDonnell Douglas Astronautics Company (MDAC) performed the work with Dr. W. David English as Principal Investigator, under the administration of Mr. P. L. Klevatt, Chief Advance Technology Engineer, Advance Propulsion Department. This report was prepared by W. David English and H. D. Samuel, Jr. In addition to the authors, Dr. S. Asumaa and Leo R. Donahue, R. M. Joyce and F. J. Fahey have made substantial contributions to this work.

This manuscript was released by the authors in March, 1971 for publication as an Air Force Materials Laboratory (AFML) Technical Report.

This technical report has been reviewed and is approved.


D. A. SHINN, Chief
Aeronautical Systems Support Branch
Materials Support Division
AF Materials Laboratory

CONTENTS

Section 1	INTRODUCTION AND SUMMARY	1
Section 2	ACS VALVE FOR STORABLE PROPELLANTS	7
2.1	Valve Development	7
2.2	Valve Description	7
2.3	Valve Test Results	13
2.4	Current Status	17
Section 3	ANALYSIS OF VALVE FAILURE PROCESSES	19
3.1	Introductory Background	19
3.1.1	Objectives and Approach	19
3.1.2	Examination of Tested Parts	19
3.2	Basic Mathematical Model of ACS Valve	25
3.2.1	Leak Rate Model	25
3.2.2	Model of Valve Dynamics	28
3.2.3	Dynamic and Static Closure Loads	30
3.2.4	Conclusions	33
3.3	Surface Wear Process Analysis	34
3.3.1	Objectives and Approach	34
3.3.2	Wear Theory	34
3.3.3	Adhesive Wear in the ACS Valve	37
3.3.4	Conclusions	51
3.4	Corrosion and Corrosive Wear	51
3.4.1	General	51
3.4.2	Corrosion and Wear	52
3.4.3	Chemical Corrosion of ACS Valve Closures	53
3.4.4	Film Fracture Corrosion	57
3.4.5	MDAC Corrosion Tests in HF	60
3.4.6	Conclusions	60
3.5	Chemomechanical Reaction Initiation	61
3.5.1	Observations	61
3.5.2	Impact Initiation	61
3.5.3	Localized Impact Heating	64
3.5.4	Conclusions	67
3.6	Other Wear Processes	67
3.6.1	Abrasive Wear	67
3.6.2	Surface Fatigue Wear	72
3.6.3	Other Factors	73
3.7	Analysis Conclusions	74

Section 4	TEST PROGRAM	75
4.1	Objectives and Approach	75
4.2	Test Results	76
4.2.1	Corrosion Tests	76
4.2.2	Interpretation	76
4.3	Impact Initiation Tests	78
4.3.1	Tests Conducted	78
4.3.2	Observations	79
4.3.3	Calculations	80
4.3.4	Analysis and Discussion	82
4.4	Rotary Friction Initiation Tests	93
4.4.1	Tests Conducted	93
4.4.2	General Observations	94
4.4.3	Calculations	96
4.4.4	Analysis and Discussion	96
4.5	Conclusions	102
Section 5	MATERIALS PARAMETERS	103
5.1	Valve Wear Threshold Considerations	103
5.2	Material Selection Parameters	106
Section 6	RECOMMENDED FUTURE WORK	111
	REFERENCES	113
Appendix A	DYNAMIC AND STATIC CLOSURE LOADS	117
Appendix B	ADHESIVE WEAR	125
Appendix C	RATE OF WEAR OF CLOSURE SURFACES	129
Appendix D	IMPACT HEATING	137
Appendix E	ROTARY SLIDING FRICTION AND PLASTIC DEFORMATION INITIATION	145
Appendix F	DATA FOR CALCULATION	149
Appendix G	GLOSSARY OF SYMBOLS	153
Appendix H	SURFACE FLUORINATION REACTIONS	155
Appendix I	TEST PROGRAM	165
Appendix J	MATERIAL PARAMETERS	169

FIGURES

<u>Number</u>		<u>Page</u>
2-1	Single-Armature Valve Configuration	10
2-2	Bipropellant Valve Configuration	11
2-3	Consolidated Leak Development Data	15
3-1	ACS Valve Parts After Operation in CPF	20
3-2	Berylco Nickel 440 Valve Seat	21
3-3	Poppet Wear Pattern	22
3-4	Selective Wear of Composite Materials (Suggested Mode)	23
3-5	Mating Roughness Nomenclature	26
3-6	Arithmetic Average Surface Roughness	27
3-7	ACS Valve Leak Versus Surface Roughness	29
3-8	Poppet Motion Model	30
3-9	Surface Energy Versus Hardness	38
3-10	Ratio γ/p Versus Hardness	38
3-11	Wear Particle Size Versus G/p Ratio	41
3-12	Surface Film Configuration	55
3-13	Reaction Film Thickness Versus Reaction Time in F_2 , CTF, and CPF	58
3-14	Wear Rate Versus Abrasive Grain Size	70
3-15	Bearing Life as a Function of Hardness Difference	72
4-1	Impact Initiation Energy in CPF as a Function of Material Hardness	76

<u>Number</u>		<u>Page</u>
4-2	ABMA Initiation Energy Parameters	86
4-3	Comparison of Tungston Carbide Cernnet Test Specimens	95
4-4	Fractured Tungston Carbide Specimen, Edge View	95
4-5	Rotary Friction Initiation of Duranickel 301 in CPF	99

TABLES

<u>Number</u>		<u>Page</u>
2-1	Valve Test Summary	8
2-2	Magnetically Linked Bipropellant Valve Performance Requirements	9
2-3	Magnetically Linked Bipropellant Valve Seat Closure Construction Materials	12
2-4	Summary of Valve Tests at Valve Manufacturer	14
2-5	Summary of Valve Tests at AFRPL	16
3-1	Calculated Forces and Stresses at Impact	33
3-2	Wear-Related Properties of Solid Materials	40
3-3	Effect of Environment on Size of Loose Wear Particles	43
3-4	Adhesive Wear Constants	46
3-5	Closure Surface Finish Change with Valve Cycling	48
3-6	Hardness Data	68
3-7	Abrasion Resistance of Alloys	71
4-1	Aqueous HF Corrosion Test Conditions	76
4-2	Corrosion in Hydrofluoric Acid - Test Data	77
4-3	HF Corrosion Resistance Ranking	78
4-4	Drop Weight Impact Initiation Test Summary, Valve Closure Materials in CPF	78
4-5	Calculation of E_{50}	81

<u>Number</u>		<u>Page</u>
4-6	Reaction Initiation by ABMA Impact in CPF	82
4-7	ABMA Initiation Data, Duranickel in CPF	84
4-8	Energy Flux and Interface Temperature for ABMA Tests of Duranickel 301 in CPF	90
4-9	ABMA Reaction of SS-304-L in CPF	91
4-10	Impact Initiation of WC-Co in CPF	92
4-11	Rotary Friction Initiation Tests Summary	93
4-12	Rotary Friction Tests in CPF	97
4-13	Rotary Friction Initiation in CPF	98
4-14	Comparison of ABMA and Rotary Friction Initiation of Metals in CPF	101
5-1	Materials Selection Data Check Sheet	108
5-2	Corrosion Wear Material Selection Check List	110

Section 1

INTRODUCTION AND SUMMARY

Recently, an attitude control system (ACS) valve designed under an Air Force contract for service with chlorine pentafluoride (CPF) and monomethylhydrazine (MMH) was found to develop an unacceptable internal leak rate in comparatively few cycles when operated in CPF. Preliminary analysis showed that this valve performed well with other propellants and that the seat materials are compatible with CPF under static test conditions. As leakage was caused by roughening of the closure surfaces only in CPF service, it was postulated that the failures occurred because of the addition of energy at the valve seat under dynamic conditions.

Components and systems designed and fabricated for service in contact with advanced, high-energy propellants must withstand severe environments. An important circumstance observed in such environments, typically in fluorinating agents, is the coupling of chemical attack and dynamic loads to produce greatly accelerated attack on structural materials. Such chemomechanical effects probably occur because the energy released in localized regions by the dynamic processes is great enough to activate a small number of molecules and initiate local hot-spot reactions. Most of the advanced high energy liquid propellants require much less activation energy than do fluids used currently.

All current and conceptual rocket systems designed for operation with high-energy liquid propellants have inherent chemical instabilities as a consequence of the chemical properties of the propellants. High-energy oxidizers may react catastrophically with common structural alloys. Also, alloying elements in structural materials may cause high-energy fuels to undergo spontaneous rearrangement into more stable chemical compounds, releasing energy and gaseous products. In addition to these violent reactions, slow degradation of the system may occur to produce changes in propellant characteristics and corrosion of containment materials.

During operation of all propellant systems, whether they are test facilities, Ground Support Equipment, or flight systems, the dynamic functions of components and fluid flow increase the total energy in the system. Because of the relatively low reaction initiation energies associated with advanced liquid propellants, there is an increased probability of reactions occurring from the energy added to the system from the dynamic environment. Thus, an understanding of propellant-materials dynamic compatibility and availability of design data are mandatory if this potential source of mission failure is to be avoided.

The ACS valve failed by an increase in leak rate to beyond the design maximum in less than the design cycle life. Failure of the original version of the valve occurred in a very few cycles. However, the valve performed well beyond design requirements with all other propellants tested: viz, dinitrogen tetroxide, fluorine, monomethylhydrazine, and methane. It was also operated successfully with fluorine-oxygen solutions, but the tests were not run to the full design cycle life.

McDonnell Douglas Astronautics Company (MDAC) has conducted this program to define the failure mechanism of the ACS valve and to evaluate and recommend specific materials that will not be subject to the failure mode observed. Since the failure mode apparently involved dynamic conditions in the presence of propellant, the program was designed to analyze and test chemomechanical processes in the valve and determine the manner in which the energy affected the closure surfaces.

Phase I of the program included the analyses of the dynamic processes occurring in the ACS valve when operated in CPF, and correlation of material properties with the wear observed. Equations were derived that relate the closure dynamics, wear process rates, and thermal energy deposition rates to the properties of structural materials used and to the specific valve design features. Chemical reactions involved in the interaction of CPF with the seat and poppet were analyzed, but unavailability of data on the energetics and mechanisms of the reactions of CPF with the materials used in the valve prevented the development of specific numerical results for correlation and prediction based on chemical reaction mechanisms at this time.

Phase II, Part I of this program consisted of dynamic tests of CPF with two alloys: Duranickel 301 and stainless steel 304-L, conducted with the ABMA impact tester and the rotary friction tester. The energy necessary to cause initiation of surface reactions on each device was determined. The Duranickel 301 was tested in several hardnesses to determine the effect of hardness on initiation. Stainless steel 304-L was tested in the air-melt and vacuum-melt conditions to investigate the effects of impurities. The following results were obtained:

- A. Initiation of burning occurred only when sufficient energy was introduced to cause damage by plastic deformation.
- B. The minimum energy required was a linear function of both the yield strength and the hardness of Duranickel 301.
- C. The purer (vacuum melt) stainless steel 304-L required greater energy to initiate a reaction.
- D. The interface temperatures on the specimens were calculated from the energy supplied in the ABMA tester. In the tests where reaction occurred, the temperatures calculated were very close to those reported for thermal ignition of the metals. In tests with no reaction, the temperatures calculated were much lower.

Phase II, Part II of this program consisted of tests to demonstrate the suitability of candidate materials for use in the ACS valve closure. The results of the Phase I analysis were used to select materials which would have the best combination of properties predicted to provide resistance to seat surface roughening. Three materials were selected for testing, with the approval of the AFML Project Engineer. The materials consisted of 99-percent pure polycrystalline aluminum oxide (Al_2O_3), tungsten carbide in a 6-percent cobalt binder, and silver-plated Duranickel 301.

The aluminum oxide proved to be too brittle and suffered mechanical fractures at test loads well below the levels expected to be required to initiate reaction. No evidence of chemical reactions at the fractured surfaces could be detected.

The silver-plated Duranickel 301 was unsatisfactory, but this was traced to carbon and sulfur impurity inclusions in the plated layer of silver. No conclusions can be drawn as to the suitability of good quality silver plate.

Tungsten carbide - 6 percent cobalt cermet is the most satisfactory material tested for closures. There are indications that its ignition temperature in CPF is higher than most metals¹.

The initiation test methods used in this program, ABMA impact tests and rotary-friction initiation tests supplied hitherto unavailable and potentially useful information on the behavior of materials in contact with propellants under dynamic load conditions. The interrelation of material properties and reaction behavior observed in the test results paralleled those predicted by the analytical equations, but energies found necessary for positive reactions in the tests were much greater than those released by the valve closure processes. It was concluded that the valve failures involved additional factors.

Evaluation of the suitability of the various test methods was part of this program. Specific points for future consideration are:

- A. The MDAC model of the ABMA tester is not suitable for initiation tests of materials harder than 300 on the Vickers penetration hardness scale because the necessary energies are beyond the maximum capacity of the apparatus.
- B. The rotary friction tester was marginally suitable for substances as hard as 1800 on the Vickers scale. These tests were run far below the maximum capacity of the apparatus; however, brittle fracture of hard, brittle materials made interpretation of test data difficult (tungsten carbide cermet) or prevented valid tests (alumina).
- C. The rotary friction tester is capable of better discriminating the tendency toward reaction than is the ABMA tester.

Corrosion rates measured by means of static tests of closure materials in aqueous HF were in accord with expectations. However, the ACS valve wear rates of the same closure materials were not proportional to static corrosion rates. This was interpreted to mean that HF corrosion in the absence of dynamic loads was not a significant factor in the valve closure degradation.

ABMA impact tests in CPF of tungsten carbide cermet specimens that had been equilibrated in an atmosphere of 100 percent relative humidity, demonstrated that in the presence of absorbed moisture, initiation occurred at greatly reduced impact energies. In the same time period, tests by the

Air Force Rocket Propulsion Laboratory, in which extremely great care was taken to remove all traces of moisture from the test valve before exposure to CPF, demonstrated that under these test conditions the valve with tungsten carbide cermet closures easily met the required design cycle life leak rate.

It was concluded that the earlier failures of the valves were due to the combined effects of dynamic loads and CPF with contaminants present.

This report presents the MDAC study in the following sequence:

- A. Description of ACS valve.
- B. Summary of results from valve tests.
- C. Description of failed closures.
- D. Separate analyses of possible failure modes, with conclusions for each analysis.
 - 1. Leak rate model applying to all analyses.
 - 2. Dynamic load.
 - 3. Adhesive wear.
 - 4. Corrosive wear—CPF and HF.
 - 5. Chemomechanical reactions.
 - 6. Abrasive wear.
 - 7. Surface fatigue.
- E. General conclusions as to causes of failure.
- F. Test program.
 - 1. Materials.
 - 2. Test procedures.
 - 3. Impact initiation.
 - 4. Rotary friction initiation.
 - 5. Corrosion in aqueous HF.
 - 6. Conclusions.

Section 2

ACS VALVE FOR STORABLE PROPELLANTS

2.1 VALVE DEVELOPMENT

As part of a continuing Air Force effort to develop component technology for high-energy propulsion systems, an attitude control system (ACS) valve was developed by a contractor for the Air Force Rocket Propulsion Laboratory (AFRPL). This all-metal poppet valve was designed for use in a pulsed ACS using high-energy storable liquid propellants (Ref 1), specifically for CPF and MMH.

The design life requirement of this ACS valve is 100,000 cycles of operation with a maximum helium leak rate of 30 scc/hr.

Several valves of this design have been built and tested with a variety of propellants. With all fluids tested, except for CPF and GF_2 , the valve has been very successful. Table 2-1, which is copied in modified form from Ref 2, is a summary of the performance in pre- and postoperation leak tests reported prior to the start of the MDAC program. The valves failed all the CPF tests. Service leakage rates reach 30 scc/hr after an average of only 100 cycles; whereas in other propellants the valves performed admirably, except for a single series of GF_2 tests.

2.2 VALVE DESCRIPTION

The specified valve, which is described in AFRPL-TR-69-250 (Ref 1), is a "Magnetically Linked Bipropellant Valve" designed for pulsed operation on an ACS operated with CPF and monomethylhydrazine. Table 2-2 lists the performance requirements given in the referenced report. The solenoid-operated valve was built in two basic configurations—a single armature valve (Figure 2-1), which was used for initial testing; and a bipropellant arrangement consisting of two single-armature valves energized by a common coil

Table 2-1
VALVE TEST SUMMARY
(Ref 2)

Fluid	Cycles	Leakage (100 psi GN ₂)		Number of Valves Tested
		Before	After	
Cold Flow Tests				
Gas He	3,000	Zero	Zero	2
CPF	45,000	Zero	Too high (varied)	6
N ₂ O ₄	100,000	Zero	3 scc/hr	1
N ₂ H ₄	100,000	Zero	Zero	2
MMH	200,000	Zero	Zero	3
Hot Firing Test				
80-FLOX*	80	Zero	Zero	1
CH ₄	80	Zero	Zero	1

*One other unit tested in FLOX developed unacceptable leakage before operation due to access of moisture into the oxidizer system (Ref 3).

(Figure 2-2). which was intended for the ultimate system application. Both the single armature and the bipropellant valve configuration feature a metal-to-metal poppet and seat with a flat sealing interface. Both of these configurations use flexure guidance of the armature-poppet assembly to provide precise axial guidance and poppet self-alignment without sliding fits. For the purpose of this analysis, there does not appear to be any significant difference between the single armature valve and the bipropellant valve mechanisms that affect the type and magnitude of wear produced.

The basic design features adopted by the contractor to meet the performance requirements included the following:

- A. Metal-to-metal, hard surface on hard surface, poppet-seat interfaces.
- B. Flat poppet; flat seat with circular flat land.

Table 2-2
MAGNETICALLY LINKED BIPROPELLANT VALVE
PERFORMANCE REQUIREMENTS*

Pressure drop (max)	40 psi at 0.167 lb/sec ClF_5 40 psi at 0.0757 lb/sec monomethylhydrazine
Dribble volume (max)	Less than 0.02 in. ³ per valve
Operating pressure	450 psia
Proof pressure	675 psia
Burst pressure	900 psia
Opening response (max)	8 ms at 28 vdc, 450 psia, and 70°F
Closing response (max)	8 ms at 28 vdc, 70°F, and nominal flow rate
Operating voltage range	18 to 32 vdc
Operating temperature range	-100° to +350°F**
Operating current (max)	2 amps at 28 vdc and 70°F
Response mismatch (max)	0.5 ms
Internal leakage (max)	5 SCC***/hr helium at 0 to 435 psig initially; 30 SCC/hr helium at 0 to 435 psig after 100,000 cycles in propellant
Internal leakage (optimum)	2 scc/hr helium at 50 to 450 psia initially
External leakage (max)	10^{-7} scc/sec helium at 675 psia
Operating life (min)	100,000 cycles
Acceleration	0-10 g's in any direction
Vibration	6 g's sinusoidal and 31.6 g's rms random
Inlet filter rating	18 μ absolute, 5 psi ΔP at nominal flow rates

* From Ref 1

** CPF - $T_c = 290^\circ\text{F}$; MMH - $T_c = 595^\circ\text{F}$

***SCC (standard cubic centimeter) is one cubic centimeter of gas measured at 25°C and 1 atmosphere pressure.

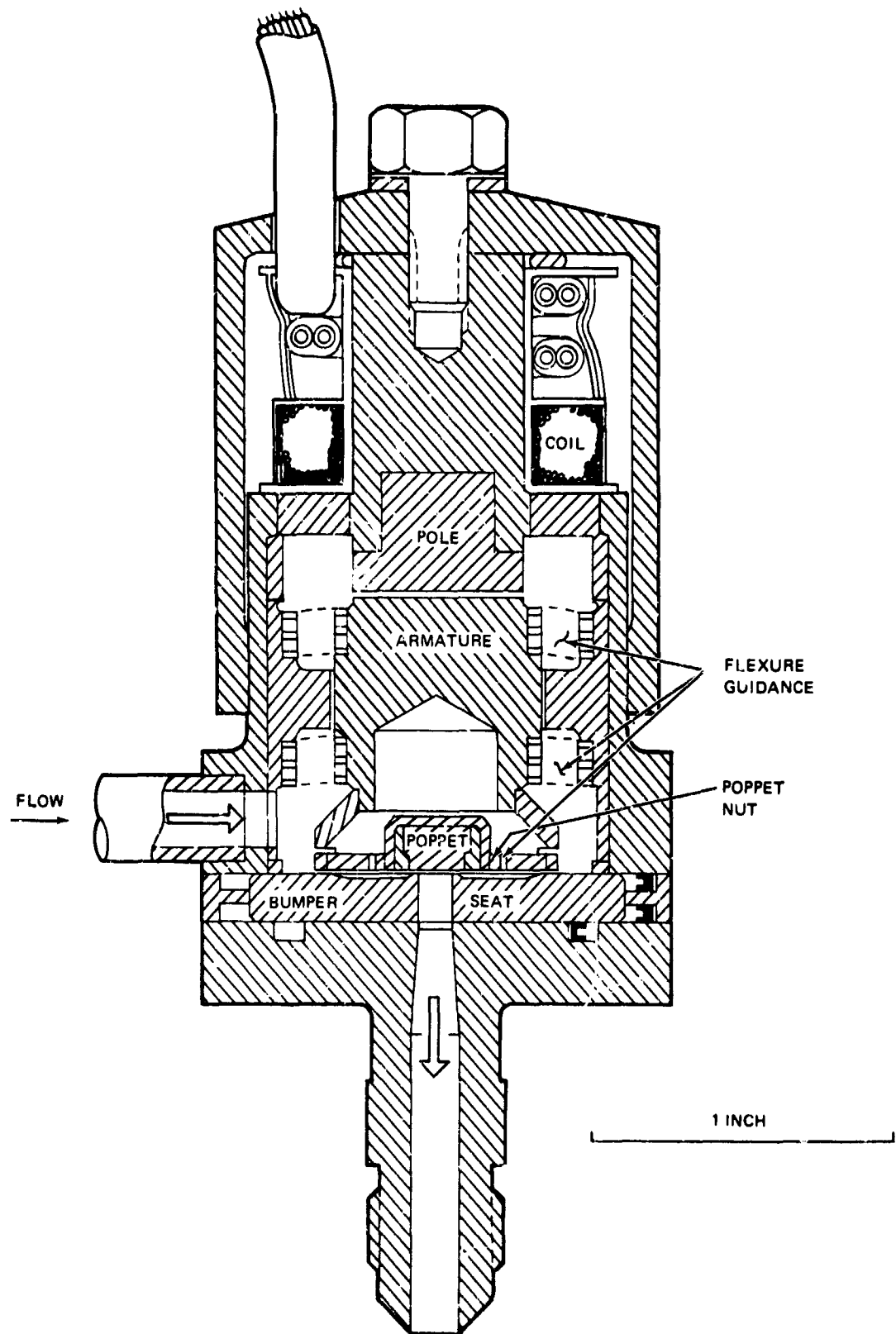


Figure 2-1. Single Armature Valve Configuration (Ref 1)

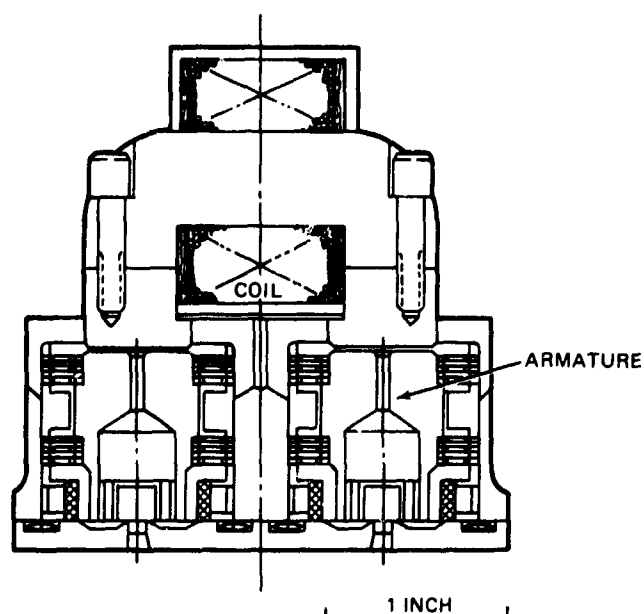


Figure 2-2. Bipropellant Valve Configuration (Ref 1)

C. No sliding fits; self-aligning poppet.

D. Integral propellant filters with cartridge elements.

Analysis of the mode and functioning of the valve resulted in selection by the valve manufacturer of the following design specifications for the poppet and seat:

Surface finish, H°	1 μ in. AA (improved to < 1 μ in. in recent models)
Surface flatness	1 Helium light band
Seating stress*, σ_c	710 psi (=3-lb force); later reduced to 300 psi (=1.2-lb force): at 450 psi fluid pressure, 2, 100 psi (=8.5-lb force)
Land width (seat), w	0.012 in.
Land inside diameter (seat), D_i	0.100 in.
Oxidizer poppet stroke, h	0.010 in.

*The terms stress and load indicate compression conditions throughout this report, unless specially noted.

The construction materials selected are listed in Table 2-3. Each pair of the poppet and seat closure seals was made of the same material. Initially, Duranickel 301 was used on the oxidizer valve closure and Pyromet X-15 on the fuel valve closure, but eventually all materials listed for the poppet and seat were tested for CPF service.

Table 2-3
MAGNETICALLY LINKED BIROPELLANT VALVE POPPET AND
SEAT CLOSURE CONSTRUCTION MATERIALS

Material (Ref 1)
Chromium-plated Kennametal K801 ^{1,2}
Duranickel 301
Pyromet X-15
Silicon carbide KT
Kennametal K602 ¹
Berylco nickel 440
Kennametal K96 ¹
Kennametal K801 ^{1,2}
Silicon carbide RM-005 ³
Rhenium ⁴
Multiphase nickel cobalt MP35N ⁴
¹ All Kennametal alloys tested are basically tungsten carbide, usually in a matrix of a softer metal.
² Components fabricated but not tested in CPF (July 1970).
³ Compatible in static exposure, but rejected due to fabrication problems.
⁴ Incompatible in static tests; rejected.

2.3 VALVE TEST RESULTS

Tests in CPF of the ACS valve were conducted in several configurations and using several material combinations. Most of these tests were conducted by the valve manufacturer, and are reported in Ref 1. A summary of the results of these tests is presented in Table 2-4.

In an effort to improve cycle life in CPF, the poppet support system was redesigned to reduce the magnitude of the impact loads on the sealing surfaces during closing. Several candidate materials were tested in this new configuration, but excessive leakage developed in all cases in less than 1,000 cycles.

Tests were conducted at ambient temperature in GF_2 at another contractor's facility (Ref 4), and at Edwards Air Force Base—Air Force Rocket Propulsion Laboratory (AFRPL) (Ref 5). At the contractor's facility in a test system to which water vapor had access, the He leak rate reached 257 scc/hr after 50,000 cycles. At AFRPL, where great care was exercised to reduce moisture access to the test, the valve leak rate was still less than 30 scc/hr after 165,000 cycles in GF_2 .

The final report of the ACS valve development program (Ref 1) concluded that deterioration of the surfaces of the poppet and seat sealing areas occurs when the valve is operated while exposed to chlorine pentafluoride. The report recommended that a program be initiated to determine the mechanism of deterioration of these smooth metal surfaces in CPF service, and to identify materials and design modifications that will permit the valve to achieve the design life requirements in CPF.

Review of the manufacturer's tests, Table 2-4, discloses the following information:

- A. All of the valves tested developed excessive leakage in less than 1,000 cycles of operation in CPF.
- B. There is evidence that hard materials have a longer life, if porosity and surface cracking do not occur.

The data on He leak rate versus number of cycles in CPF from all tests of all configurations presented in AFRPL-TR-69-250 (Ref 1), Figures VII-4 through -7 of the reference, have been replotted as change in leak rate

Table 2-4
SUMMARY OF VALVE TESTS AT VALVE MANUFACTURER

Test Series Number	Poppet and Seat Material	Cycle Test Fluid	Total No. of Cycles	Helium Leak Rate (scc/hr)		Remarks
				Initial	Final	
1	Pyromet X-15	MMH	100,000	2.75	6	
2	Pyromet X-15	MMH	47,800	2.5	110	Metal chip embedded in closure.*
3	International Nickel Duranickel 301 (DNi-301)	CPF	200	2.5	100	
4	DNi 301	CPF	5,000	3.0	300	
5	DNi 301	CPF	200	7.5	1,500	2 in parallel
6	Pyromet X-15	CPF	1,000	7.5	900	
7	Pyromet X-15	CPF	10,000	3.5	9,000	
8	DNi 301	CPF	10,000	3.5	4,000	
9	DNi 301	CPF	10,000	4.0	900	
10	DNi 301	CPF	5,000	3.0	600	
11	Pyromet X-15	CPF	5,000	2.75	800	
12	Berylco Ni 440	CPF	1,000	0.2	1,000	
13	Berylco Ni 440	CPF	1,000	3.0	800	
14	Kennametal K-602	CPF	9,000	100.0	90,000	
15	Kennametal K-602	CPF	29,000	5.0	7,000	
16	Kennametal K-602	CPF	1,000	60.0	900	Low Impact
17	Kennametal K-602	CPF	1,000	60.0	4,000	High Impact
18	Kennametal K-96	CPF	1,000	10.0	50	
19	Kennametal K-96	CPF	1,000	12.0	70	

*This type of failure is discussed by Tellier in Ref 6.

versus cumulative operating cycles on a single log-log graph (Figure 2-3). All data obtained during passivation or periods of flow exposure with the valve not operated have been deleted. A straight line was drawn as a mean correlation value through the remaining points, having a slope of 35 degrees. Considering the number of other variables, the scatter is surprisingly small, indicating that there is probably a single overriding mechanism responsible for leak development. All materials tested give points on both sides of the correlation band.

Subsequent to the release of the final report on the initial program (Ref 1) and prior to this MDAC evaluation contract, additional tests in CPF were conducted by AFRPL personnel. The results of these tests are summarized in Table 2-5.

The data in Table 2-5 confirm that the harder materials have longer service lives. Test number 2 shows the best performance. In this test, 50,000 cycles of operation in CPF were completed before leakage had increased to the design limit of 30 scc He/hr.

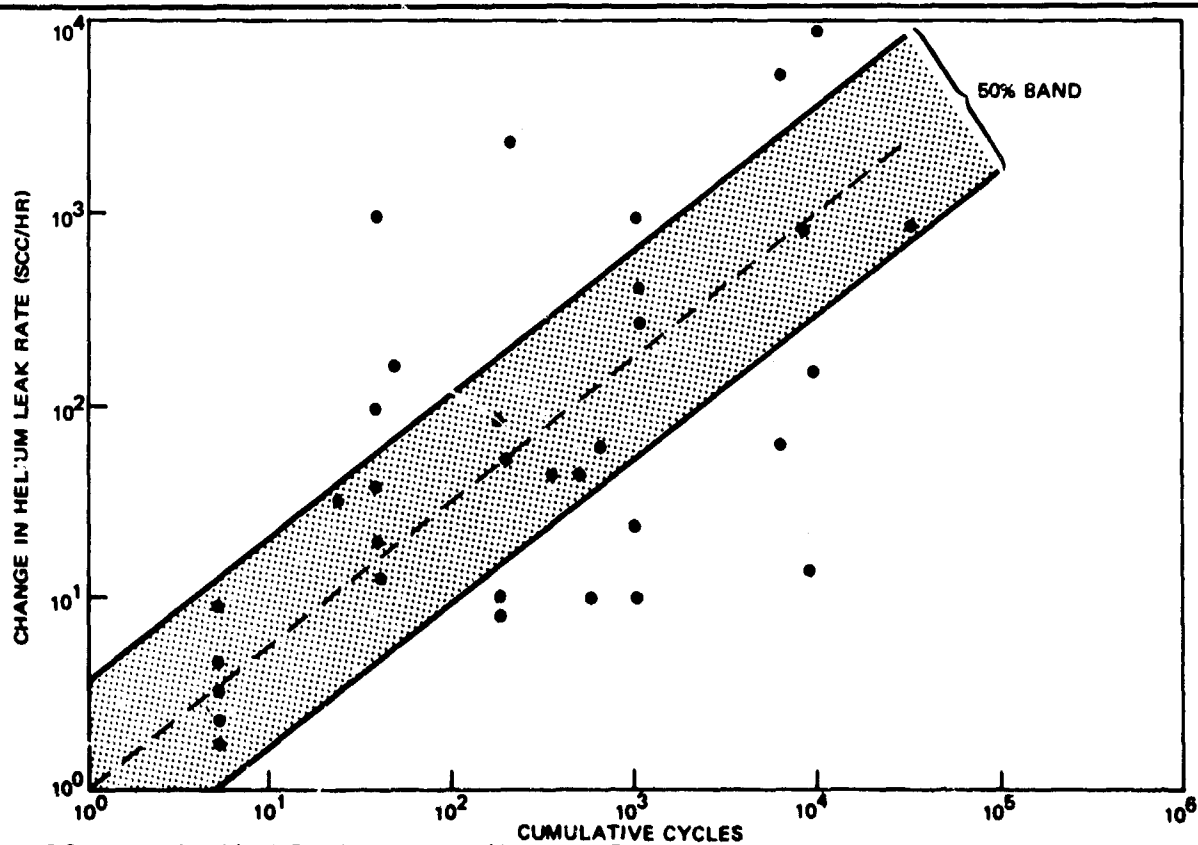


Figure 2-3. Consolidated Leak Development Data (Calculated From Reference 1)

Table 2-5
SUMMARY OF EARLY VALVE TESTS AT AFRPL

Test Number	Poppet and Seat Material	Cycle Test Fluid	Total No. of Test Cycles	Helium Leak Rate (scc/hr) Initial	Final	Remarks
1	K-96	GF ₂	50,000	13	29	Low impact
		GF ₂	+65,000 additional	30	120	High impact
		GF ₂	+50,000 additional	30	3	Low impact
		CPF	+40,000 additional	21	18	Low impact, Low flow rate
2	K-96	CPF	+15,000 additional	20	103	Low impact, 0.167-lb/sec flow rate, contamination
		CPF	50,000	10	30	Low impact, 0.167 lb/sec flow rate
		Helium	50,000	-	2	
3	Duranickel 301	CPF	6,000	33	456	Low impact, Very low flow rate

Shortly after completion of Phase II, Part 1 (Verification Tests) for the current contract at MDAC, new test results from AFRPL became available (Ref 7). Tests of several specially prepared valves with tungsten carbide-cobalt cermet closures were completely successful. All of the valves have leak rates of less than 30 scc He/hr after more than 100,000 cycles in CPF. The special preparation consisted of a very thorough pretest bakeout to remove all traces of moisture. This evidence supports the statements in the MDAC Phase I Interim Report, (Ref 8), that trace contamination by water could cause surface damage by ignition of local hot spots even at reduced closure impact loads.

2.4 CURRENT STATUS

These recent Air Force test results have demonstrated that the particular ACS valve is adequately designed for service in CPF. In addition, the tests have again demonstrated the absolute necessity of ensuring that systems for fluorine oxidizers must be cleaned to rigid specifications, must include positive barriers preventing access of contaminants (including water), and that operating techniques must maintain the clean, moisture-free condition.

Section 3

ANALYSIS OF VALVE FAILURE PROCESSES

3.1 INTRODUCTORY BACKGROUND

3.1.1 Objectives and Approach

The Air Force Material Laboratory (AFML) and AFRPL have supported this present program to define the valve failure mechanism, and to evaluate and recommend specific materials that will not be subject to the observed failure modes in CPF. This program contained three phases. Phase I consisted of an analysis of the failure process, including limited testing to support the establishment of a wear model. Phase II consisted of tests to evaluate candidate materials and to confirm the validity of the wear model. Phase III consisted of preparation of program documentation.

The purpose of the analysis of the ACS valve failure mechanism was to identify the failure mode and establish criteria that can be used to extend the valve operating life in CPF.

A review of valve test parameters and observed valve performance in tests previous to and during the early stages of the MDAC program was conducted. Meetings with engineers from the valve manufacturer and with cognizant Air Force personnel were held. Thorough discussions of the valve design and operating parameters, details of test procedures, posttest specimen examinations and test results were held. Closure poppets and seats, which had been tested in various fluids, were supplied to MDAC by the manufacturer and by the Air Force.

3.1.2 Examination of Tested Parts

Observation of failed seats and poppets showed that surface finish changes are concentrated in local areas (Figure 3-1). Micrographs at higher magnification show the existence of pits and built-up deposits (Figure 3-2). Initial



U.S. AIR FORCE PHOTO

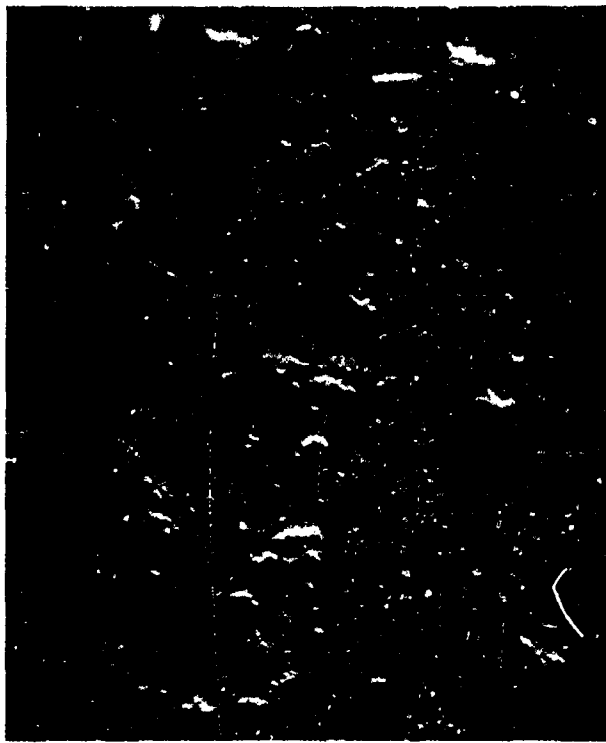
- a. VALVE POPPET (20X). NOTE GREATER WEAR
BETWEEN 6 O'CLOCK AND 12 O'CLOCK



U.S. AIR FORCE PHOTO

- b. VALVE SEAT (20X). NOTE WHITE FILM BETWEEN
6 O'CLOCK AND 12 O'CLOCK

Figure 3-1. ACS Valve Parts After Operation in CPF



U. S. AIR FORCE PHOTO

Figure 3-2. Berylco Nickel 440 Valve Seat (300X)

wear is more severe near the seat OD and extends inward as the number of operating cycles is increased.

The surface irregularity of a Berylco 440 seat land, measured with a Profilometer, increased from 5.5×10^{-6} to 25×10^{-6} inches after 1,000 cycles in CPF.

An electron microprobe test of a failed valve poppet (Ref 5) showed that the film contained fluorine, chlorine, and oxygen atoms, suggesting that the film is a metal fluoride-chloride conversion coating of a previously existing oxide, in agreement with previously published information (Ref 9).

The poppet that exhibited the smallest increase in leak rate (Test 2, Table 2-5) was inspected at MDAC. The finish of the surface of this poppet was examined with a proficorder, an interference microscope, and a stereo-microscope. Figure 3-3 is a sketch showing the observed wear. It is apparent that the poppet sealing surface has been coined by the multiple impact contacts with the seat sealing land. The maximum wear and

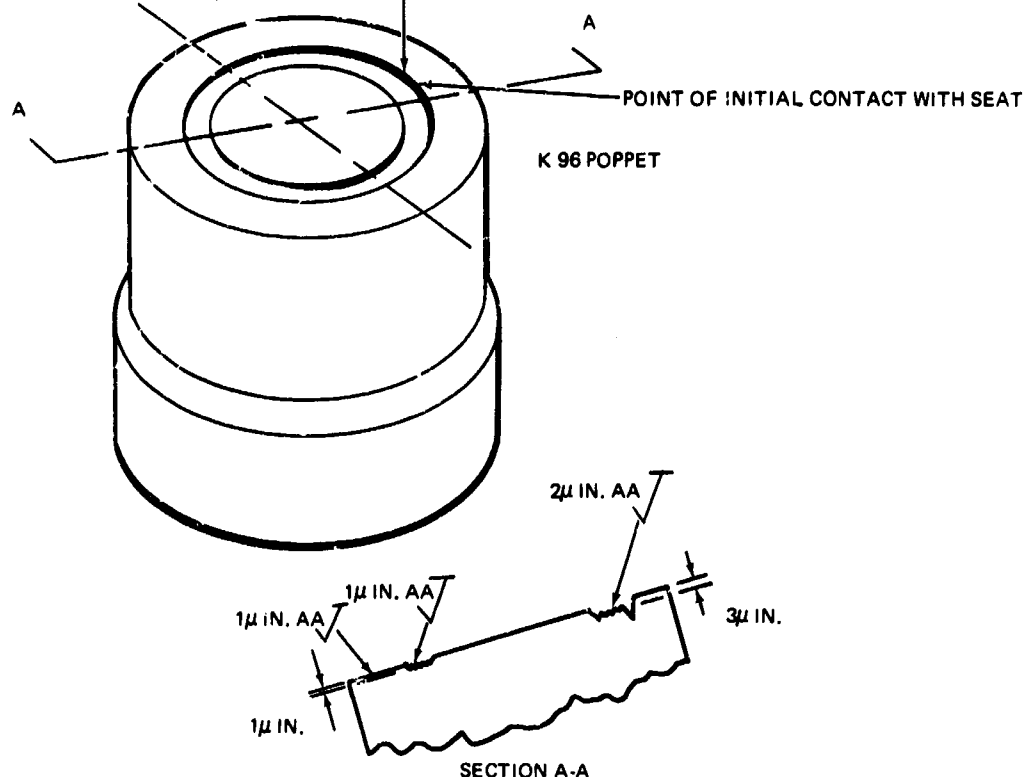


Figure 3-3. Poppet Wear Pattern

depression of the surface occur at one location on the outside diameter of the sealing land, where the poppet initially contacted the seat. The depressed sealing surface shows general signs of adhesive wear, resulting in an increase of the initial surface roughness. Maximum roughness occurred in the region of initial contact, tapering to negligible increase in roughness at the opposite side.

The mating surface on the seat land had surface roughness values that matched those of corresponding poppet locations. The wear pattern shown in Figure 3-3 is typical although the extent of wear is less than that observed on other poppets and seats after test. The material of which this poppet was fabricated consists of tungsten carbide particles in a cobalt matrix. The adhesive wear observed probably occurred primarily in the softer cobalt.

Examination under an interference microscope suggested that the cobalt had been worn down about 1 microinch below the level of the tungsten carbide (Figure 3-4). The depth of this selective wear is probably controlled by,

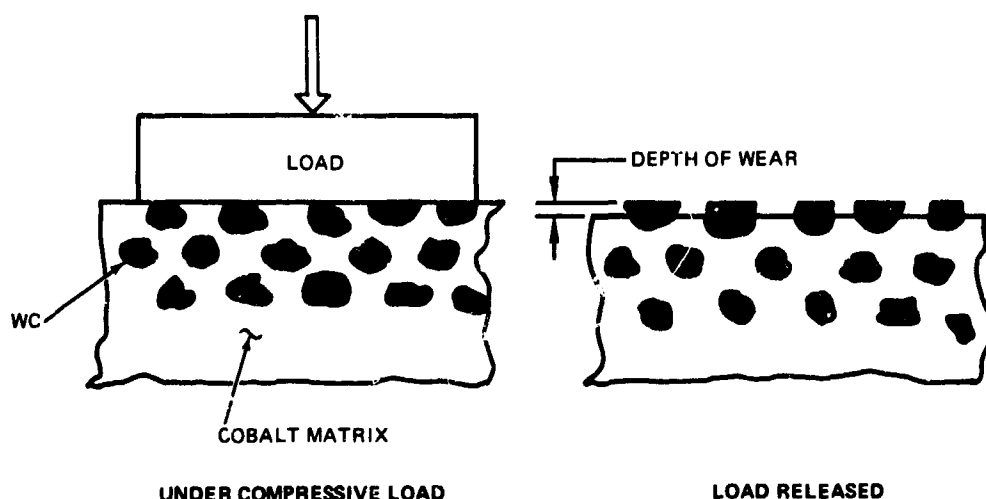


Figure 3-4. Selective Wear of Composite Materials (Suggested Mode)

and equal to, the amount of compressive deflection of the tungsten carbide surface under load. The cobalt matrix is probably flush with the tungsten carbide particles when the surface is under load, but lies below the carbide particles when the load is released.

Duranickel 301 showed evidence of some conventional abrasive wear, and considerable chemical impact initiation. Local craters—signs of impact-initiated nonpropagating ignition—are reported in Ref 1 for the materials Duranickel 301, Pyromet X-15, and Kennametal K-602.

Kennametal K602 showed signs of slight abrasive wear and considerable surface cracking and porosity. K602 is a sintered tungsten carbide without a binder. Historically, this class of material has developed porosity and cracking, particularly in a chemically reactive environment.

All of the poppets and seats, except those from test number 3 at AFRPL, were exposed to ambient air for a considerable time after testing before they

were sent to MDAC for inspection. Therefore, some of the observed surface conditions may have been produced after the parts were removed from the valve, and may not have contributed to the measured leakage. After test number 3 (Table 2-5) was completed, the valve was disassembled in a glove-bag in a dry nitrogen atmosphere and stored in plastic bags under dry gaseous nitrogen (GN_2). These parts were also examined in a dry GN_2 environment. They had much less evidence of surface corrosion.

Chemical corrosion was reported as quite evident on many closures immediately after testing (Ref 1). The corrosion was probably caused by access of water vapor, which reacted with CPF to form hydrofluoric acid. The tungsten carbide cermet alloys were apparently more sensitive to this attack than the Duranickel or Berylco nickel. This was confirmed in static corrosion tests conducted at MDAC (see Subsection 4.5).

In an attempt to enhance the stability of the passive film, the valve manufacturer passivated all valves in GF_2 before exposure to CPF (Ref 1). It had been demonstrated previously at MDAC that F_2 -formed films are less sensitive to corrosion when exposed to moisture than those from halogen fluorides (Ref 10).

The observations of liquid residues on the valve surfaces after operation in CPF systems to which water vapor had access (Ref 1), the different behaviors in "wet" and "dry" systems (Ref 5 and 7), and green "hydrated" corrosion deposits from FLOX service (Ref 3) emphasize that the corrosion is accelerated in the presence of moisture.

It is difficult to estimate to what extent simple corrosion reactions degraded valve closures during the testing because the access of moisture can also accelerate other mechanisms for valve degradation, a point discussed in Subsection 3.5. In the test programs at various test centers, as experience with the problems of the valve accumulated, increasingly sophisticated methods were used to reduce contamination by water. This makes it difficult to be certain whether a decrease in wear rate after a design change or operation cycle change was due to the change, or to a cleaner system, or both.

The overall results, especially the most recent successful tests at AFRPL, reemphasize the absolute necessity of ensuring that the highest possible standards of cleanliness are applied for fluorine oxidizers, and also the recognition that water is an impurity which contributes to generating the most corrosive conditions. Although comparative test data are not available, it can be confidently asserted that corrosive effects of water are much more serious with the warm storable oxidizers when compared with liquid fluorine at cryogenic temperatures.

3.2 BASIC MATHEMATICAL MODELS OF ACS VALVE

In order to analyze the closure wear processes quantitatively, it is first necessary to derive models of the basic operations and conditions occurring in the valve.

3.2.1 Leak Rate Model

In this subsection, the relation between surface finish and leak rate is described quantitatively. The equations are applied later to determine the effects of specific wear processes.

Leakage through the closure of a flat-face poppet valve depends primarily on the mating roughness of the sealing surfaces. For leak rates in the range allowed for the ACS valve, leakage (which will occur primarily by laminar flow) can be calculated for surfaces with a multidirectional lay finish using the relationship.*

$$Q = 5.54 * 10^{-8} \left(\frac{S}{w} \frac{H^3}{\sigma_c^{2/3}} \right) \left(\frac{P_1^2 - P_2^2}{\eta T} \right), \text{ (sccHe/hr)} \quad (1)$$

where

Q = leak rate, scc He/hr

S = circumference of (seat) land, in.

H = seal surface finish (arithmetic average, AA), in. * 10^{-6} (= μ in.)

*Symbols are defined the first time that they are introduced in equations or figures. A complete glossary of symbols is given in Appendix F.

w = width of seal (seat land), in.
 σ_c = compressive stress, lb/in.²
 P_1 = upstream pressure, lb/in.²
 P_2 = downstream pressure, lb/in.²
 η = fluid viscosity at $T^\circ\text{R}$, lb-sec/ft²
 T = fluid temperature, $^\circ\text{R}$

As shown in Figure 3-5 the arithmetic average (AA) mating roughness height H is the sum of the arithmetic average peak-to-valley (PTV) heights y of each of the contacting surfaces,

$$H = y_p + y_s, (\mu\text{ in}) \quad (2)$$

The arithmetic average of the surface roughness of each surface shown in Figure 3-6 is defined by

$$y = \frac{1}{S} \int_{x=0}^{x=S} |y| dx, (\mu\text{ in}) \quad (3)$$

R87

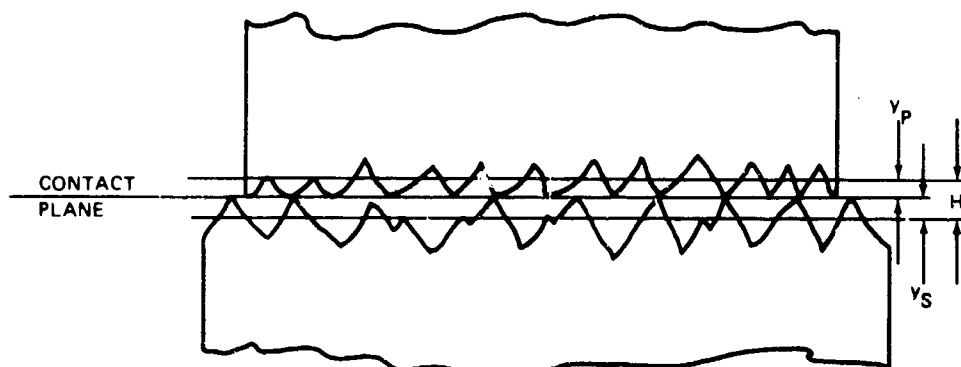


Figure 3-5. Mating Roughness Nomenclature

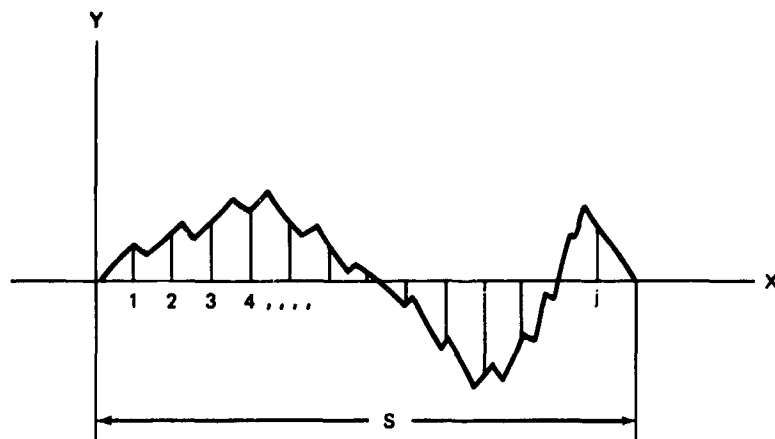


Figure 3-6. Arithmetic Average Surface Roughness

Equation (3) can be approximated by

$$y \approx \frac{y_1 + y_2 + y_3 + \cdots + y_j}{j}, (\mu \text{ in.}) \quad (4)$$

According to Ref 11,

$$y \approx \frac{1}{3} y_{\max}, (\mu \text{ in.}) \quad (5)$$

is a reasonable approximation of arithmetic average if the surface roughness is small, as in the case of the ACS valve. In the local region near to and including a pit or peak, according to Ref 12,

$$y = \frac{1}{4} y_{\text{measured}}, (\mu \text{ in.}) \quad (6)$$

Equation (1) shows that the leak rate increases with the cube of the surface roughness, with approximately the square of the pressure, and linearly with the circumferential seal length. The leak rate decreases linearly with the seal width and with a fractional power of sealing stress. Figure 3-7 is a plot of the predicted ACS valve leak rate versus surface roughness for several sealing stresses. At a nominal operating sealing stress of 1,500 psi (calculated for typical operating conditions reported in Ref 1), a leak rate of approximately 50 scc/hr is predicted for the 1.5- μ in. AA average surface roughness, estimated from the data shown in Figure 2-6 for a used poppet. This value compares reasonably well with the measured leak rate of 30 scc/hr for the K 96 poppet illustrated.

3.2.2 Model of Valve Dynamics

In this subsection, the effects of the forces and stresses applied to the sealing surfaces during normal valve operation are analyzed. Both parallel and cocked impact are considered. Quantitative equations are presented relating the valve design and operating parameters to impact forces, surface stresses, and extent of yielding. The equation for impact force is based on an approach different from the usual formulation. The analysis demonstrates that the valve will not develop excessive leakage due to normal forces and stresses.

Because the development of leakage occurs only when the valve is operated, understanding the mode of failure requires that the internal dynamics of the valve be accurately represented.

Figure 3-8 illustrates the proposed model of valve motion. The poppet moves through a full stroke, h , from open to closed, in time τ_c . The poppet makes an initial contact with the seat at angle α , and then tilts to parallel compliance with the seat. During this tilting, some lateral motion of the poppet occurs, which moves the poppet a distance s towards the side of the seat where initial contact was made. Some rotation of the poppet about its centerline may also occur, but its magnitude will be very small because of the torsional stiffness of the poppet spring support. Bouncing of the poppet on the seat is assumed to have a negligible effect on the wear in this valve design.

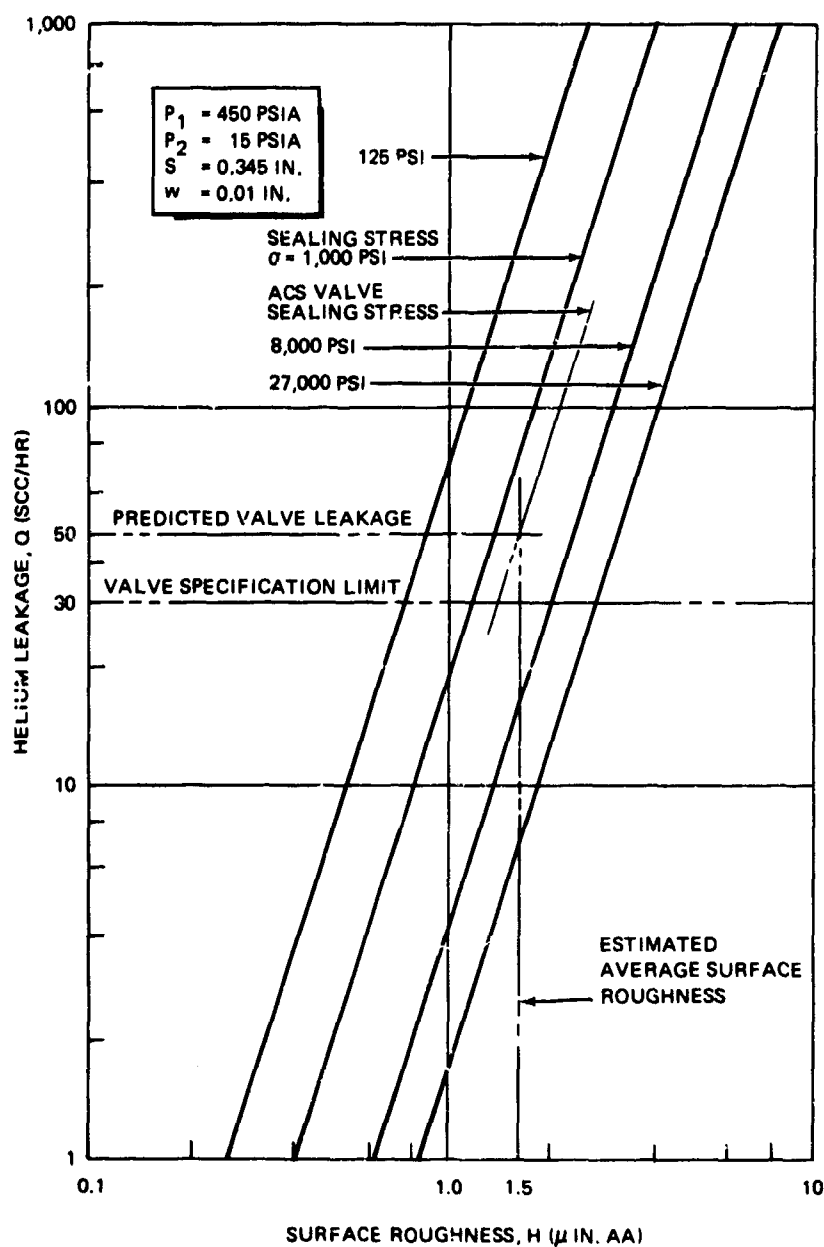


Figure 3-7. ACS Valve Leak Rate Versus Surface Roughness

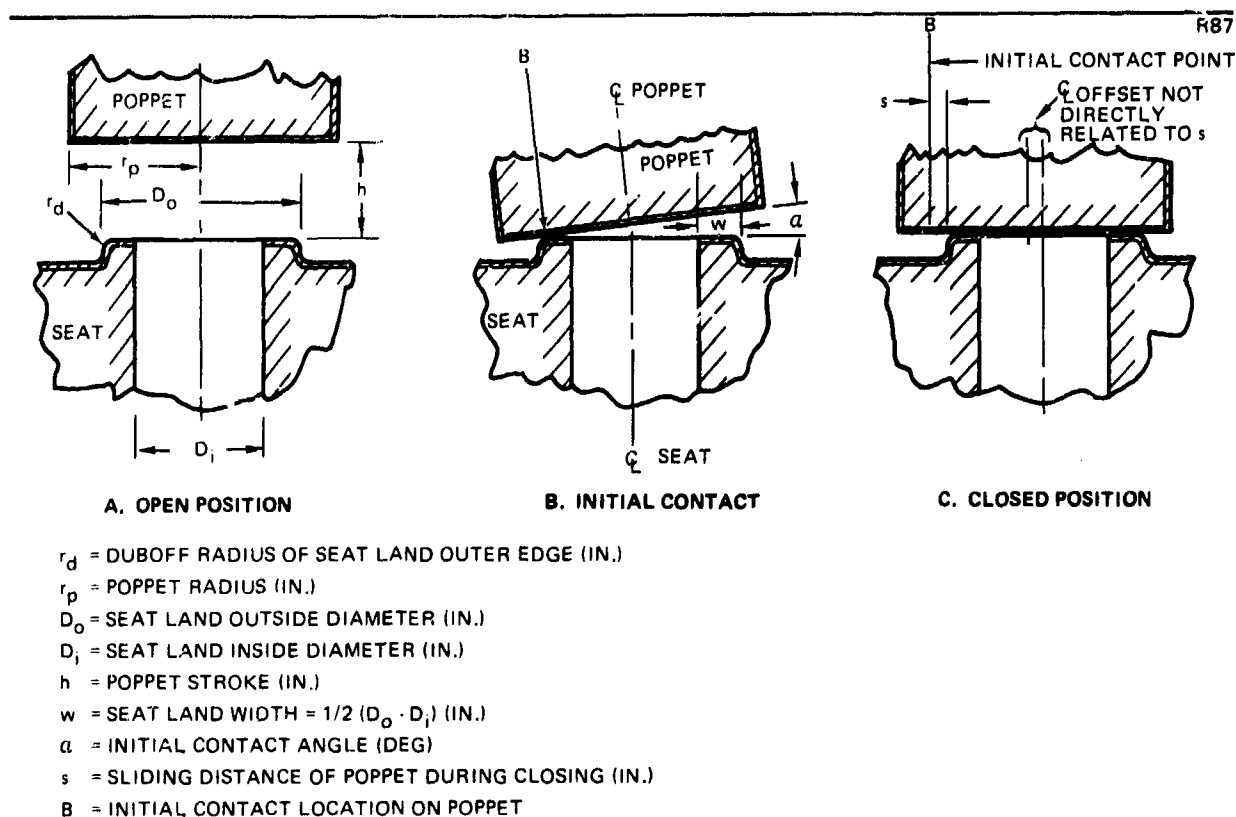


Figure 3-8. Poppet Motion Model

During the poppet opening stroke, some tilting of the poppet may occur because of local cavitation of the fluid film in the interface. This tilting may cause some small lateral movement on the opposite diameter under light load, which should not produce any significant wear.

3. 2. 3 Dynamic and Static Closure Loads

To evaluate the performance of seat materials and to predict cyclic wear it is necessary to consider the repetitive impact loading and stresses on the seat. A study of the forces and interactions, including the spring mass system, that effect the closure during operation of the valve was conducted to provide a mathematical model for performance analyses.

Details of the logic and derivation of the various equations are presented in Appendix A. The impact force on the seat in a dry condition when the poppet and seat are made of the same material is there shown (Equation A-11) to be:

$$F_I = 6.22 \times 10^{-2} \left(\frac{E}{\sigma_y} \right) \left(\frac{h}{t_T} \right) \left(\frac{W I_e}{r_c} \right) \quad , \quad (lb) \quad (7)$$

where

F_I = impact force (lb)

E = bulk modulus (Young's modulus) (lb/in.²)

σ_y = compressive yield stress (lb/in.²)

h = poppet stroke (in.)

t_T = thickness of poppet and seat, total (in.)

$W_{I, e}$ = effective weight of poppet at impact (lb)

τ_c = poppet close time (sec)

The factor (E/σ_y) is a function of the poppet and seat material. the factor (h/t_T) is a function of the valve configuration, and the factor $(W_{I, e}/\tau_c)$ is a function of the flexure spring suspension system which isolates part of the armature loads from the seat; it also depends on one material property, the density of the materials used.

The surface stresses at impact (Equation A-13) are

$$\sigma_I = \frac{F_I}{A}, \quad (\text{lb/in.}^2) \quad (8)$$

where

σ_I = impact stress (lb/in.²)

A = contact area (in.²)

Note that if the poppet impacts the seat while the surfaces are parallel, the apparent contact area, A , may be assumed to be equal to the real contact area because of the smooth finish of the poppet and seat surfaces used in this valve.

At the usual initial contact, when the poppet surface impacts the edge of the seat sealing land (Figure 2-5b), the contact angle, α , is greater than zero. The impact force is decreased because energy is absorbed in the process of rotating the poppet to a parallel position, but the stresses are increased

because the contact area is smaller. The equation for the impact force in a cocked position from Equation (A-15) is

$$F_{I,\alpha} = \frac{0.5 r_N F_I}{2 \sqrt{r_N^2 + 3B}}, \quad (\text{lb}) \quad (9)$$

where

$F_{I,\alpha}$ = impact force at contact angle α (lb)

r_N = poppet nut radius (in.) (Figure 2-1)

B = radial distance of contact on poppet (in.)

The relation for the contact stress (Equation (A-16)) is

$$\sigma_{I,\alpha} = \frac{0.395}{\alpha\beta} \sqrt[3]{\frac{E^2 r_{I,\alpha}}{d_d^2}}, \quad (\text{lb/in.}^2) \quad (10)$$

where

$\sigma_{I,\alpha}$ = contact stress at angle α (lb/in.²)

d_d = diameter of seat duboff (in.)*

α = angle between seat and poppet (deg)

β = angular position of contact on duboff relative to perpendicular (deg) (Figure A-2)

When the poppet is in the final closed position, the closed stress σ_c is defined by

$$\sigma_c = \frac{P_1 D_o^2 - P_2 D_i^2 + \sigma_S (D_o^2 - D_i^2)}{D_o^2 - D_i^2}, \quad (\text{lb/in.}^2) \quad (11)$$

Typical values for F_P , σ_P , $F_{I,\alpha}$ and $\sigma_{I,\alpha}$ calculated by means of Equations (7) to (11) using the numerical data presented in Appendix F are given in Table 3-1. The values for copper and steel are included for comparative purposes.

Table 3-1
CALCULATED FORCES AND STRESSES AT IMPACT

	Copper*	Steel	Duranickel 301	Tungsten Carbide in Cobalt Matrix
F_I (lb)	1680	24.6	89.1	58.7
σ_I (lb/in. ²)	(3.95*10 ⁵)**	5.8*10 ³	2.1*10 ⁴	1.4*10 ⁴
$F_{I,\alpha}$ (lb)	654	9.7	34.7	22.9
$\sigma_{I,\alpha}$ (lb/in. ²)	(7.6*10 ⁶)	(2.84*10 ⁶)	(4.3*10 ⁶)	(7.7*10 ⁶)
σ_y (lb/in. ²)	4.5*10 ³	5.6*10 ⁵	1.5*10 ⁵	6.9*10 ⁵

$$\sigma_c, \text{ all materials} = 1.55*10^3 \text{ lb/in.}^2$$

*Though the consideration of a soft metal, such as copper, in a model for this specific ACS valve may seem inappropriate, it is included because most of the concordant data for metallic wear have been obtained using copper as the test material; so this metal is an appropriate test of the mathematical models.

**Values in parentheses are greater than the yield stress and indicate plastic flow of the closure material.

The data indicate that the ACS valves are stable if the contact angle is held to a minimum or to zero. For the hard materials used, the stress values calculated do not indicate much damage. The width of the flattened area due to impact at an angle was calculated, using Equation (A-18). The calculations gave the widths as $2 * 10^{-5}$ for K-96 and $4 * 10^{-3}$ for steel. These are maxima; when they are reached $\sigma_{I,\alpha}$ is equal to σ_y and growth of the flattened area ceases. These calculations were made for a dry condition. The presence of liquid in the valve is reported to reduce the impact force by a factor that ranges from 1.5 to 3; other forces and stresses will be reduced proportionally.

3.2.4 Conclusions

The ACS valve is obviously stable and can withstand the ordinary dynamic loads in the service for which it is intended. The observed minor damage is

*According to Tellier, (Ref. 11), a sharp cornered seat (no duboff) experiences extremely high stresses at the edge, resulting in plastic flow or fracturing.

due to angular impact, but its effect is not serious. Additional factors must enter those cases where failure occurred.

3.3 SURFACE WEAR PROCESS ANALYSIS

3.3.1 Objectives and Approach

The purpose of this analysis of the ACS valve failure mechanism is to identify the failure mode and establish criteria that will extend the valve operating life in CPF. A wear model was developed, and appropriate wear equations predicting surface roughness were derived. This wear model was checked against the measured roughness of tested poppets and seats. The results of the analysis were used to develop material property parameters for selecting poppet and seat materials, and to identify changes in the valve design that should extend the operating life.

3.3.2 Wear Theory

The four principal wear processes that can roughen a surface are adhesion, abrasion, corrosion, and surface fatigue. Each of these wear processes is unique, but frequently one mode of wear acts in such a way as to affect the other wear modes. Additional modes of wear, which are variations or combinations of the principal wear processes, include fretting, erosion, and cavitation. Information presented on wear theory is based on discussions in Rabinowicz (Ref 13) adapted by MDAC to the particular situation in the ACS valve.

3.3.2.1 Adhesion

Adhesive wear is the most common wear mode, and it is the most difficult to eliminate. Adhesive wear occurs when two smooth surfaces in contact move relative to each other and fragments are pulled off the surfaces. Larger fragments fall free, while smaller ones adhere to the other surface. During subsequent relative movement, the adherent fragments may come off the adherend surface and be transferred back to the original surface, or else may agglomerate to form loose particles.

Adhesive wear arises from the strong forces of attraction occurring whenever atoms come into intimate contact. During the closure process of contacting and sliding of two surfaces, small asperities on one of the surfaces come into intimate contact with similar asperities on the other surface, and adhesive bonds are formed. Then, when the surfaces continue their relative motion or separate, bonds must be broken. There is a small but finite probability that when these bonds are broken, separation will occur within one of the materials, rather than at the original surface. Such fractures usually result in a surface roughness that is greater than the roughness of the original surface.

Adhesive wear is the most universal form of wear in mechanical systems in which two solids in contact move relative to each other. Adhesive wear cannot be eliminated, only reduced in severity. However, adhesive wear is not necessarily the most dangerous form of wear, because adhesive wear rates are usually fairly low. Unexpectedly high wear rates are usually caused by other forms of wear.

If flowing liquids wash the surfaces, it is assumed that free particles, formed by the adhesive wear process, are swept from the wear zone as they are formed and have no further effects. In static or quasi-static systems this is not the case, and the particles generated can become involved in abrasive wear.

3.3.2.2 Corrosion

Corrosive wear occurs when sliding or impact of two surfaces takes place in a corrosive environment. In the absence of mechanical motion, the products of corrosion form a film on the surfaces that tends to slow down the rate of, or even halt, corrosion. Sliding action wears this film away, and impact processes may fracture it, allowing the corrosive attack of the surface to continue. The physical characteristics of the corrosion film affect the wear rate and the roughness of the surface. Materials that form ductile, dense, and tenacious films resist corrosive wear most effectively.

3. 3. 2. 3 Abrasion

Abrasive wear occurs when a rough hard surface, or a soft surface containing hard particles, slides on a softer surface and ploughs grooves in it. The material from the grooves is displaced in the form of wear particles, generally loose, which cause additional abrasive wear if the particles are harder than the surfaces. In general, the magnitude of surface roughness produced is proportional to the diameter of the adhesive bonding area or of the loose abrasive particles.

3. 3. 2. 4 Surface Fatigue

Surface fatigue wear occurs after repeated working of the surfaces by sliding or impact. The repeated loading and unloading stress cycles to which the materials are exposed induces the formation of surface or subsurface fatigue cracks. These cracks eventually result in the formation of large loose fragments, leaving pits in the surface. Materials that are hard, but not brittle, generally resist surface fatigue wear.

3. 3. 2. 5 Combined Modes

Fretting

Fretting wear occurs when contacting surfaces undergo oscillatory tangential displacement of small amplitude. This movement causes adhesive wear, which produces loose particles. The surface exposed by this wear may be corroded by the ambient environment. The particles may also be corroded by the environment and work hardened sufficiently to cause abrasive wear of the surfaces. Thus, fretting may be a combination of adhesive, corrosive, and abrasive wear.

Erosion

Erosion is a form of abrasive wear in which sharp particles impinge on a surface. Surface roughness produced by erosion may be relatively greater than that produced by conventional abrasive wear, because impinging particles may readily remove material from a low point on the surface.

Cavitation

Cavitation occurs when vapor bubbles in a liquid collapse abruptly, producing a mechanical shock. Cavitation wear is similar to surface fatigue wear, and materials that are resistant to surface fatigue wear are also resistant to cavitation wear. However, the materials selected to resist the mechanical shock of cavitation must also resist corrosion attack by the liquid which is cavitating.

3. 3. 3 Adhesive Wear in the ACS Valve

In this subsection, surface wear by means of an adhesion mechanism is analyzed quantitatively. The results indicate that the valve will not wear appreciably in operations with liquid propellants, but it may fail when used in inert gases.

3. 3. 3. 1 Wear Particle Generation

According to Rabinowicz (Re 13), the extent of adhesive wear and the resultant surface roughness depend primarily on two properties of the contacting materials and on the contact load applied. The properties are the hardness, p , and the surface energy γ . Hardness is readily determined by conventional penetration hardness tests, such as Vickers diamond pyramid hardness. For many solid materials, surface energy is proportional to the cube root of hardness, as shown in Figure 3-9. This relationship is brought out more clearly in Figure 3-10 in which the ratio of surface energy to hardness is plotted against hardness. Appendix B, Subsection B. 1, contains descriptions of several methods for determining the surface energy of solid materials. Note, however, that the immediate environment will affect both the hardness and the surface energy; this is discussed later. The energy of adhesion G_{AB} between 1-cm² plates of two materials, A and B (of which A is the softer), is given by the relationship (Ref 13)

$$G_{AB} = \gamma_A + \gamma_B - \gamma_{AB} \quad (\text{erg/cm}^2) \quad (12)$$

(see also Appendix B, Subsection B. 2).

*Surface energy and surface tension are the same parameter. Usually the term energy is used for solids and tension for liquids, but these are simply conventions among different groups of workers.

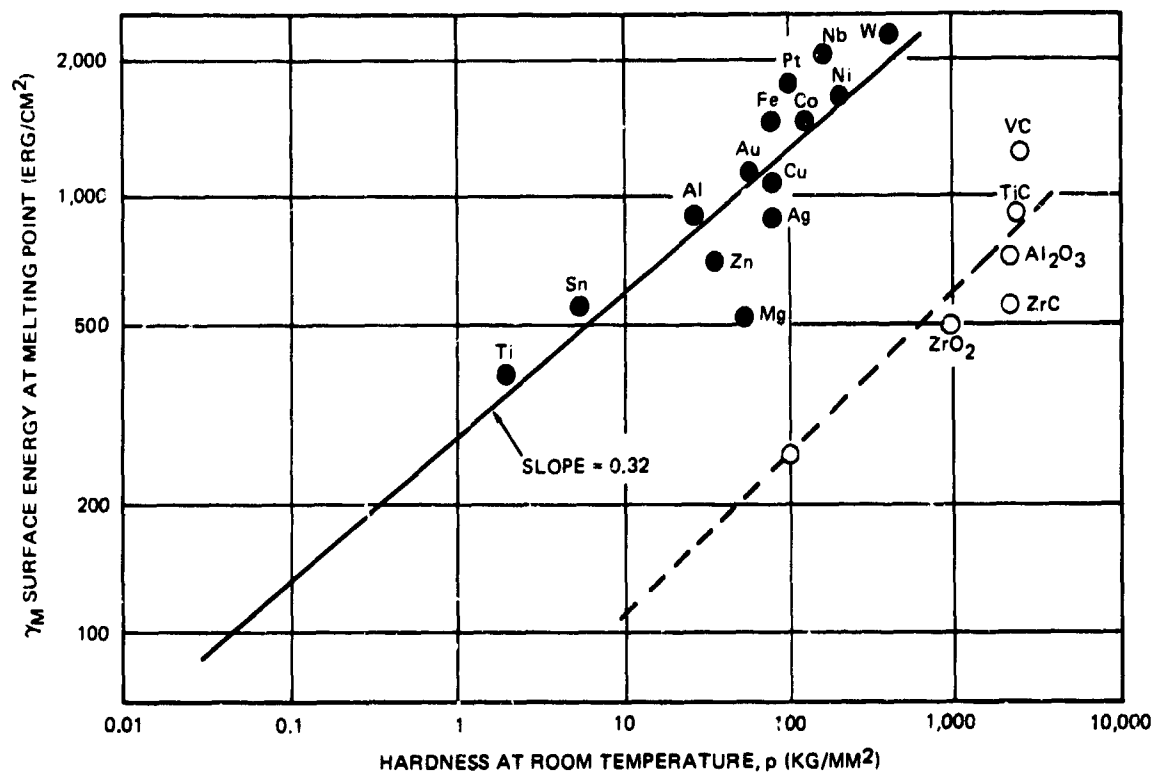


Figure 3-9. Surface Energy Versus Hardness (Ref 13)

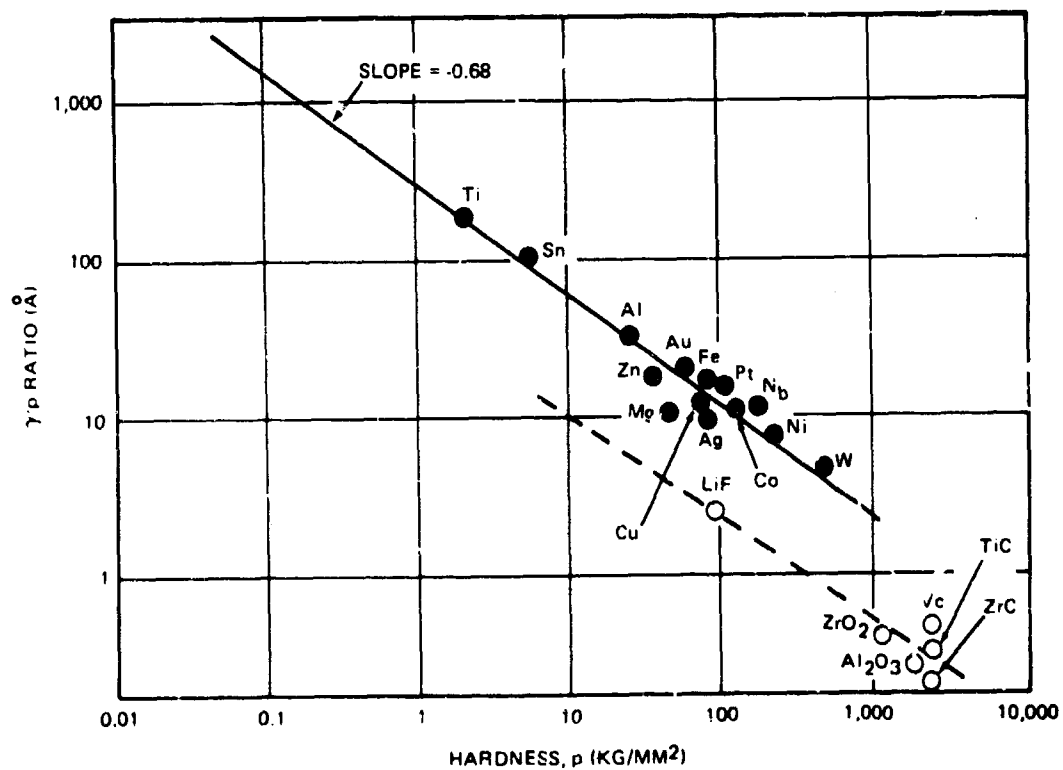


Figure 3-10. Ratio γ/p Versus Hardness (Ref 13)

The relationship of G_{AB} to various types of materials and their interactions is discussed in Appendix B, Subsection B. 2. Large values of G_{AB} are associated with increased wear and surface roughness, since they indicate that the intermaterial bond strength is greater. Therefore, the use of noninteracting materials will minimize both wear and roughness increase. Note that the adhesion energy between two pieces of a single material is equal to twice the surface energy, since the term γ_{AB} vanishes for this condition.

Values of surface energy, hardness, and other significant properties of several materials are listed in Table 3-2. Surface energy values calculated by means of Equation (B-4) are given in parentheses in this table.

The data listed for the surface energies of metals (Table 3-2) have in many cases been obtained from the surface tensions of the molten metal (Ref 16); then these values were corrected appropriately for the cooling to room temperature. Such surface tension measurements are conducted on a clean liquid surface in an inert atmosphere to reduce problems due to oxides and slags. But the solid metal of interest for use in fabricating components normally has an oxide film on its surface. It may be seen from Table 3-2 that the surface energies of the bulk oxides are usually considerably less than those of the metals. The surface tension of mercury is 10 percent less in air than in a vacuum (Ref 16), that of silver is 12 percent less (Ref 17). The structural metals of ordinary use then probably have true surface energies that fall between the values in the table for the clean metal and its bulk oxide. Rabinowicz assumes that the increase in γ as the temperature decreases below the melting point compensates for the decrease in γ due to oxide film formations. Fluorine passivation is expected to lower the true surface energy even more.

3. 3. 3. 2 Wear Particle Size and Configuration

The roughness produced by adhesive wear depends on the size of the loose particles generated. The average diameter, C_l , measured parallel to the wear surface, of a loose wear particle can be calculated (Ref 13) from

$$C_l = 6.5 \frac{G_{AB}}{P_A}, \text{ (microns)}^* \quad (13)$$

* Note that p_A is the hardness of the softer material in a bimaterial interface.

Table 3-2
WEAR-RELATED PROPERTIES OF SOLID MATERIALS

Material	Melting Temp (°C)	Young's Modulus, E		Compressive Yield Strength, σ_y		Maximum Hardness, p (Kg/mm ²)	Surface Energy, γ (erg/cm ²)	Calculated G_A/pA (Å)	Observed Particle Sizes (μ -in.)
		10^{12} (Dyne/cm ²)	(psi) $\times 10^3$	(Kg/mm ²)	(psi) $\times 10^3$				
Aluminum	933	3.65	0.98	1.1	1.6	27	900	66	140
Aluminum oxide	2400	3.0	4.4	3.2	4.5	150	1,000	13	
Aluminum nitride	3210	3.70	0.83	0.72	1.0	22	620	56	320
Aluminum nitride	3200	2.6	5.8	1.6	2.3	935	1,600	3.4	
Aluminum nitride	3440	2.1	3.0	7.8	11.1	125	1,530	24	
Copper	1358	1.2	1.7	3.2	4.5	80	1,100	28	250
Brass	1600	-	2.98	-	100	253	-	-	
Brass	1600	0.81	1.1	2.1	3.0	58	1,120	38	
Brass	1670	-	3.1	-	115	301	-	-	
Brass	1684	2.04	3.0	2.5	3.5	82	1,500	36	
Brass	1690	0.39	0.57	1.9	2.7	150	450	(29)	270
Brass	650	0.44	0.64	1.5	2.1	46	560(?)	24	
Brass	1,245	-	-	2.5	3.5	3,300	(4,100)	(2.5)	
Brass	2,610	3.0	4.4	8.4	11.9	240	(1,700)	(14)	
Brass	1,443	2.08	3.0	3.2	4.5	210	1,700	16	35
Brass	2,468	1.05	1.5	2.0	4.0	160	2,100	26	
Brass	1,761	1.5	2.2	1.6	2.3	100	1,800	36	
Silver	961	0.78	1.1	2.0	2.8	80	920(S09)	22	330
Tantalum	2,990	1.9	2.7	3.5	5.0	-	-	-	
Titanium	3551	0.44	0.64	0.15	0.21	5.3	470	220	120
Titanium	1,670	1.13	1.6	1.4	2.0	65	(1,100)	(34)	
Tungsten	3,410	3.51	5.1	18.0	26.0	435	2,300	11	
Tungsten	420	0.91	1.3	1.3	1.8	38	790	42	440
Tungsten	1,832	0.96	2.4	2.0	2.8	145	(1,500)	(20)	
Al ₂ O ₃	2,045	-	7.0	-	-	2,100	740	0.68	1
Ba F ₂	1,260	-	-	-	-	-	210	-	
Ca F ₂	1,360	-	-	-	-	160	340	4.2	
Ca O	2,550	-	-	-	-	-	360	-	
Fe ₂ O ₃	2,550	-	-	-	-	2,000	600	0.6	1
Mg O	2,550	-	-	-	-	500	670	2.6	
Si	1,410	-	1.6	-	-	-	930	-	
Si O ₂	3,100	-	1.0	-	-	800	-	-	
Ti C	3,140	-	5.0	-	-	2,400	900	0.76	
V C	2,810	-	-	-	-	2,500	1,250	1.0	
W C	2,870	-	8.6	-	900	1,900	848	1.1	1.1
Zr C	3,540	-	-	-	-	2,100	600	0.56	
Zr O ₂	2,715	-	-	-	-	1,150	530	0.92	
Mild steel	1,525	-	3.0	-	-	200	1,000	10	60
Tool steel	1,525	2.2	3.1	-	560	1,100	1,500	3	
Steelite 1	1,430	-	3.5	-	-	690	5,430	16	
WC in Co	-	-	9.1	-	690	1,800	(780)	(0.8)	
Matrix	-	-	0.009	-	2.0	4	15	8	90
Teflon	220	-	0.05	-	14	20	30	3	100
Nylon	930	-	-	-	-	120	700	12	
Brass	460	0.66	0.99	-	-	550	200	0.8	1

Parenthears indicate surface energies calculated by means of Equation (B-4) and G_A/pA values calculated from these energies. Most of these data were taken from Ref 13. Other sources included Ref 11, 14, 15, and product brochure from several alloy suppliers.

where subscript ℓ = average loose particle.

This equation gives the result in metric units. In order to compare the data with common measures of roughness, c_ℓ in microinch units, is defined by

$$c_\ell = 40 C_\ell = 2.60 \times 10^2 \frac{G_{AB}}{P_A}, \quad (\mu \text{ in.}) \quad (14)$$

The points on Figure 3-11 are observed particle sizes (Ref 13) plotted against the calculated G/p ratio. The line drawn through the points is a plot of Equation (13) showing the calculated sizes of the average wear particle for several materials rubbed against themselves in a laboratory air environment.

Recently, MDAC prepared a number of scanning electron photomicrographs of hardened 17-4 PH stainless steel surfaces after the surfaces had been worn by a process that emphasized adhesive wear. (This work was done on an IRAD program related to dry helium gas flow rates through small passages.) The photographs revealed plainly that pits had been formed, apparently by the adhesion mechanism. The pits range in diameter from

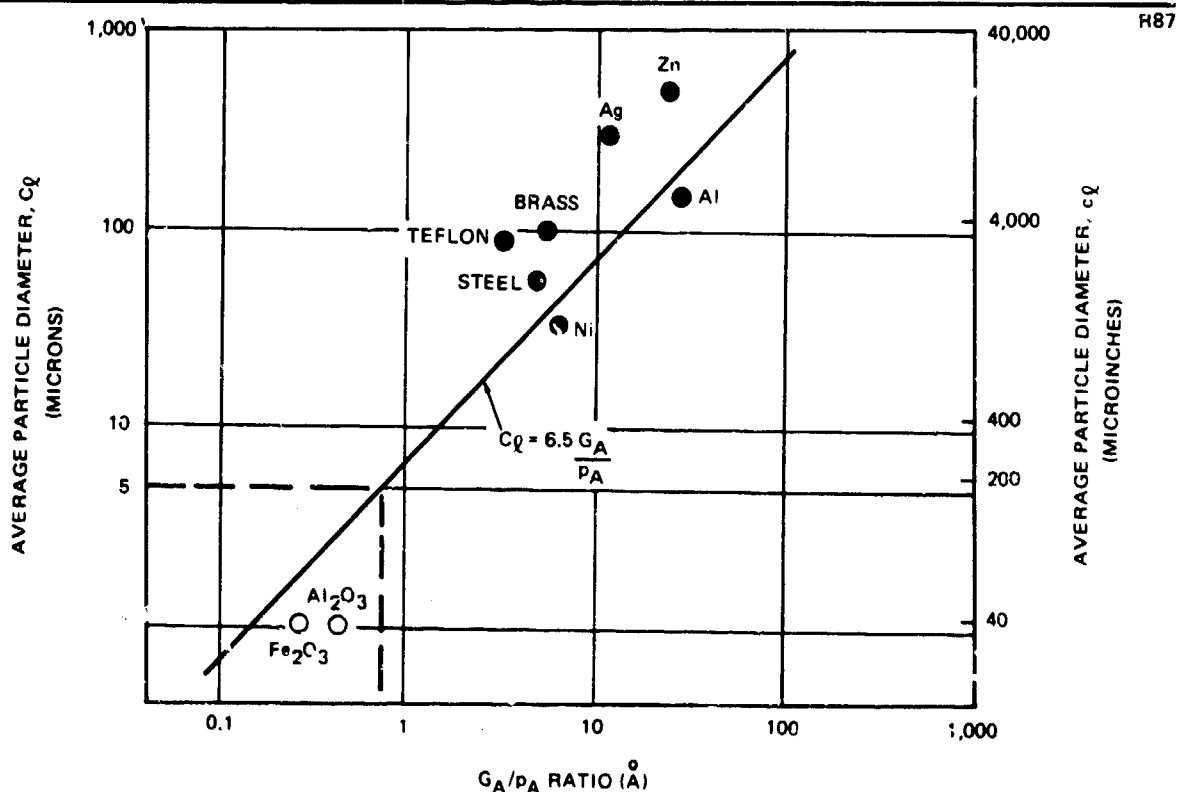


Figure 3-11. Wear Particle Size Versus G/p Ratio (Data from Ref 13)

6.9×10^2 to 1.7×10^3 μ in. However the pits are not hemispherical, but instead are fairly shallow. The depths are about 1/4 of the pit radius.

Examination of adhesion-worn CRES 21-6-9 surfaces under high magnification resulted in detection of adherent particles, since both pits and particles were visible. The smallest particles and pits detected were 40 μ in. in diameter, and again the depth of the pits and thickness of the particles was about 1/4 of the radius, or 5 μ in. The pit bottoms and particle tops were flat and parallel to the original surface, so the cross sections were trapezoidal. But wall angles were not the same from particle to particle. Hence, for calculating volumes, it is more convenient to assume a shape equivalent to a spherical segment, as is done in Appendix C, Subsection C.1.

The Berylco nickel 440 seat surface in Figure 3-2 has both pits and adherent materials. Sizes of both range from 65 to 800 μ in. (not considering the large shallow depression, which is over 4,000 μ in. long). Again, the pits are usually shallower than their radii. The adherent material does not match the pits; it seems to be fluffy and irregular, and appears to have undergone hydrolysis during unprotected storage.

The average wear particle diameter is influenced by the amount of lubricant at the rubbing interface. A dry inert atmosphere will increase and a lubricant will decrease the particle size from those shown in Figure 3-11. Table 3-3 shows measured sizes of wear particles formed in various environments. The changes in particle sizes can be attributed to changes in both G_{AB} and p_A in the various environments. The surface energy of the substrate is strongly affected by the environment. The energy is generally reduced by the presence of surface films, oxides, absorbed gases, or lubricants. This is due simply to the fact that if a heat of reaction is released (e.g., heat of oxidation, heat of absorption, heat of wetting, etc.) this output of energy reduces the potential energy still present in the system, and surface energy is a potential energy (i.e., energy of position).

The hardness changes are obvious—the reacted or absorbed film on the surface is almost always of a hardness different from that of the substrate.

Table 3-3
EFFECT OF ENVIRONMENT ON SIZE OF LOOSE WEAR PARTICLES

Environment	γ Surface Energy (erg/cm ²)	Measured Average Loose Fragment Diameter	
		(μ)	(μ in.)
Copper on Copper (Ref. 13)			
Nitrogen	2,000	480	1.8×10^4
Helium		380	1.5×10^4
Carbon dioxide		300	1.2×10^4
Dry air		224	8.8×10^3
Oxygen		201	7.9×10^3
Laboratory air (50% RH)	1,380	177	7.0×10^3
Laboratory air—calculated	1,100	182	7.3×10^3
Wet air (100% RH)		144	5.7×10^3
Cetane	240	12.0	4.7×10^2
Silicone DC200-100 cst	180	9.5	3.7×10^2
Ucon fluid LB-70X	140	9.5	3.7×10^2
Palmitic acid in cetane	100	8.0	3.1×10^2
Gold on Gold (Ref. 38)			
Laboratory Air	1,780	275	1.1×10^4
Vacuum	1,360	200	8.0×10^3
Hydrochloric Acid	670	100	4.0×10^3

There is no necessity that G_{AB} and p_A should change in the same direction; in fact the alteration of an oxide film to a fluoride probably causes a decrease in G_{AB} and an increase in p_A , whereas a lubricant would decrease both.

Because particle sizes are determined by the G_{AB}/p_A ratio the changes in particle size as caused by changes in the environment (Table 3-3) are directly due to the effect of the environment on the G_{AB}/p_A ratio. The particle sizes of copper decrease roughly 15 fold from laboratory air to lubricated conditions. Hence, G_{AB}/p_A must decrease by the same factor. This would imply that if lubrication has approximately the same effect on the forces for all metals, then if a material has G_{AB}/p_A of 15 Å or less under ordinary circumstances (dry laboratory air), this value will reduce below 1 Å when the

surfaces are well lubricated, and the material will be polished when loaded by cyclic impact, instead of wearing. The metals beryllium, chromium, manganese, molybdenum, tool steel, and tungsten meet this criterion (Table 3-2). Observed behavior is generally in accord with this prediction, which is a partial explanation of how a lubricant functions.

The assumption that most metals will behave in similar fashion in a single fluid or a series of similar chemically related fluids cannot be extended to assuming similar behavior in fluids of widely different chemical constitution, even for a single metal. The effects on G_{AB} and p_A should be evaluated separately before prediction is made.

3.3.3.3 Surface Wear Volume

In Appendix B, Section B. 3, it is shown that for the ACS valve design, if the impact force F_I is less than the value calculated by the formula,

$$F_{I, \text{ no wear }} \leq 3.76 * 10^{-7} \frac{y^2}{p_A}, \quad (\text{lb}) \quad (15)$$

no wear particles will be generated. Typical solutions of this equation are, for copper, 5.5×10^{-3} lb, and for WC, 2.3×10^{-5} lb. F_I is used in this expression because it is typically one or two orders of magnitude greater than

$$F_c = W_{I, e} / g, \quad (\text{lb}) \quad (16)$$

The force in the closed position, F_c , approximately equals 3 lb. Even this low value is great enough to generate adhesive wear particles from some materials. Tests made with 1020 steel on 1020 showed that at low loads the wear debris is an oxide and at higher loads it is metallic (Ref 13).

The volume of material, V_w , removed as free particles per stroke by adhesive wear can be calculated (Ref 13) from

$$V_{w, l} = 7.04 * 10^{-4} \frac{k_{ad} F_I^s}{p_A}, \quad (\text{in.}^3) \quad (17)$$

where

k_{ad} = adhesive wear constant

subscript w = worn away

The wear adhesive constant, k_{ad} , is a measure of the probability that any surface junction will result in a transferred fragment rather than failure of the junction along the original interface. The wear constant, like the coefficient of friction, is dimensionless and can be determined empirically.

Experimental values of the adhesive wear constant k_{ad} for several materials, with corresponding values of G_{AB}/p_A , are shown in Table 3-4. No values of k_{ad} for tungsten carbide in cobalt matrix are available at this time. Consideration of the tabulated data again suggests that wear decreases as G_{AB}/p_A decreases.

The calculated values of V_w are very small, due in part to the very small sliding component s in the ACS valve. The observed average sizes (diameter) of individual loose copper particles are $7.0 \times 10^3 \mu \text{ in.}$ (dry) and $3.7 \times 10^2 \mu \text{ in.}$ (lubricated) for laboratory test conditions (not the ACS valve) (Table 3-3). Equation (17) gives similar calculated values. These diameters are equivalent to total particle volumes which fall in the range of 10^{-9} in.^3 (dry) and 10^{-12} in.^3 (lubricated). This implies that many valve closings are needed to form an applicable number of loose adhesive wear particles even when copper is used for the closures.

3. 3. 3. 4 Surface Roughness Change Due to Adhesive Wear

The removal of small particles of the closure surface material by adhesive wear causes the formation of pits, and the presence of steadily increasing numbers of pits causes roughening of the surface or degradation of the surface finish. Hence, if the quantity of material removed and the sizes of the individual particles formed are known, it becomes possible to estimate the average surface finish at any time after the adhesive wear process has started.

The important assumptions are

- A. The total number of pits formed is equal to the number of particles generated.

Table 3-4
ADHESIVE WEAR CONSTANTS

Material	Environment				
	Clean Lab Air				
	k_{ad}	GAB/PA (Å)	k_{ad} Poor Lubricant	k_{ad} Good Lubricant	k_{ad} Special Conditions
Zinc on zinc	1.6×10^{-1}	42	6.4×10^{-3}	6×10^{-5}	-
Steel on steel (low carbon)	4.5×10^{-2}	36	1.8×10^{-3}	2×10^{-5}	-
Copper on copper	3.2×10^{-2}	28	1.3×10^{-3}	1×10^{-5}	-
CRES on CRES	2.1×10^{-2}	-	1.8×10^{-3}	1×10^{-5}	LO_2 4×10^{-5} $RP-1$ 2×10^{-5} N_2H_4 1×10^{-5} N_2O_4 5×10^{-6}
Hard steel on hard steel	1.3×10^{-3}	14			
Low carbon steel on copper	5×10^{-4}	16	5×10^{-4}	1×10^{-5}	
CRES on tool steel	1.7×10^{-4}	-	-	-	
WC on mild steel	4×10^{-5}	9	-	-	
Bakelite on bakelite	2×10^{-5}	-	2×10^{-5}	1×10^{-5}	
Al_2O_3 on Steel 135M	-	2.2	-	-	$RP-1$ 2×10^{-5}
WC on WC	1×10^{-5}	1.1	-	-	
Bakelite on tool steel	7.5×10^{-6}	-	-	-	
Polyethylene on tool steel	1.3×10^{-6}	-	-	-	

Based on data in Refs 13 and 39

- B. The area of the surface degraded is related to the shape, size and number of particles generated.
- C. The surface finish of the worn surface is related to the depth of the pits formed, and reaches a maximum when the whole surface is worn.
- D. The location of new wear pits formed in any individual closure stroke is statistically random over the unworn area.

It is assumed that the surface roughness from removal of particles is directly proportional to the size of the particles removed. Measured in the usual manner then,

$$\bar{y} = \frac{1}{16} c, \quad (\mu \text{ in.}) \quad (18)$$

Some of the previously given equations can be combined to give a formal quantification of the increase of surface degradation. This derivation is presented in Appendix C, Subsections C. 1 and C. 2. It is shown in the derivation that the fraction of the closure surface worn at each stroke, which is due almost entirely to generation of adherent particles, is

$$Z_w = 6.95 \times 10^3 \left(\frac{k_{ad} E}{G_{AB} \sigma_y} \right) \left(\frac{sh}{t_T} \right) \left(\frac{W_{I, e}}{\tau_c} \right) \quad (19)$$

The average surface finish of the valve closure in the local region where a particle, j , is generated, is

$$y_j = \frac{1}{16} c_j, \quad (\mu \text{ in.}) \quad (20)$$

and the overall average surface finish after n closing strokes can be calculated using the formula

$$\bar{y}_{n, j} = y^\circ + n \bar{y}_j Z_w - n y^\circ Z_w, \quad (\mu \text{ in.}) \quad (21)$$

where

y° = the initial surface finish

Calculated values for the wear rate parameters defined are presented in Table 3-5. Again, noncandidate materials are included for comparison.

Table 3-5
CLOSURE SURFACE FINISH CHANGE WITH VALVE CYCLING

Initial Conditions $H = 0.75$
($y_p = y_s = 0.375$)

Cumulative Number of Cycles	Copper		Steel		Duranickel ^c		Tungsten Carbide ^c	
	Dry	Propellant	Dry	Propellant	Dry	Propellant	Dry	Propellant
n = 0	0.75	0.75	0.75	0.75	0.75	0.75	0.75	0.75
1	2.53	0.75	4.59	0.75	0.75	0.75	0.75	0.75
10	18.6 ^a	0.74	39.1 ^a	0.75	0.76	0.75	0.75	0.75
102	-	0.67 ^b	-	0.77	0.85	0.72 ^b	0.75	0.75
103	-	-	-	1.03	1.76	-	0.75	0.75
104	-	-	-	4.55	10.85 ^a	-	0.79	0.75
105	-	-	-	38.75 ^a	-	-	1.14 ^a	0.73

a. Roughening greater than particle size; beyond limit of accuracy of unexpanded equation.

b. Polishing: applicability of the equation to a polishing situation is questionable, so prediction of extent of polishing should be regarded as doubtful.

c. Estimated k_{ad} used; see Table C-1.

Note added in proof (Personal communication, H. Wietmann, July 1971): Summary of test results on closure materials at this date: a) WC in Co tested more than 4 x 105 cycles in CIPF-leak rate is still within design limit; b) boron carbide appears more wear-resistant than WC from initial tests; c) Duranickel 301, no matter how well cleaned and dried, develops too great a leak rate and has noticeable buildup of deposits. The results for Duranickel indicate that the value for the k_{ad} of nickel, estimated by MDAc to be 7×10^{-3} , is too small.

The behavior of the valve closures when operating in liquid propellant is of considerably greater interest than the dry wear characteristics. Accurate values for such terms as γ_A , p_A , etc., are not available for metal surfaces passivated in CPF. However, it is possible to make fairly good estimates of the net effects, using available data. This was done (see Appendix C, Subsection C.3) and wet wear rates calculated. The results from these calculations are also given in Table 3-5.

Review of the application of the equations and the tabulated data points up the following interesting and important conclusions.

- A. Remembering that $y_{n,i} = 1/16$ of the particle diameter, solution of Equation (21) for $\bar{y}_{n,i} = y^*$ indicates that adhesive wear becomes negligible when the particles generated are smaller than 8 μ in. or 0.2-micron in diameter. Abrasive wear is reported to become negligible at 5 microns (200 μ in.).
- B. In the derivation of Equation (21), neglect of higher order terms allows the calculated roughness to exceed the wear particle size, contrary to assumption. This type of result can be avoided by using the full binomial expansion of Equation (C-27). Such an expansion is generally unnecessary, since the region of interest for valves is that of very low roughness, not the upper limit.
- C. This is a dramatic change in wear rates in the presence of a fluid. Three out of the four materials are no longer roughened, instead they now become polished. Only steel gives an indication of still wearing, but at a rate one-ten thousandth as fast as for the dry condition.
- D. Generally, all the results of application of the equations lie in the direction which experience indicates is correct. However, lack of sufficient numerical test data prevents the desirable close check with experience and refining of the various parameters and constants used.

The equations for this analysis are based on the assumption that only the softer material in a sealing interface will wear, and that there is wear on both sides only in cases in which identical materials are used for seat and poppet. Of course, wear occurs on both surfaces, even when they are of different hardnesses. But the softer material wears faster and thus has the major effect on leak development. Even so, the applications for the current program are for use of a single material for both poppet and seat, and the approximation of wear on a single surface does not apply; instead equal wear will occur on both surfaces.

Another point is that work hardening of the surfaces will occur, so that p will change during valve cycling. It is possible to use a variable, $p = f(n)$, but this would add considerable complexity. It would be satisfactory to assume that p reaches its maximum value in a relatively few cycles, and to use p for a work hardened condition in the calculations. This was not done in the above examples, because the data were not available.

In the above analysis, it has also been necessary to ignore a number of other factors due to lack of data. These factors include specific changes in surface energy γ , surface hardness p , and adhesive wear constant k_{ad} , when a fluoride or chloride-fluoride film forms on the metal. Instead, estimates of the changes in the G/p ratio and in k_{ad} were used.

However, the failure to include them may not be of significant importance. The available values of γ and p for commonly used metals in ordinary environments are those for the substrate metal, and the fact that the metals have oxide-hydroxide coatings of considerably lower γ is not usually considered. The effects of change from oxide to fluoride in both γ and p will be in the same direction as the change from metal to oxide. This may account for the very severe effect of environment on particle size demonstrated by the test data in Table 3-3. In addition, k_{ad} is used in the equations, and this factor seems to parallel G/p at constant lubrication conditions (Table 3-4). The wear constant k_{ad} is very sensitive to the environment at the sealing interface (see Table 3-4 for effects). It seems probable that k_{ad} is a function of G/p , tensile yield strength, and the coefficient of friction. No attempt to derive such a relationship was made on this program. Instead, it was assumed that the use of k_{ad} in discussions E and F above would supply the necessary corrections to take care of changes in G/p .

It must also be pointed out that the leak rate Equation (1) has no terms to take care of surface films which have properties different from those of the substrate metal. Horizontal transport through the film could be treated as increased surface roughness, H , and the mechanical properties of the film would entail a correction in σ_c . However, the overall tribological theory presented in this report is not yet sufficiently accurate, and any modifications to Equation (1) are probably only 3rd order effects.

3.3.4 Conclusions

This analysis leads to the conclusion that the valve design is more than adequate; it will readily withstand the effects of simple adhesive wear due to mechanical loads. The leakage problems that were encountered must hence relate directly to a chemical interaction related to the CPF environment. This conclusion is in agreement with the findings from the valve wear test data.

3.4 CORROSION AND CORROSIVE WEAR

In these subsections, corrosion as a mechanism of closure surface roughening is analyzed qualitatively. The analyses suggest that corrosion, by the oxidizer, CPF, in a contaminant-free system, even when accelerated by mechanical action, or simple corrosion by aqueous HF in the absence of dynamic loads, are not significant factors in causing increased leakage.

3.4.1 General

Corrosive wear occurs when the attack of the environment on a surface is either accelerated, increased, or both because of dynamic processes occurring at the same surface. In most instances, corrosive wear takes place when the environment interacts chemically with a surface, and then the reaction products are removed by some mechanical process; adhesion is one such mechanism. The exposed surface then reacts further with the environment.

A different process is possible in some cases when the corrosive agent is sufficiently active. The agent can diffuse through the protective layer of reaction product and then react with the substrate if sufficient energy for activation is supplied by the mechanical process. There are some indications that the ordinary reaction of copper with F_2 occurs by diffusion of F_2 molecules or atoms through the oxide and fluoride coatings, even in the absence of additional energy inputs (Ref 18).

There is a third process which is possible in the presence of high energy propellants; that is the initiation of a combustion type reaction. Combustion is different from corrosion in that combustion is progressive, it can become self supporting, and if it does so, it will completely consume one of the reactants with the evolution of heat and light. Combustion reactions can be initiated by a number of types of processes, including mechanical actions which release energy into the system. This type of chemomechanical interaction is discussed later, in Subsection 3.5.

A discussion of the chemical process that occurs in the fluorination reaction, and of the way that impurities can affect the reaction may be found in Appendix H.

4.2 Corrosion and Wear

For the usual corrosive wear process, there is a chemical attack on the material surface. The chemical reaction rate is usually rapid at first, but decreases as the corrosion product film thickness increases. In the case of aluminum in air, the reaction ceases when the oxide film thickness reaches 2×10^{-6} cm (200Å). In some cases the chemical reaction continues indefinitely at the initial rate because the reaction products do not act as a protective film. The reaction will then continue until one reactant is used up. For the ACS valve application, it is essential that the poppet and seat materials form coherent protective films in the presence of CPF, over the temperature range of -100° to 350°F.

The essential step of the usual corrosive wear process consists of stressing the film to such an extent that it fails and is removed, either locally or over large areas, by means of a mechanical action. When the film is thus removed, the exposed surface is again subjected to chemical reaction with the environment, and the corrosive attack begins again. The removal of the reaction product film also results in release of energy in the reaction zone due to bond fracture, frictional heating, and other similar processes. The new corrosive attack may then be much more vigorous than the original because of the initiation energy available. This can result in severe local effects, such as pitting or cratering, resulting in a roughened surface. In some instances it might even result in a self-propagating ignition.

Usually, the corrosion products are harder and more brittle than the metal alloy surfaces on which they form. The corrosion film tends to be reasonably resistant to wear as long as the film is thin. However, above some critical thickness, wear occurs at a rate which is dependent on the conditions of the sliding process. If the thick film is brittle, the total thickness tends to flake off, forming large particles. However, if the film is ductile and less cohesive than the surface on which it forms, it is probable that only part of the film thickness will be removed, and that the wear rate will be less than for brittle films. Thus, it is desirable that the materials selected for the ACS valve

poppet and seat be able to form relatively soft and tenacious films in the presence of CPF; however most fluorides are hard and brittle.

The alternative process of corrosive wear can occur without rupture of the corrosion film if the film is permeated with reactant fluid after formation. While it is possible to remove the fluid (dry the film), the moment a new exposure to the fluid occurs, the film becomes permeated to saturation again. The strong affinity of the film and fluid suggests that some type of solvation or complexation occurs between the species.

The wet film holds some of the fluid directly against the substrate. Since further film formation does not usually occur, it is probable that there is a chemical complexation reaction of the permeated fluid with the film material which reduces any tendency to react with the substrate. An example would be formation of $(AlF_4)^-$ ions. Hence, a greater initiation energy is required to start a reaction. Friction and impact will release energy in the film system, even if they do not destroy the corrosion film. Under some circumstances this energy may be sufficient to initiate corrosion reactions between the permeant fluid and the substrate.

3.4.3 Chemical Corrosion of ACS Valve Closures

The excessive leakage observed when a specific propellant, CPF, is used, but only if the system has not been thoroughly dried, occurs with several seat structural materials. Several metals or cermets of widely different composition all degrade at about the same rate.

The presence of impurities in the CPF, in the valves or inclusions in the materials, as well as the continued access of moisture, will account for the above effects. The valve has a built-in upstream filter, but it is not very efficient, because particles known to be generated upstream of the filter were found downstream of it (see Page 75 in Ref 1). The observations of liquid residues on the valve surfaces after operation in CPF systems to which water vapor had access (Ref 1), the different behaviors in wet and dry systems (Ref 5 and 7), and green "hydrated" corrosion deposits from FLOX service (Ref 3) emphasize that the corrosion is accelerated in the presence of moisture.

It has been demonstrated at MDAC that metal fluoride films on metals will absorb oxidizer up to 50 percent of their dry weight and that simple purging will not remove fluorine oxidizers absorbed in passivation films (Ref 18 and 10). Therefore, diffusion of any water vapor which gains entry can be expected to reach the valve sealing surfaces and hydrolyze the absorbed oxidizer to aqueous HF (hydrofluoric acid). This acid is very corrosive, much more so than fluorine or CPF. It is also relatively non-volatile and will remain on surfaces, causing appreciable corrosion. The hydrated "passive" films which result are much weaker than anhydrous films and can be easily broken by mechanical action such as closing of the valve.

This mechanism is supported by the test data in Figures VII-4 through -7 in Ref 1. When new valve parts were tested, there was no increase in leak rate during the first 5 or so cycles (the passivation period). Only Berylon nickel 440 and one set with Kennametal K-601 (K602, sic, in Ref 1 text) showed leak rate increases during passivation. The temporary stability might occur because the initial leak rate (1 cycle) was measured before exposure to fluorine. Therefore, an absorbed fluorinating agent was not present and the water vapor from the 1-cycle leak test could not form HF. The leak test after 6 cycles in F_2 caused HF formation from diffused moisture. Subsequently, corrosion occurred during the next set of actuation cycles, and leakage was detected in the third leak check.

In an attempt to enhance the stability of the fluoride film, the fabricator passivated all valves in GF_2 before exposure to CPF (Ref 1). It has been demonstrated at MDAC that F_2 -formed films are less subject to corrosion when exposed to moisture than those from halogen fluorides (Ref 10). Again, this property could explain the flat initial portion of the corrosion versus operating cycle curves in Ref 1, but the film forms on a metal by conversion of only the upper part of the normal oxide layer on the metal surface, leaving the bulk of the oxide still present (Ref 10). This lower layer could possibly react with a halogen fluoride to form the moisture-sensitive component. No data are available about the effects on the passive film caused by sequential exposure to fluorine and then to halogen fluorides.

Most metals form tenacious metal-oxide films about 100\AA thick. When these metals are placed in a CPF environment, the more active fluorine and chlorine atoms tend to replace the oxygen and form metal-fluorides and metal-chlorides. The metal-fluorides are probably concentrated closer to the outer surface of the film than are the metal-chlorides, because fluorine is more active than chlorine and so reacts before the chlorine can. For most surfaces, the metal-fluorides and chlorides are limited to the upper 10 to 20\AA , and the rest of the film remains as metal-oxides. The thickness of these films, relative to the surface roughness is illustrated in Figure 3-12. Oxygen displacement becomes more complete only if the surface is exposed to CPF at an elevated temperature for an extended time.

The demonstrated presence of chloride in the films (Ref 5 and 10) suggests that the initial metal fluoride might fracture because of subsurface mechanical expansion when metal chlorides form with their much larger chlorine atoms.

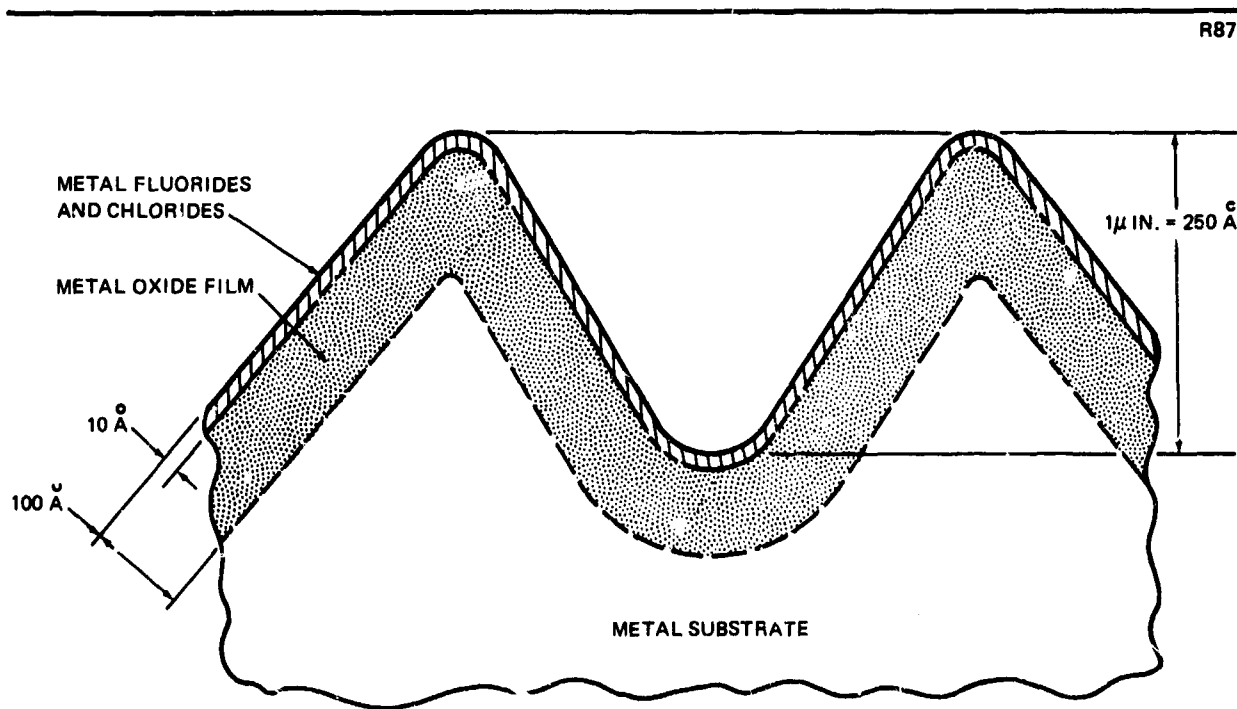


Figure 3-12. Surface Film Configuration

Also, it is known that very few metal chloride-fluorides are stable in the form of free compounds; most tend to disproportionate or break up into separate molecules of metal chlorides and metal fluorides. A similar reaction in the film would lead to segregated areas of metal fluorides and chlorides, with the latter not stabilized against attack by fluorinating agents.

The fracture of these composite surface films may occur in a complex manner. In order to establish a realistic model of film fracture, the physical characteristics of the fluoride, chloride, and oxide films of candidate materials must be known.

There are no mechanical property data available on the properties of the fluoride-chloride films. It is desirable to obtain property information on metal fluoride-chlorides including film thickness and leakage (transverse permeability) of the passivation film as functions of temperature, pressure, time of exposure, and moisture content in the CPF. Other important parameters that should be determined include surface energy and film hardness. The actual performance of such measurements is beyond the scope of the current program.

The valve contractor suggested (Ref 1) that the failure is due to mechanical destruction of the passive film followed by repassivation. This would gradually eat into the substrate and cause roughening. The suggestion is supported by (1) the observation that the film on the roughened surface is a mixed chloride-fluoride and (2) a normal passive film is about 10 \AA thick ($40 \times 10^{-9} \text{ in.}$) (Ref 18). Figure VII-10 in Ref 1 indicates that the Beryleo nickel 440 sealing surface has a roughness profile equivalent to $25 \times 10^{-6} \text{ in.}$ after 1,000 cycles in CPF, which is a change of about $20 \times 10^{-9} \text{ in. / cycle}$. At the test frequency of 22 cycles/sec (15 ms closed, 30 ms open), it would be unlikely that a full passivation film could be built up during each open cycle. Hence the agreement between normal passivation film thickness and change of surface per cycle is excellent. However, this agreement is probably only coincidental, because the roughness profile measurements indicate that the roughness is due to a buildup on the surface, with resultant increase in thickness. The passivation etching would erode the surface away, resulting in a depression, unless the fractured passive film does not break

off completely. If it remains while new film is formed underneath, then a buildup can be expected. However, if the surface is then cleaned by dissolving the film away, the profile should show a depressed area, corresponding to the metal removed. Such a test has not been reported.

A further argument against simple brittle failure of the passivation film followed by repassivation is that tests demonstrate that fluoride films are not easily broken and detached by abrasion (Ref 19) or flexure (Ref 20), if the substrate is in its elastic deformation region. When a load is great enough to cause film fracture, the substrate is scored by the hard fluoride particles that are released (Ref 19). The only score lines visible in Figure 3-2 are those from the polishing operation. On the other hand, films established by exposure to hydrofluoric acid and those converted by hydrolysis of ordinary passive films are quite weak and poorly adherent. They are frequently green and often fluffy or flaky. Such films are readily fractured by abrasion, exposing bare metal.

3.4.4 Film Fracture Corrosion

In the ACS valve operating in CPF, there are two separate reaction paths defined for the interaction of the CPF and the closure materials.

The first reaction path (discussed above) is the formation of the passive film on the surface of the metals. The exact chemical mechanisms of this reaction have not been studied sufficiently to give a detailed predictive description, but the following points have been established. First, the reaction usually does not involve the metal alloy, but instead it occurs between the CPF or other fluorinating agent and the normal hydrated oxide film found on structural metals. The activation energy required is very low because the reaction occurs even at -320°F with F_2 . However the reaction is not very rapid; and at room temperature, although only about 10 to 15 percent of the oxide film is converted to fluoride or chloride fluoride and the product film is only 10 to 20\AA thick, it requires about 15 minutes for the reaction to be completed.

Figure 3-13 summarizes experimental data for film thickness in F_2 , CTF, and CPF. The data are for a number of exposure durations and conditions.

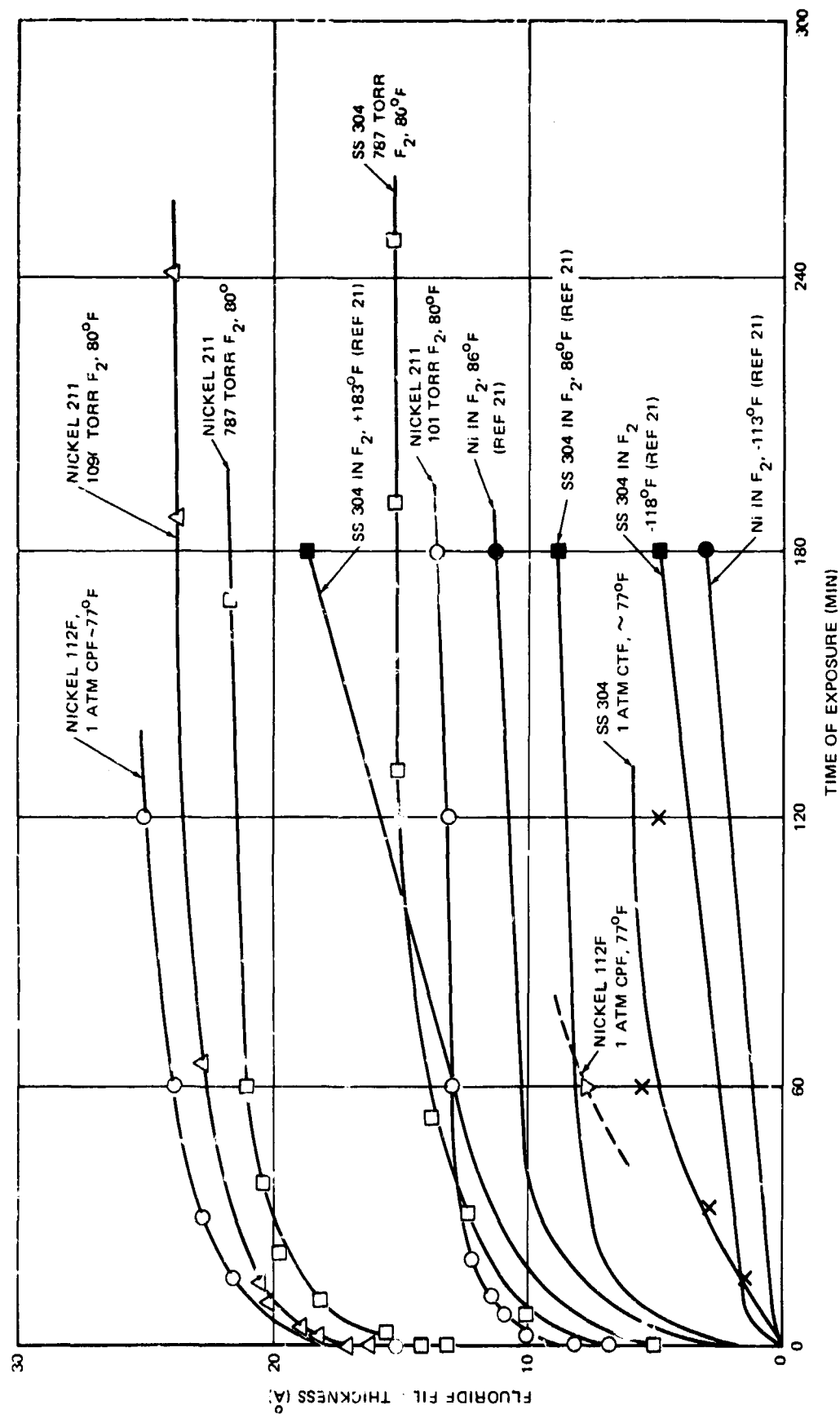


Figure 3-13. Reaction Film Thickness Versus Exposure Time in F₂, CTF, and CPF (Ref 18 except where noted)

A rate equation for film formation by elemental F_2 can be obtained by combining the unnumbered equations on pages 40 and 42 of Ref 18. The combined equation is

$$\dot{M} = P^{0.33k} \log(j\tau + \tau^0) \quad (22)$$

where

\dot{M} = rate of mass increase

k = constant specific for the substrate

j = term which can be called a pseudo concentration

τ = time after start of reaction

τ^0 = initial time.

Although no comparable equation was presented, it was concluded in Ref 18 that film formation by CTF and CPF appeared to occur by similar processes, but with greater ranges of rates for different substrates.

At higher temperatures, $\approx 350^\circ F$, complete conversion of the oxide film takes about one hour in GF_2 , but there are insufficient data to establish rate as a function of temperature. Because heat is released due to impact when the valve closes, there will be further conversion of the oxides to fluorides during service in CPF. However, the extent cannot be calculated because the basic chemical data are not available. The reaction rate is proportional to the one-third power of the concentration (pressure) of the fluorinating agent. The product film from CPF contains chlorine, fluorine, and oxygen atoms (Ref 18). The metal ions found in the films correspond to all those in the substrate alloy, except that metals which form volatile fluorides are absent.

The behavior of bare metals without oxide films when exposed to fluorinating agents has not been studied quantitatively. It has been noted that they appear to form a fluoride film with little tendency for the reaction to go over into a propagating combustion mode in tests which consist of fracture of the metal while it is immersed in liquid fluorine. The passivation of bare metal corresponds to the process after valve closure impact breaks off the original film, but there is insufficient information to develop equations relating the process to conditions in the valve.

The initial passivation by oxide film conversion is probably not of great significance during ACS valve operation. Since the passive films are about 10 to 20 Å thick (2.5 to 5×10^{-5} μ in.), and since the time to form a complete film is much longer than the 30 msec that the valve is open on each stroke, it is unlikely that successive mechanical removal and chemical reformation at each stroke would have an appreciable effect on the surface finish. Assuming that all traces of CPF are absent from the interface during the period that the valve is closed, if the valve were run to 1×10^5 cycles in one operation, the wear due to simple passivation should be no greater than 20 Å. Of course, if the valve were to operate in periodic cycles, with appreciable durations while it is open and not functioning, thus allowing complete film formation, the effect would be greater, reaching a maximum roughening of 2×10^6 Å (5 μ in.), if there were 15 minutes between each stroke. However, the evidence indicates that the valve does not fail due to successive removal of the film and repassivation.

3.4.5 MDAC Corrosion Tests in HF

The access of water into the CPF system will result in the formation of hydrofluoric acid. The relatively nonvolatile liquid droplets observed on closures after some tests (Ref 1) are probably this acid. HF is a very corrosive fluid—much more corrosive than CPF. However, there are few data on the corrosion rates during HF exposure of the closure materials.

A series of tests were conducted to determine the corrosion rates for several valve closure materials in contact with vapor and liquid 50 percent aqueous hydrofluoric acid (Subsection 4.5). The test results are presented in Table 4-22. The materials tested include three that have already been used in the ACS valve—Duranickel 301, Berylco nickel 440 and tungsten carbide-cobalt cermet. The respective corrosion rates were 3.0, 3.4 and 29 mils per year. This variance is certainly greater than the difference in failure rates of the valve closures, and since the material most sensitive to HF, the carbide cermet, shows the lowest rate of leak development, the results are interpreted to mean that corrosion by hydrofluoric acid is not a significant factor in the development of leakage in the ACS valves.

3.4.6 Conclusions

It is concluded that neither simple corrosion nor corrosive wear mechanisms could account for the development of leakage in the ACS valve.

3.5 CHEMOMECHANICAL REACTION INITIATION

In this subsection, the possibility of ignition of local hot-spot CPF-metal combustion nuclei on the closure surfaces by heating due to impact forces is investigated. Equations to define the temperature rise are presented. It is shown that this process alone cannot account for the observed closure surface roughening if the system is free of contaminants*. Insufficient data prevent mathematical analysis of the effect of contaminants, but observations indicate a significant reduction of the minimum energy to initiate reactions.

3.5.1 Observations

Key observations of the behavior of the ACS valve are:

- A. Unacceptable leakage develops only in CPF, and then only when the presence of contaminants is suspected.
- B. In the presence of CPF and contaminants, the leak increases only if the valve is actuated.
- C. When the valve is actuated, leakage increases linearly as a function of the number of cycles; other factors tested such as material composition or rate of closure have only a second-order effects.
- D. Changes in appearance of the metal surfaces are observed only on the sealing (contacting) areas of the poppet and seat.

These observations suggest that leak development is due to a chemical interaction involving contaminants, CPF, and the structural alloys and is initiated by the kinetic energy released when the poppet impacts the seat.

This chemomechanical interaction is an instance of dynamic corrosion originating from the repeated application of high loads to a metal-metal interface in the presence of CPF. It can result in local hot-spot nonpropagating ignition of metal due to plastic deformation.

3.5.2 Impact Initiation

Previous studies at MDAC have shown that under conditions of metal-metal impact or friction in CPF, localized reaction initiation occurs when there is plastic flow or galling (Ref 9). In tests documented in Ref 9 the reaction did not propagate; instead it was confined to microscopic locations in which

*In this report, Contaminant means a material whose presence is undesired, and which is either not carried by flowing propellant, or if it is moved by the propellant, it moves much more slowly than the propellant. Alloy inclusions, free metal particles, and solid HF frozen on a surface are classed as contaminants. Materials which move at the same velocity as the propellant are called Impurities; examples are dissolved CF_4 and free-floating Teflon shreds.

small, rough craters formed. When local areas of the metal undergo plastic deformation, the heating of the metal releases sufficient energy in hot spots to activate the CPF, which in turn reacts with the metal. However, these hot spots are not frequent enough to cause a generally propagating reaction. The result of these localized reactions is a roughening of the metal surface. Impact-initiated nonpropagating reactions of tungsten carbide in LF_2 were observed at MDAC during materials evaluation for the LF_2 shutoff valve (Ref. 22).

For the reactions of structural metal alloys with fluorinating agents, most recorded ignition temperatures are considerably above 200°C , at which formation of active fluorine atoms takes place. For a number of metals ignition occurs at the melting temperature of the metal. The presence of localized combustion sites (hot spots) and local melting would indicate release of sufficient heat energy to start a reaction with the metal.

One factor that decreases the initiation energy for the reaction is the presence of reactive contaminants. Local concentrations of substances that react more readily than the structural materials can start to react at lower applied energies. These reactions may then release enough energy to kindle the main material. These impurities may be included in the structural material, they may be brought in by the fluid, or they may enter the system due to improper handling.

Some unpublished results obtained by Aerojet General Corporation and made available by W. Britsch, NASA-LeRC (Ref 23) are of interest. AGC has been testing ball bearings operating at high speed in liquid fluorine. In the first tests, using Berylco nickel 440, they found that considerable surface roughening occurring, which was traced to formation of tiny burn craters in the nickel. These seem to be similar to the burn pits formed upon impact or friction in F_2 and CPF (Ref 9). Substituting high purity vacuum cast 440 did away with the problem; the purer alloy is less prone to react under the test conditions. The explanation currently offered is that minute carbon inclusions were the actual initiation sites, and that brief local hot-spot combustion of the nickel followed. Removal of the easily initiated sites stabilized the system.

If contaminants are deposited between the closures, the impact from closing will initiate them as local hot spots, while similar deposits elsewhere in the system may not react at all, or only slowly. The heat of reaction from the fluorination may be sufficient to cause local initiation of the substrate, forming small craters, even if the metal cannot sustain the reaction.

This appears to be the explanation for the pits observed in Berylco nickel 440 bearings in fluorine (Ref 23).

Because the occurrence of contamination is random or uncontrolled, prediction of its effects as a specific occurrence for the ACS valve is not feasible. For most ordinary contaminants, the energy yield from fluorination is 3 to 6 Kcal/g or 0.7 to 1.4×10^{-3} Btu/grain. (Note that there are 440 grains in an ounce. Grains are often used in measurement of impurity concentration. *) This is several orders of magnitude greater than the total heat released by the impact process in the ABMA tester ($\tau \cdot dU/d\tau \approx 10^{-8}$ Btu) and results in temperatures high enough to initiate local burning of any metal in CPF. This inevitable initiation is the reason that scrupulous cleanliness is necessary in CPF and similar propellant systems.

These observations reinforce the suggestion that the valve process is an impact initiated chemical reaction and that the activated chemical species is not derived from the metal. The reaction of this active species then heats the structural alloy in a local, nonpropagating reaction. The location of the attack is limited to the contacting metal surfaces, ruling out a general initiation mechanism, which is not specific to the closing process. Also, the local reaction does not release sufficient energy to become self-sustaining.

The access of water can supply a lower energy initiation path for hot-spot reaction. If the water reacts with film-absorbed CPF to form aqueous hydrofluoric acid, then when the valve is actuated to close, the known impact sensitivity of water in fluorinating agents could cause local explosions, triggering local CPF-metal reactions. This mechanism can account for the fact that the corrosion rate is relatively insensitive to the composition of the substrate metal and also for the fact that even when moisture invades the valve, the serious corrosion is confined to the sealing surfaces. The tendency of fluorinating agents to react only partially with water, even in excess fluorinating agent, has been established at MDAC for both fluorine and oxygen

*The solid (at -320°F) impurities in MIL-P-27405 liquid fluorine are equivalent to 7 grains/ft³. A gas with a dew point of -92°F has 1×10^{-3} grains H₂O/ft³.

difluoride (Ref 19 and 24). The impact sensitivity of water in fluorinating agents at low energy levels is well known (Ref 19).

In order to properly evaluate this impact-triggered reaction, it is necessary to determine the amount of energy deposited at the closure interface. Then a comparison can be made between the requirements for initiation of the closure material in clean and in contaminated systems.

3.5.3 Localized Impact Heating

In previous work at MDAC (Ref 9), it was shown that impact energy available for reaction initiation appears as a friction at the metal-metal interface due to radial expansion of the vertically compressed parts. Only a small portion of the impact energy is actually available for reaction initiation at the material-propellant interface. It was estimated that only the energy released in the top 0.002 in. of the surfaces was effective, and it was shown that the maximum release took place at the exterior edge of the member with the smaller radius. The tests discussed later in this report show that less than 1/10 of 1 percent of the impact energy input is released at the interface in a form suitable for reaction initiation. The maximum rate of energy release can be calculated by Equation (23), which was derived for the contact of two flat components of different radii (specifically for the striker pin-specimen interface in an ABMA impact tester).

$$\frac{dU(\tau)}{d\tau} = \frac{\mu_{sp} r_p P(\tau)}{12} \cdot \frac{dP(\tau)}{d\tau} \cdot \left[\frac{\Lambda_p}{E_p} - \frac{\Lambda_s}{E_s} \cdot \left(1 - \frac{1 - \Lambda_s}{2} \right) \cdot \left(\frac{r_s^2 - r_p^2}{r_s^2} \right) \right], \text{ (ft-lb/sec-in.}^2\text{)}$$

(23)

where

$dU(\tau)/d\tau$ rate of energy release at edge of smaller radius component at time τ after impact.

μ coefficient of friction or rigidity between surfaces of materials

$P(\tau)$ pressure at time, τ , due to compression

Λ Poisson's ratio

E = bulk modulus

r = component radius

and subscripts

s = specimen

p = striker pin

with the provision that $r_s > r_p$.

To apply Equation (23), the appropriate values must be substituted for the various terms. The values of r_p and r_s are defined by the configuration of the apparatus; μ , Λ_s , Λ_p , E_s , and E_p , are material properties; however, $P(\tau)$ and $dP(\tau)/d\tau$ must be calculated from the functional characteristics of the operating parts. Both $P(\tau)$ and $dP(\tau)/d\tau$ vary with time, and values for the same instant must be used in the solution of Equation (23).

The same calculation with appropriate parameters for the ACS valve with a single material for both seat and poppet can be made by means of

$$\frac{dU(\tau)}{d\tau} = 4.17 * 10^{-2} \frac{\Lambda \mu F_I D_o}{AE} \left(\frac{1 - \Lambda}{2} \right) \left(\frac{r_p^2 - (D_o/2)^2}{r_p^2} \right) \frac{dF_I(\tau)}{d\tau}, (\text{ft-lb/sec}) \quad (24)$$

Of greater interest for evaluating the initiation of interface reactions is the energy release rate averaged over the time period in which closure is occurring. The symbol $dU/d\tau$ is used for this value.

The energy flux can be used to calculate the temperature change at the interface by using Equation (25).

$$\Delta T = \frac{1.288 * 10^{-3} \frac{dU}{d\tau} r_c - (2\pi K_f \rho_f r \exp^{r_H d_{\min}}) (L_v - (T_B - T)(\Gamma_f - \Gamma_p))}{2\pi r \exp^{r_H d_{\min}} (K_{up} \rho_{up} \Gamma_{up} + K_{lo} \rho_{lo} \Gamma_{lo} + K_f \rho_f \Gamma_p)}, (^\circ F) \quad (25)$$

where

- τ_c = duration of impact, sec = 1×10^{-4} sec for valve closures.
- K = arbitrary constant
- ρ = density, lb/in.³
- r_{exp} = expansion radius difference, in.
- r_H = heated zone radius, in. = 0.002 in.
- d_{min} = diameter of smaller member of closure, in.
- L_v = latent heat of evaporation, Btu/lb
- T_B = boiling point at 450 psi
- T_{INIT} = initial temperature
- Γ = heat capacity

and subscripts

- f = fluid
- P (on gamma) = constant pressure
- up = upper member
- lo = lower member

The method of solution used for these equations is described later in this report, when the test data are discussed. However, it is of interest at this point to mention typical values obtained from use of the equations. As an example, theoretical solutions of the equations applied to the ACS valve gave temperature increases at the closure of 22°F for Durnickel 301 and 23°F for tungsten carbide-cobalt cermet. These temperatures indicate that there is no chance for local ignition of the metal closures in CPF if contaminants are not present. Note added in proof: In a personal communication (July 15, 1971), H. Wichmann stated that even after rigorous cleaning and baking, closures made from Durnickel 301 still developed unacceptable leakage in CPF. He attributed the failures to buildup of excessively thick fluoride films because of heating from the poppet impact. The thick films were observed on the failed closures.

3.5.4 Conclusions

This portion of the analysis demonstrates that the valve design is adequate for the design operating conditions, and that the failures were due to some uncontrolled factor, such as contamination. Unfortunately, there are insufficient data available for calculating the likelihood of ignition of contaminants. Test results indicate that contaminants significantly lower the minimum energy required for initiation of hot spot reactions (See Subsections 5.1.3.2, 5.1.4, and 5.2)

3.6 OTHER WEAR PROCESSES

3.6.1 Abrasive Wear

The effect of abrasive wear conditions are analyzed in this subsection, and it is concluded that the ACS valve did not undergo such a process.

There are two types of abrasive wear, two-body and three-body. Two-body wear occurs when a harder rough surface slides against a softer surface, digs into it, and removes material from it, usually in the form of loose fragments, having ploughed grooves. Three-body wear involves the presence of loose grains between the two surfaces. Three-body abrasive wear is usually considered to occur only if the particles are harder than surfaces they contact. Table 3-6 presents hardness values of many materials of interest.

For a model surface with conical asperities, the volume of material removed by abrasive wear can be estimated from

$$V_{ab} = k_{ab} \frac{F I^s}{p}, (\text{in.}^3) \quad (26)$$

Equation (26) has the same form as Equation (17) for adhesive wear, with k_{ab} , the abrasive wear coefficient, replacing k_{ad} . Typical experimental values of k_{ab} are 0.150 for two-body wear, and 0.080 for three-body wear.

Three-body wear has a smaller k_{ab} than does two-body, because, in the former case, the free bodies tend to roll over the surface most of the time.

Some observations which indicate that Equation (26) does not include all of the significant factors are worthy of consideration for future analysis. The

Table 3-6 (Page 1 of 2)

HARDNESS DATA

Material	Composition	Hardness - Kg/mm ² p
Diamond	C	8,000
Titanium boride	TiB ₂	3,000
Boron carbide	B ₄	2,750
Ditungsten carbide	W ₂ C	2,600
Silicon carbide	SiC	2,500
Titanium carbide	TiC	2,400
Alumina	Al ₂ O ₃	2,100
Zirconium carbide	ZrC	2,100
Tungsten carbide	WC	1,900
Tungsten silicide	WSi ₂	1,300
Zirconia	ZrC ₂	1,150
Silica, sand	SiO ₂	800
Bearing steel	-	700 to 900
Steel 440C	-	735
Tool steel	-	700 to 1,000
Chromium electroplated	-	900
Carburized steel	-	900
Nitrided steel	-	900 to 1,250
Tungsten carbide (cobalt binder)	-	1,400 to 1,800
Stellite	-	700
Ferritic CRES	-	250
Beryllium Copper	-	210
347 CRES	-	164
Aluminum 7079-T6	-	184
Aluminum 5083-H32	-	92
Copper 102	-	76
Tin bronze	-	60 to 80
Aluminum alloy	-	45 to 50
Cadmium base	-	20 to 40

Table 3-6 (Page 2 of 2)
HARDNESS DATA

Material	Composition	Hardness - Kg/mm ² P
Silver (overplated)	-	25 to 50
Tin-base babbitt	-	20 to 30
Lead	Pb	9
Teflon	(C ₂ F ₄) _n	5
Polyethylene	(C ₂ H ₄) _n	2

resistance to abrasive wear increases as material hardness increases. For example, the wear resistance of steel varies approximately as the 1/3 power of the hardness. The rate of abrasive wear decreases as the size of the particles decrease as shown in Figure 3-14.

Experience has shown that if the loose particle size is less than 5 μ (200 μ in.) the surfaces will be polished rather than roughened.

Figure 3-11 indicates that the ratio G/p must be less than 1Å if the particle size is to be less than 5 microns. Referring to Table 3-2 it is apparent that all metals rubbing against themselves in a nonlubricated environment will produce loose particles large enough to cause abrasive wear and surface roughening. Only a few ceramics will be polished by their own particles in a dry environment.

An abrasion resistance factor has been used by Kennametal Inc., (Ref 25) for rating of alloys. It is "the reciprocal of the volume lost in a 30-minute period in which a flow of silica sand is rubbed against the specimen by a rubber wheel." Data obtained by this test method are given in Table 3-7. These data clearly indicate that abrasion occurs even when the wearing surface is harder than the particles, and that the wear rate is somewhat proportional to the hardness difference or ratio.

Experience with roller bearings indicates that a small difference in hardness between two bearing surfaces can have dramatic effects on the wear life of the system. Figure 3-15 copied in modified form from Ref 26, shows the

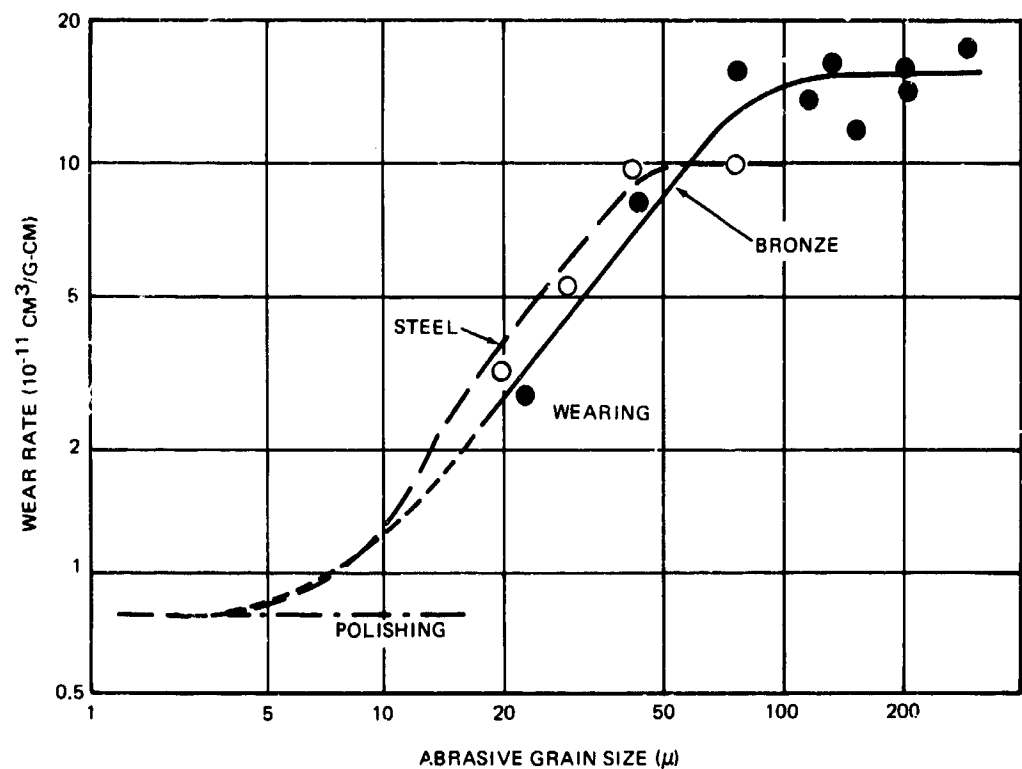


Figure 3-14. Wear Rate Versus Abrasive Grain Size (Ref 13)

effect on life span caused by a hardness difference for SAE 52100 steel balls and races. The life span peaks at a ΔR_c of 1.5 units, where the increase in life span achieved is greater than eight fold compared with the condition where both parts are of the same hardness.

Equation (26) is thus not a complete representation of actual abrasion.

There are two processes that occur during abrasion. First, the wearing agent (particle or asperity) must penetrate the surface which is going to be abraded or lock in an existing asperity. Then the agent moves relative to the surface, causing the removal of material in a gouge.

The formation of grooves and scratches which lie parallel on the two sealing surfaces has the effect of changing the equation applicable to the leak rate estimation. Equation (1) applies to a multidirectional lay of the surface, and the rate for parallel radial lay is a priori appreciably higher. No equation is available for the condition of radial lay on both closure surfaces.

Table 3-7
ABRASION RESISTANCE OF ALLOYS

Material	Hardness		Kennametal Abrasion Resistance	Wear Factor (10 ³ /KAR)
	Rockwell	Vickers		
400 stainless steel	C40	392	13	77
Carbon steel 1095	C50	510	9	111
Low alloy steel 4140	C50 (A76)	510	14	71
Tool steel AISI D7	C64	800	17	59
Tool steel AISI T1	C65	830	14	71
Cast alloy (Co, Cr, Ni, W)	N. R.	N. R.	32 to 36	30
K-801	A 89.5	>1,100	110	9
K-96	A 92.0	>1,100	165	6
K-701	A 92.0	>1,100	825	1.2
K-602	A 94.3	>1,100	470	2
(Silica sand abrasive	N. R.	800	N. A.	N. A.)
N. R. = Not Reported				
N. A. = Not Applicable				

Abrasive wear is not particularly important for the ACS valve because the propellant is filtered as it enters the valve. If the filter pore size were decreased to 5 μ , the possibility for abrasive wear would be further reduced. Formation of hard metal fluoride particles inside the valve itself is possible. Nominally the passive film thickness is about 10 \AA (0.001 μ): and although the possibility of growth to 0.1 μ cannot be excluded, further thickening is very unlikely. Thus most particles generated would be below the 5 μ limit, and hence would not cause abrasion.

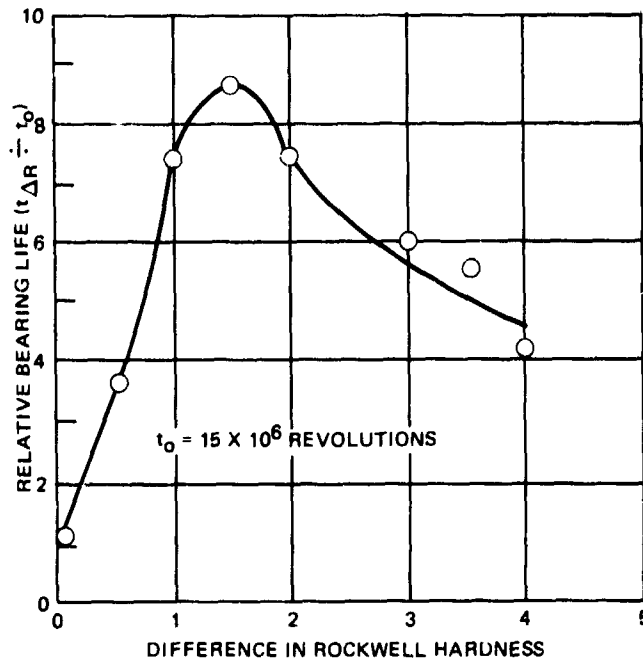


Figure 3-15. Bearing Life as a Function of Hardness Difference

3. 6. 2 Surface Fatigue Wear

Surface fatigue occurs when the magnitude of the applied loads varies cyclically. The most common example of surface fatigue occurs in rolling applications such as gears and rolling contact bearings. Surface fatigue can also occur under repeated impact and sliding loads such as those observed in the ACS valve closing motion. The applied loads produce stresses on the surface and in the material below the surface. Repeated application of these stresses can cause progressive increase in size of initially microscopic cracks or flaws in the material, until failure occurs.

For any given set of operating conditions, the service life decreases with increase of applied load, generally in accordance with the relationship

$$n = \frac{\text{constant}}{l^3} \quad (27)$$

The particles removed in surface fatigue wear tend to be as large as the area of contact under stress (approximately $1,000\mu$), rather than the characteristic adhesive wear particle size (approximately 30μ).

Surface active lubricants generally lower the fatigue life, whereas under adhesive wear conditions these lubricants may tend to raise the useful life.

Propellant CPF may be considered to be a very reactive, average quality lubricant. As such, the physical characteristics of the films produced on candidate materials will have a significant effect on fatigue and adhesive wear, hence on service life.

No data for fatigue life in CPF have been reported. Some tests which were conducted in elemental fluorine (Ref 27) may be of interest: aluminum, stainless steel, and Inconel each show reduced service life in fluorine as compared with air, oxygen, or nitrogen. The reduction was one-third (i. e. , the fatigue cycle was 67 percent that of the controls) for all three metals run at -320°F or room temperature (controls at same temperature as F_2 test).

Experimental data on surface fatigue life-versus-load is subject to wide scatter, making it difficult to predict fatigue life accurately. However, if surface fatigue wear becomes a problem, a small decrease in applied loads will produce a large increase in cycle life.

3.6.3 Other Factors

Similarly, because of the low number of cycles to failure, erosion and cavitation probably are not significant causes of wear. Erosive wear occurs when sharp particles in the flowing fluid impinge on, and remove material from the wearing surfaces. Erosive wear is similar to abrasive wear, but it can produce greater surface roughness, because an impinging particle can remove material from a low point on the surface. Hard surfaces resist erosion.

When the poppet closes on the seat, some of the flowing liquid is held in the interface by surface tension. During subsequent separation of the interface, the liquid is placed in tension and boils, producing vapor bubbles. Later, abrupt collapse of the bubble produces a mechanical shock that may damage the interface surfaces. This process, known as cavitation, produces wear

which is similar to the wear that is produced by surface fatigue. Materials which are hard, but not brittle, are resistant to both cavitation and surface fatigue wear.

3.7 ANALYSIS CONCLUSIONS

Analysis of the ACS valve and its operation in CPF in terms of possible reasons for reported failures by development of excessive leaks while functioning under what were supposed to be design operating limits indicates that the valve is not subject to such failures.

The causes of failure must be sought elsewhere.

Information released by AFRPL during the course of the MDAC program supports this conclusion. The failures of tungsten carbide-cobalt cermet closures were overcome by more thorough cleaning of the valves before exposure to CPF. This extra cleaning consists of a careful vacuum bake-out. Thus it can be concluded that contamination by absorbed water was the proximate cause of failure. The presence of water in fluorine oxidizer systems is unacceptable for normal operating designs or procedures.

The mechanism of failure appears to be an impact-initiated reaction of the contaminant water or a reactive intermediate from water on the closure surfaces. Evidence for this mechanism will be found in the next section.

Section 4

TEST PROGRAM

4.1 OBJECTIVES AND APPROACH

In addition to investigating the failure mechanism of a specific ACS value in CPF service, major objectives of this program have been to develop analytical methods for predicting wear and chemodynamics characteristics for designing values for high energy storable liquid propellants, and determining the utility and compatibility of specific closure materials in environments related to the service in the ACS valve, by means of static corrosion and static dynamic and initiation tests.

The test program was conducted in three parts. The first was tests conducted during Phase I, Part 2 with the objective of supplying data needed to support the Phase I analysis of the valve failure mechanism. The second series of tests were conducted during Phase II, Part 1 with the objective of verifying the conclusions from the Phase I analysis. The Phase II, Part 2 tests had the objective of determining the suitability of several candidate closure materials.

There were three types of tests conducted:

- A. Static corrosion in 50-percent aqueous hydrofluoric acid.
- B. Drop-weight impact initiation, using the MDAC modified ABMA impact tester.
- C. Friction initiation, using the rotary friction tester.

All three types were used in all parts of the test program.

Details of the tests, including materials, apparatus, and procedures can be found in Appendix I.

4.2 TEST RESULTS

4.2.1 Corrosion Tests

The test conditions listed in Table 4-1 were followed. Test data are recorded in Table 4-2.

Table 4-1
AQUEOUS HF CORROSION TEST CONDITIONS

Material	Duration (hr)	Temperature (°F)
Duranickel 301	90	32 ± 3
Alumina	115	70 ± 5
Berylco nickel 440	24	70 ± 5
Silver plated Duranickel 301	71 1/4	70 ± 5
Tungsten Carbide in Cobalt Matrix	24	70 ± 5

4.2.2 Interpretation

In all cases, the corrosion appears to be of the film type. No evidence of pitting was noted. The Berylco nickel had the appearance of a galvanic effect. Hard white crystals, insoluble in water, formed where the two nickel specimens were in contact. The impurities in silver plate on DN-301 did not appear to affect its corrosion. The minor change in surface finish of the tungsten carbide contrasted with the relatively high corrosion rate is not easily explained. Perhaps the attack was concentrated on the cobalt matrix (CoF_2 is pink), but did not proceed far enough in the short duration test to free an appreciable number of WC grains. This mode of attack in a purely mechanical wear environment has been reported (Ref 40).

From the data on corrosion rates and surface finish presented in Table 4-2, the materials tested are ranked in the order shown in Table 4-3 for consideration as valve closure materials where the possibility of exposure to liquid HF exists.

Table 4-2
CORROSION IN HYDROFLUORIC ACID-TEST DATA

Pretest					Posttest					
Material	Dimensions (in.)	Weight (g)	Appearance	Average Surface Finish (μ in.)	Weight (g)	Appearance	Surface Finish (μ in.)	Weight Change (mg)	Corrosion Rate	
									(mg/sq in. -day)	Mean (mils/year)
Duranickel 301- Wff	2-15/16 by 3/4 by 1/16	A: 17.3616	Shiny metallic	5	17.3415	Unchanged	7	20.1	1.22	3.0
		B: 27.2302	Shiny metallic	-	17.2132	Unchanged	9	17.0	1.03	
Alumina	1 by 1 by 1/16	3.9537	Shiny grey	8	3.9524	Somewhat dulled, darker grey	8	1.3	0.12	0.6
Berylco Nickel 440	2-3/4 by 3/4 by 1/16 with single 1/4 dia hole	A: 16.7402	Metallic	2	16.7217	Dulled, dark areas, crystals	3-20	18.5	4.01	3.4
		B: 17.3253	Metallic	-	17.2791	Same	5-100	46.2	10.0	
Silver Plated Duranickel 301	2-15/16 by 3/4 by 1/16	C: 17.0091 (vapor only)	Metallic	-	17.0024	Dulled	5	6.7	1.45	0.7
		A: 18.2030	Silvery	2	18.2012	Tarnished	3-30	1.8	0.122	
Tungsten Carbide in Cobalt Matrix	1-3/4 by 3/4 by 1/16	B: 18.2683	Silvery		16.2873	Tarnished	3-10	0.5	0.034	29.
		A: 22.9389	Mirror finish	1.5	22.8828	Dark patches	1-3	56.1	19.1	
		B: 22.8450	Mirror finish	-	22.7859	Dark patches and lines. HF solution turned bright pink	2-3	59.1	20.1	

Table 4-3
HF CORROSION RESISTANCE RANKING

Rank in Test	Test 1 Corrosion Rate	Test 2 Surface Finish Changes Effects	Averaged Rating
Best	Ag Plated on DN 301	Alumina	Alumina
	Alumina	WC in Co	{ DN-301
	DN - 301	DN - 301	{ Ag Plated DN 301
	Berylco Nickel 440	Ag Plated on DN-301	{ WC in Co
Worst	WC in Co	Berylco Nickel 440	Berylco Nickel 440

Note that these ratings are based on static corrosion effects in HF only, and do not include considerations of dynamic factors in CPF.

4.3 IMPACT INITIATION TESTS

4.3.1 Test Conducted

The tests conducted are summarized in Table 4-4.

Table 4-4
DROPT WEIGHT IMPACT INITIATION TEST SUMMARY
VALVE CLOSURE MATERIALS IN CPF

Material	Impact Energy Range (ft-lb)	Number of Test Drops	Program Phase
DN-301-WH	71	20	Phase I, Part 2
DN-301, Various Hardness Condition	165 to 293	67	Phase II, Part 1
Stainless Steel 304-L Air and Vacuum Cast	183 to 275	26	Phase II, Part 1
Tungsten Carbide - Cobalt Cermet	146 to 293	16	Phase II, Part 2
Silver Plated DN-301	110 to 293	16	Phase II, Part 2

The tests of DN-301-WH at 71 ft-lb were conducted to prove that this nickel alloy is stable and not sensitive to impact in CPF at energy levels that would bar it from flight service. Titanium and some aluminum alloys do react at this energy level (Ref 9).

The tests of DN-301 at higher energy levels were conducted to determine the relationship between material hardness and initiation energy for a single material composition. Those with the stainless steel 304-L were designed to study the relation between material purity and ease of initiation. The latter relationship was not found in the drop weight tests (it was shown in rotary friction tests).

The tests with tungsten carbide-cobalt cermet and silver-plated DN-301 were designed to help determine which was the most suitable material for ACS valve closure service. Included in the tungsten-carbide series were three drop tests in which the specimens were purposely allowed to become contaminated with moisture before exposure to CPF.

Alumina was not included in the drop weight impact tests because previous experience at MDAC had demonstrated that the material is pulverized even at 72 ft-lb, and reaction sites, if any, cannot be detected.

4.3.2 Observations

In all cases in which reaction spots were observed on the specimens, the impact load had been great enough to cause plastic yielding or fracture of the test discs and the reaction sites were near the outside edge of the yielded zone, which corresponds to the circumference of the striker pin. However, minor plastic deformation of the discs did not invariably result in reaction spots.

No reactions were detected on DN-301 in CPF at 71 ± 1 ft-lb input energy. Reactions were detected at the higher energy levels during Phase II tests. The reactions seldom emitted visible light, but small burn craters and melted edges were readily detected when the specimens were examined with a 20X microscope. The 304-L specimens showed the same signs.

All tungsten carbide specimens shattered during the tests, but they yielded fairly large shards. Two types of indication of reaction were detected. One was burn traces or hot spots. These were typically very shallow, hardly more than surface roughening plus discoloration when in the unbroken surface of the specimen. When they occurred along fracture edges, they were considerably deeper, perhaps 1×10^{-3} in. The other type of reaction indication depended on the occurrence of fracture. In a nonreactive case, the intersection of fracture cones gave rise to very sharp edges. If reaction had occurred, some of these intersection edges were smoothly rounded due to removal of material by chemical reaction. The two reaction indicators always accompanied each other, except for one case. The exception was the water-equilibrated specimens. With these three specimens, a considerable number of tiny reaction sites were observed through the area covered by the striker pin, instead of being concentrated at the outside edge of the pin. Surface degradation at these reaction locations was not as great as for the locations on dry specimens where the alloy itself had reacted. There were no large reaction sites from reaction of substrate, nor had any sharp edges been rounded by combustion.

On the silver plated DN-301 specimens, the reaction sites were spread out under the whole of the striker pin. In addition, silver foil was extruded from under the pin, and this foil ignited in two instances. In one of these cases, and for one other specimen, sustained combustion of the substrate DN-301 had evidently occurred. On many specimens, the DN-301-silver bond parted and/or the plating cracked.

4.3.3 Calculations

Table 4-5 is an illustration of the method of calculation of the 50-percent reaction threshold energy (E_{50}), using the data from Figure I-9. The threshold initiation energy, TIE, is greatest energy at which no reaction is observed.

Note that in the calculation of E_{50} , all tests below the TIE level are ignored.

Table 4-5
CALCULATION OF E_{50}

Energy Level (ft-lb)	Test Level No. Assigned (i)	Total Burn Crater Reactions	Total No. of Inert (N_i)	Product (iN_i)
238	0	0	10	0
256	1	4	1	1
275	2	2	1	2
293	3	3	0	0
$\Delta E = 18.3 = \text{Energy Level Difference}$			$\Sigma N_i = 12$	$\Sigma iN_i = 3$
$E_{50} = 238 + 18.3 (3/12 + 0.5)$				(38)
$= 252 \text{ ft-lb}$				
TIE = 238 ft-lb				

Data from all ABMA impact tests in CFF were treated in the same fashion to obtain E_{50} and TIE. The results of these calculations are tabulated in Table 4-6. DN 301 and SS-304L results are plotted as a function of material hardness in Figure 4-1.

Test data for silver plated DN-301 showed such a great dispersion, due to the inclusions, that calculations of E_{50} was impossible. Some specimens ignited at 110 ft-lb, others were stable at 293.

The three water-vapor equilibrated tungsten carbide-cobalt cement specimens all reacted at energies below those for the dried specimens. The energies tested were 220, 183, and 146 ft-lb, and the three specimens behaved in identical fashion.

Table 4-6
REACTION INITIATION BY ABMA IMPACT IN CPF

Test Material	Vickers Hardness (kg/mm ²)	50% Reaction Energy (E ₅₀) (ft-lb)	Threshold Initiation Energy (TIE) (ft-lb)
Stainless 304-L; Air Melt	89	241	228
Stainless 304-L; Vacuum Melt	89	239	228
Duranickel 301; Annealed	147	252	238
Duranickel 301; Work hardened	179	264	238
Duranickel 301; Thermally aged	247	286	256
Duranickel 301; 3/4-Hard	326	-	293
Carbet CA-4 (WC in Co)	1800 (Nominal)	233	220
Ag-Plated DN-301	50 (Nominal)	Not Calculated	<110

NOTES: The E₅₀ values for the two 304-L are considered to be the same.
The Vickers hardness was calculated from Rockwell hardness values.

4.3.4 Analysis and Discussion

These tests were conducted because they are considered to model certain aspects of the dynamics of the ACS valve-closing process. The test data are analyzed: (1) to compare surface damage as a function of energy input with material characteristics, and (2) to calculate the temperatures which are reached on the interfaces as a function of impact energy.

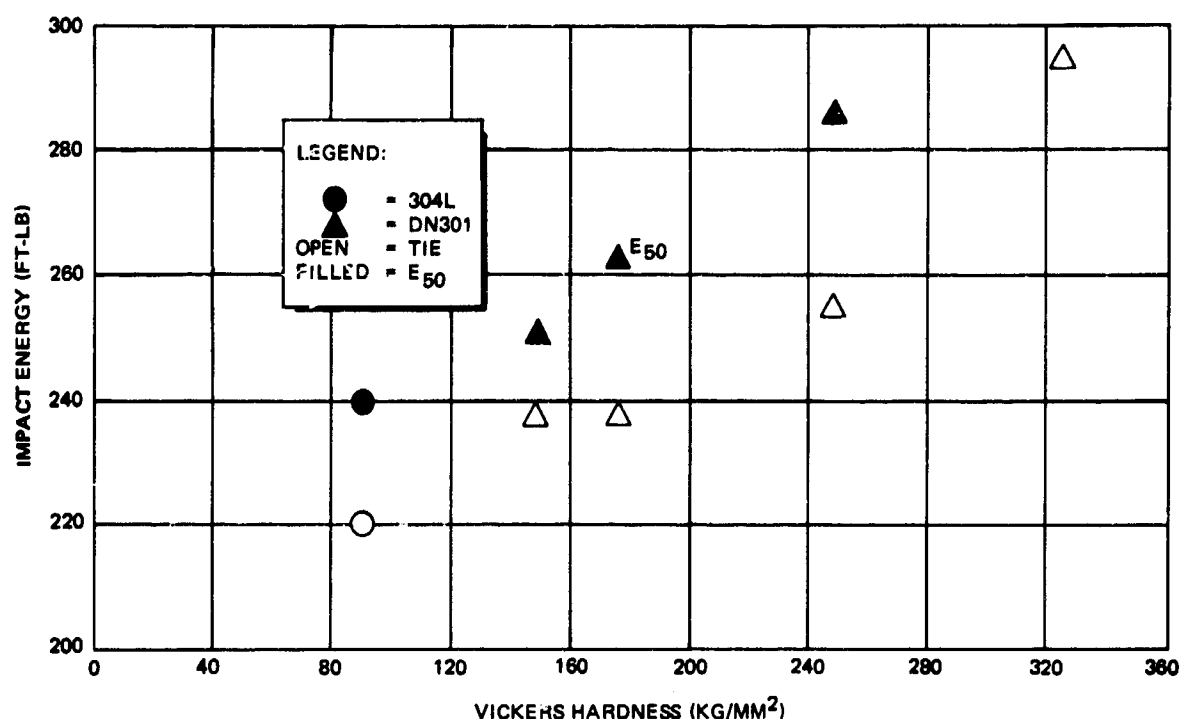


Figure 4-1. Impact Initiation Energy in CPF as a Function of Material Hardness

4.3.4.1 Duranickel 301

Several different metallurgical conditions of this alloy were tested to provide data that could be analyzed to provide correlations between behavior in the tests and the materials properties of specimens tested. In the analysis developed in Section 3 it was predicted that surface damage could be correlated with various material properties including hardness and yield strength. The relationships are discussed in this section.

The equations derived during Phase I of this study predict that the mechanical damage done by an impact F_I , of a particular energy level is inversely proportional to the hardness, p_A , of the material. Conversely, as the hardness of the material increases, greater impact energy is needed to

cause the same damage. An example is the relation for calculating the adhesive wear volume per stroke, V_w as a function of p_A , k_{ad} , F_I , and s (the sliding distance).

$$V_w = 7.04 * 10^{-4} \frac{k_{ad} F_I s}{p_A} \quad (28)$$

In addition, the basic relationship between energy of impact and valve wear includes a term for the yield stress of the closure materials. This energy-yield stress relation can be summarized as

$$F_I = f \left(\frac{1}{\sigma_y} \right) \quad (29)$$

This relationship indicates that as the yield strength of the material increases, a greater energy input is needed to cause the same amount of damage.

The numerical data to demonstrate these relationships are presented in Table 4-7.

Table 4-7
ABMA INITIATION ENERGY DATA, DURANICKEL IN CPF

Duranickel 301 Condition	Hardness, (p) (kg/mm ²)	Yield Strength (σ_y) (psi)	TIE (ft - lb)	E ₅₀ (ft - lb)	$\frac{p^2}{E_{50} \sigma_y}$, in. ⁻³
Annealed	147	30,000	238	252	$4.8 * 10^2$
Work Hardened	179	45,000	238	264	$4.6 * 10^2$
Thermally Aged	247	78,000	256	286	$4.8 * 10^2$
3/4 Hard	326	118,000	293	>293	$< 5.2 * 10^2$

Empirical manipulation of the data disclosed an interesting fact: the ratio $p^2/E_{50} \sigma_y$ is a constant. The last column in Table 4-7 is a list of the values calculated by the formula in Equation (31).

$$K = \frac{\left(1422 \frac{\text{lb/in.}^2}{\text{kg/mm}^2} * p \text{ kg/mm}^2\right)^2}{12 \text{ in./ft} * E_{50} \text{ ft lb} * \sigma_y \text{ lb/in.}^2} \quad (30)$$

$$K = 1.68 * 10^5 \frac{p^2}{E_{50} \sigma_y}, \text{ in.}^{-3} \quad (31)$$

Note that σ_y is not a linear or even regular function of p for the series of DN 301's. The data in Ref 28 show curved-line relationships between σ_y and p , and various thermal and work histories displace the curves and change their rate of curvature. In addition, note that tables for hardness scale conversion of steels usually give the equivalent tensile strength, but that similar tables for nickel alloys specifically exclude such an equivalence (Ref 36). Thus the term p^2/σ_y is not equivalent to a constant times " p ", which is the case for common steel alloys.

If the parameter $p^2/E_{50} \sigma_y$ equal to a constant could be shown to have general validity for chemomechanical reactions, it would be a very useful tool. At present, this relationship is supported by only very few data points, and such extrapolations may be premature. However, the relationship equated to $4.75 * 10^2$ was used to calculate E_{50} for the 3/4 H ($\sigma_y = 118$, $p = 326$) and FH ($\sigma_y = 135$, $p = 360$) Duranickel 301, neither of which could be determined using the ABMA impact tester. The values calculated were 318 foot-pound and 330-foot-pound, respectively.

A graph (Figure 4-2) has been plotted with the experimental and calculated values of E_{50} and the experimental values of TIE plotted against both p and σ_y .

The other materials parameters deemed of importance for controlling wear/reactivity (the bulk modulus, E , the surface energy, γ , and the adhesive-wear constant) are not subject to study by the methods and test plan used.

The interface temperatures corresponding to the E_{50} and TIE energy levels were calculated by using Equations (D-2) and (D-14) in Appendix D.

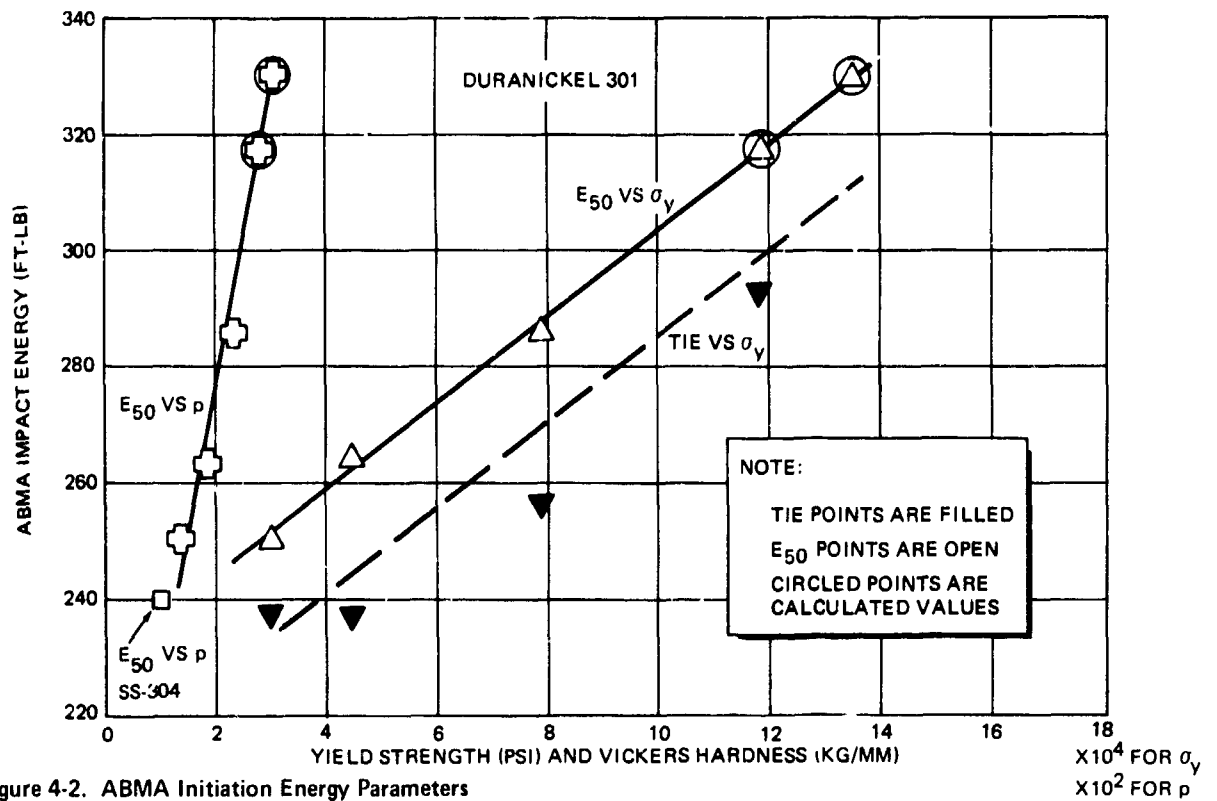


Figure 4-2. ABMA Initiation Energy Parameters

To apply Equation (D-2), the appropriate values must be substituted for the various terms. The values of r_{pn} and r_{sp} are defined by the configuration of the test apparatus; Λ_{pn} , Λ_{sp} , E_{pn} , and E_{sp} are known material properties. However, $P(\tau)$, $dP(\tau)/d\tau$ and μ must be calculated from the test data. Note that both $P(\tau)$ and $dP(\tau)/d\tau$ vary with time, and values averaged over the impact duration must be used. The method is given in Appendix D.

One other empirical term is needed to solve Equation (D-2); that term is the coefficient of friction between the striker pin and the sample disc while the interface is immersed in CPF. This datum is not available from the literature; fortunately, it can be calculated from the Rotary Friction test data. However, at this point it must be mentioned that Equation (D-2) was expressly derived for conditions in which the various parts of the system remain below their yield strengths and all

behavior is elastic. If plastic flow occurs, corrections to the equation are necessary. A complicated correction involving plastic flow and friction is given in Ref 9; it is based on a derivation of a coefficient of plastic flow resistance, K_{pl} .

$$K_{pl} = \frac{-P}{1 + 2/3 \frac{\mu R}{h}} \quad (32)$$

where h is the height of the compressed member.

An alternative procedure instead of calculating K_{pl} is to define an empirical plasticity coefficient, μ_{pl} , in place of the coefficient of friction. This coefficient is equivalent to the coefficient of friction, and determined in a like manner. This procedure has been adopted here.

In both the ABMA and rotary friction tests, it was observed that plastic deformation was necessary in order to obtain reaction initiation in CPF. This requirement has been observed by other workers in ABMA tests.

The Rotary-Friction test data given in Table 4-12 were used with Equation (33) to calculate the interaction coefficient at the interface in the rotary friction tests. Equation (33) is from Ref 9, with a factor included for the true contact area between the specimens:

$$\mu = \frac{3780 L}{\pi \alpha F R_o} \quad (33)$$

where R_o is the radius of the upper, rotating specimen, = 0.375 in. The values calculated are also given in Table 4-12. It is obvious immediately that the values for μ of Duranickel 301 fall into separate high and low groups. The high values were obtained whenever ignition occurred, and in some instances in which ignition spots were not detected. This value corresponds to the observed serious plastic deformation, and the coefficient calculated using (33) is here taken as the plasticity coefficient.

$$\text{Duranickel } \mu_{pl} = 0.61 \text{ in CPF}$$

The lower values, which occurred only if there was no detectable reaction are taken as friction coefficients of DN 301 against DN 301.

$$\text{Duranickel } \mu_{ii} = 0.33 \text{ in CPF}$$

For the ABMA tester, the use of the 17-4 PH striker pin against the Duranickel 301 specimen disc introduces a new factor, and the value for μ_{ij} is not known. However, review of the relationship of μ_{ij} for paired nickel and steel materials versus μ_{ii} for a single material, when the hardnesses are in the ratio of those for DN 301 and 17-4 PH, using the several tables of data in Ref 14, suggests as a valid approximation that $\mu_{ij} = 1/2 \mu_{ii}$. This approximation will be used in the present case, and the value $\mu_{ij} = 0.17$ for DN 301-17-4PH in CPF will be used.

On the other hand, the plastic flow of the DN 301 will not be affected much by the substitution of the harder material in the striker pin, so it is assumed that μ_{pl} is unchanged and equal to 0.61.

The data required have now been made available for calculation of the energy flux rate at the interface. Substitution of the following constants into Equation (D-2) (see Appendix F)

$$\begin{aligned} r_{pn} &= 0.25 \text{ in.} && (\text{Striker pin}) \\ \Lambda_{pn} &= 0.305 && (17-4 \text{ PH}) \\ E_{pn} &= 29 * 10^6 && (17-4 \text{ PH}) \\ \Lambda_{sp} &= 0.315 && (\text{DN 301}) \\ E_{sp} &= 30 * 10^6 && (\text{DN 301}) \\ r_{sp} &= 0.312 \text{ in.} && (\text{Specimen disc}) \end{aligned}$$

and combining reduces the equation to the form:

$$\frac{dU}{d\tau} = 2.72 * 10^{-10} P(\tau) \frac{dP(\tau)}{d\tau} \quad (34)$$

Average rate at 252 ft-lb impact, (reaction)

$$\mu_{pl} = 0.71$$

$$P(\tau)_{av} = 0.55P(\tau)_{max} = 1.640 * 10^5 \text{ psi}$$

$$\frac{dP(\tau)}{d\tau}_{av} = 4.44 * 10^8 \text{ psi/sec}$$

$$\frac{dU}{d\tau}_{av} = 1.41 * 10^3 \text{ ft-lb/sec}$$

It is interesting to calculate the total quantity of energy which is released at the interface. The time period during which the energy is released is $6 * 10^{-4}$ sec, and the area of the interface is $1.97 * 10^{-1} \text{ in.}^2$. Hence, the total energy released is:

$$\begin{aligned} U &= 1.41 * 10^3 * 6 * 10^{-4} * 1.97 * 10^{-1} \text{ ft lb} \\ &= 0.167 \text{ ft-lb} \end{aligned}$$

This is 0.07 percent of the 252 ft-lb impact.

Using appropriate values of the physical constants for CPF, DN301 and 17-4 PH, and for the geometry of the system (see Appendix F), the interface temperatures were calculated by using Equation (D-14).

The results are presented in Table 4-8.

The temperatures calculated by this method certainly seem to be related to ordinary chemical ignition processes. Nickel is known to be stable to fluorinating oxidizers in the 500°F temperature zone. The isothermal ignition temperature in CPF is not known, but a temperature range of 1928-2226°F for ignition in GF_2 is reported (Ref 37).

The large increase in temperature at the interface when plastic deformation becomes appreciable is in line with expectations as previously discussed.

Table 4-8
ENERGY FLUX AND INTERFACE TEMPERATURE FOR
ABMA TESTS OF DURANICKEL 301 IN CPF

Material Hardness (kg/mm ²)	Test Observation	dU/d τ_{av} (ft-lb/sec)	Interface Temperature (°F)
147	E ₅₀	1.41×10^3	2090
	TIE	3.19×10^2	450
179	E ₅₀	1.45×10^3	2155
	TIE	3.19×10^2	450
247	E ₅₀	1.53×10^3	2270
	TIE	3.34×10^2	472
326	E ₅₀ ^(a)	1.59×10^3	2365
	TIE	3.55×10^2	503
360	E ₅₀ ^(a)	1.62×10^3	2410
	TIE ^(a)	3.80×10^2	540

^(a) Values calculated from $p^2/E\sigma_y$ relation.

Summary

The results from ABMA impact tests with Duranickel 301 in CPF have confirmed that the materials properties of hardness (p) and yield strength (σ_y) are important criteria for defining service life at energy levels which cause surface ignition, as was postulated previously. Calculated interface temperatures are in excellent agreement with data obtained from purely chemical studies.

4.3.4.2 Stainless Steel 304-L

In the analytical phase, it was suggested that alloys of greater purity would show decreased chemomechanical reactivity. ABMA impact tests with two grades of stainless steel 304-L were conducted in CPF. The grades were air melt (ordinary purity) and vacuum melt (high purity). No difference in behavior was detected in these tests (see Table 4-9).

Table 4-9
ABMA REACTION OF SS-304L IN CPF

Condition	Energy Input (ft-lb)		Test Result	dU/dτ (ft-lb/sec)	Interface Temperature (°F)
	Test	Mean			
Air Melt	241	240	E ₅₀	7.95×10^2	1075
Vac Melt	239				
Air Melt	228	228	TIE	3.00×10^2	393
Vac Melt	228				

Using the calculation methods outlined above, maximum and average values were obtained for $P(\tau)$, $dP(\tau)/d\tau$ and $dU/d\tau$ from the E_{50} and TIE impact energy inputs. The interface temperatures were also calculated for each energy input. As with the DN 301, the temperature calculated for reaction initiation for SS 304-L in CPF, 1075°F (Table 4-9), is in the same temperature region as that reported (Ref 12) for ignition of stainless steel in F_2 , i.e., 1058 to 1465°F.

4.3.4.3 Tungsten Carbide-Cobalt Cermet (CA-4)

Dry Specimens

The behavior of the cermet in the ABMA impact tests was different from that of metals. Plastic deformation was not observed; instead the specimens shattered. However, even with this type of failure, reaction was not observed at lower energy levels. The apparent reaction threshold by ABMA test was about the same as that of the stainless steel 304-L. However, the entirely different nature of the cermet with its great hardness makes this apparent similarity quite wrong. Calculations of the reaction initiation temperature gave a very surprising result as shown in Table 4-10.

Table 4-10
IMPACT INITIATION OF WC-Co IN CPF

Energy Input (ft-lb)	Observation	dU/dr (ft-lb/sec)	Interface Temperature (°F)
220	TIE	1.27×10^3	2045
233	E_{50}	1.94×10^3	3135

It seems that this cermet is one of the most fluorine-resistant substances known — that is, if the equations, developed for metallic substances, are appropriate for these ceramics. It would certainly seem worthwhile to determine the ignition temperature of WC-Co in CPF or F_2 by a direct method.

Wet Specimens

No effort was made to determine a threshold for reaction of the specimens with absorbed water, and no difference in the positive reactions was observed for the three tests at 146, 183, and 220 ft-lbs, respectively. The threshold was not sought because it is known that water reacts spontaneously with CPF at room temperature and below. (The situation of course applies to all materials, but only the cermet was tested with absorbed water.)

4.3.4.4 Silver Plated DN-301

Evaluation tests with this candidate material were unsuccessful because of impurities in and beneath the plating (Section I.1.1.3). In two instances, the test specimens actually ignited, which is a rare circumstance in ABMA tests with metals. This again emphasizes the problems contaminants can cause in F_2 oxidizer systems. Analysis of the impurities showed that they contain sulfur and carbon.

4.4 ROTARY FRICTION INITIATION TESTS

4.4.1 Test Conducted

The tests conducted are summarized in Table 4-11.

The Phase I tests of DN-301 were conducted at the upper load capacity of the apparatus to demonstrate that hard alloys would react under achievable test conditions. All previous test programs had been conducted with much softer alloys such as aluminum and titanium.

The Phase II tests of DN-301 at lower energy levels were conducted to determine the relationship between material hardness and initiation energy, and to compare with the data found in drop-weight tests. Tests of 304-L were undertaken to demonstrate the effects of impurity inclusions in the alloy; and by this method differences in initiation energy were detected.

Table 4-11
ROTARY FRICTION INITIATION TESTS SUMMARY

Material	Compression Pressure Range (psi)	Number of Tests	Program Phase
DN-301-WH	455,000	1	Phase I, Part 2
DN-301, Various Hardness Conditions	50,000 to 101,000	13	Phase II, Part 1
Stainless Steel 304-L Air and Vacuum Cast	19,000 to 40,000	7	Phase II, Part 1
Carmet CA-4 WC in Co	12,600 to 191,000	7	Phase II, Part 2
Silver Plated DN-301	12,600	2	Phase II, Part 2
Alumina	12,600 to 76,500	4	Phase II, Part 2

The tests of candidate closure materials were conducted to evaluate these alternates. However, the tests with alumina were unsuccessful due to brittleness of the material. It shattered under test loads well below reaction initiation. The tungsten carbide cermet also shattered, but only in those cases in which a reaction was initiated—evidently the reaction caused the material fracture. The tests with silver-plated DN-301 were abandoned after it was determined that the inclusions were causing reactions and confusing the test interpretations, even when no reactions of the silver occurred.

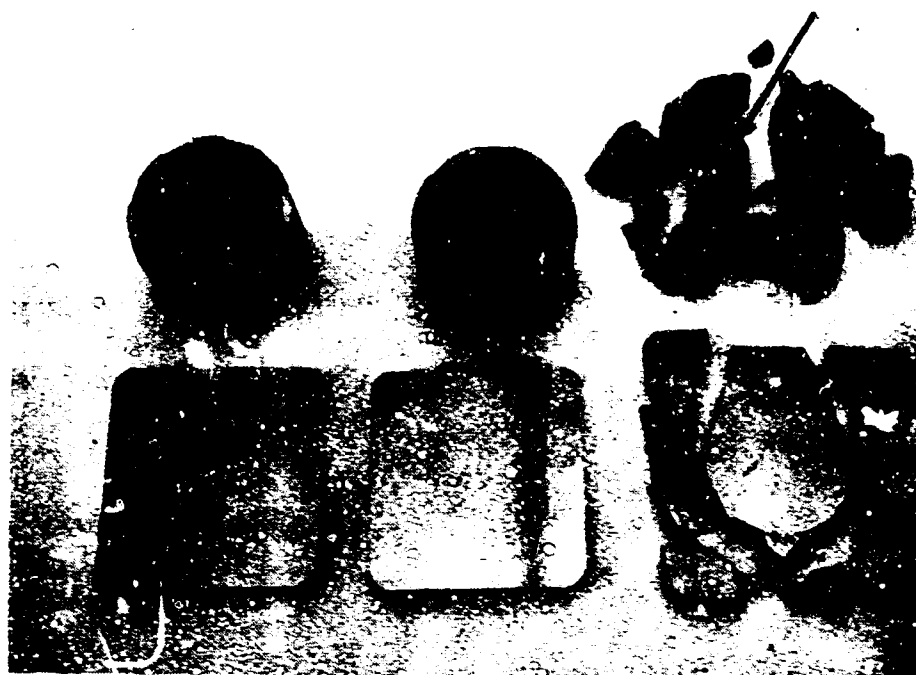
4.4.2 General Observations

It was found that visible reactions (i. e., light emission) occurred much more frequently with this test method than with the ABMA procedure. During examination of the specimens after test it was noted that, as in ABMA tests, reaction sites were found only on specimen surfaces that had undergone considerable plastic deformation or other failure. However, plastic deformation did not always lead to initiation.

The tungsten carbide cermet specimens failed by shattering, but only in those instances when reaction occurred. Although it is difficult to be certain which is the cause and which the effect, it is currently assumed that reaction caused the fracture, probably by local thermal expansion and gas generation, resulting in high local tension stresses. The pattern of failure of the specimens supports this assumption. As with the drop-weight specimens, signs of reaction were of two types, craters and smoothed edges.

Figure 4-4 shows these features.

When reaction and failure did not occur, the specimens were barely marked (see Figure 4-3). The optical ring noted for the (b) specimen cannot be detected by other than optical methods so it cannot be more than a light wavelength deep. This phenomenon has been observed by MDAC on other hard metal valve closures.



- A. UNTESTED
 B. AFTER TEST IN CPF AT 50-KSI LOAD, NO REACTION.
 (A FAINT 'OPTICAL' RING IS VISIBLE ON THE LOWER SPECIMEN IN THE ORIGINAL PHOTOGRAPH)
 C. AFTER TEST IN CPF AT 150-KSI LOAD, REACTION.
 (NOTE MANY REACTION SITES WHICH DID NOT CAUSE FRACTURE. ARROW POINTS TO REMAINS OF ONE BEARING SURFACE ON UPPER SPECIMEN)

Figure 4-3. Comparison of Tungsten Carbide Cermet Test Specimens

R87



(CENTRAL PIECE SHOWN IN FIGURE 4-3, PEAK AT TOP. THE SIDE SUBJECTED TO LOADING BY UPPER SPECIMEN IS AT LEFT. NOTE BURR LOCATIONS AND SMOOTHING OF FRACTURE EDGES ON LEFT, SHARP EDGES ON RIGHT.)

Figure 4-4. Fractured Tungsten Carbide Specimen, Edge View

4.4.3 Calculations

The load on the specimens is 12.5 times the cylinder pressure (see description in Appendix E), due to the relative areas of the piston and compression rod. The contact area at the specimen interface is 0.0495 in.², so the interface pressure is the interface load divided by 0.0495.

The angular scale for the final pendulum height is positioned so that if no energy were lost in the impact process, the scale reading would be 0 degrees. The equivalent drop height (EDH) of the pendulum—due to energy lost during impact—is calculated as follows:

$$EDH = 48 \sin \theta \quad (36)$$

when θ is the final pendulum position.

The effective mass of the pendulum at the impact point is equivalent to 18.1 pounds (Ref 9).

Tests at zero compression load were run with this pendulum to determine energy losses in the apparatus. The final height was equivalent to a loss of 10.4 ft-lb. This is slightly higher than the 9.3 ft-lb found for the lighter pendulum reported in Ref 9. The net energy released at the interface was calculated by using the relationship:

$$\text{Net Energy (ft-lb)} = \frac{EDH}{12} \times 18.1 - 10.4 \quad (37)$$

Test data and energy inputs calculated are presented in Table 4-12.

4.4.4 Analysis and Discussion

The rotary-friction tester was developed to release the major portion of its energy input in a controlled fashion at the specimen interface. Thus, it models any sliding component in the ACS valve closing mode, as well as the effects of the impact.

The theory of the mode of action of the ABMA impact tester is that radial expansion of the striker pin and specimen occurs when they are subjected to a vertical compression load (Ref 9). The differences in configuration

Table 4-i2
ROTARY FRICTION TESTS IN CPF

Material	Cylinder Pressure (psi)	Force on Specimen (lb)	Specimen Interface Pressure (psi)	Specimen Rotation Angle (°)	Final Pendulum Position (°)	Equivalent Drop Height (in.)	Net Energy Released at Interface (ft.-lb)	Reaction	Plasticity	Coefficient of Friction
Duralumin 101-A	100	1,750	75,800	60	Not Measured	---	---	Yes	---	---
	225	2,812	56,800	60	42	25.7	28.4	Yes	0.55	---
	200	2,500	50,500	60	35	21.6	22.2	Yes	0.47	---
	150	1,875	37,900	60	36	22.5	23.1	Yes	0.66	---
	100	1,250	25,100	60	19	11.8	17.4	No	0.75	---
Duralumin 101-WH	1800	22,500	455,000	15	Specimens Locked	48.0	59.1	Yes	0.56	---
Duralumin 101-1/4 H	400	5,000	101,000	60	Specimens Locked	48.0	59.1	Yes	0.64	---
	100	1,750	75,800	60	42	25.7	28.3	Yes	0.41	---
	200	3,500	70,700	60	33	20.4	20.4	No	---	0.32
	150	3,125	63,200	60	31	19.2	18.6	No	---	0.32
	100	4,375	88,400	60	Specimens Locked	48.0	59.1	Yes	0.73	---
104-1 Stainless Varnish Coat	150	4,375	88,400	50	64	36.7	43.4	Yes	0.65	---
	125	4,062	82,200	50	55	32.6	38.8	Yes	0.63	---
	100	3,750	75,800	60	36	22.2	23.7	No	---	0.34
	100	1,750	25,100	60	22	13.7	10.3	Yes	0.44	---
	75	918	19,000	60	20	12.4	8.3	Yes	0.48	---
104-1 Stainless Air Metal	75	918	19,000	60	Not Measured	---	---	Yes	---	---
	75	938	19,000	50	18	11.2	6.5	No	0.45	---
	150	1,475	37,900	60	22	13.7	10.3	Yes	0.30	---
	110	1,250	25,100	60	17	10.5	4.7	Yes	---	0.20
	75	938	19,000	60	12	---	2.7	No	---	0.16
Alumina	100	3,750	75,800	20	Shattered	---	---	No	---	---
	250	3,125	63,000	30	9(Shattered)	7.5	0.9	No	---	0.15
	110	1,375	27,800	30	9	7.5	0.9	No	---	0.15
	50	625	12,400	20	7	5.0	0	No	---	---
	50	625	12,400	15	6	5.0	0	Inclusions Only	---	---
Silver Plated (20-30)	50	625	12,400	15	6	5.0	0	Inclusions Only	---	---
	50	625	12,400	15	8	6.7	0	Inclusions Only	---	---
	50	625	12,400	40	11	9.2	3.5	Inclusions Only	---	0.04
	755	9,118	171,000	10	22	18.0	16.8	Yes (Shattered)	---	0.17
	600	7,500	151,000	45	24	19.2	18.5	Yes (Shattered)	---	0.17
Carnel C/A-4 Wt. in Cu	500	6,250	120,600	10	36	28.1	32.0	No	---	---
	200	2,500	50,500	30	15	12.4	8.3	No	---	0.55
	100	1,250	25,100	30	8	6.7	0	No	---	---
	50	625	12,400	45	11	9.2	3.5	No	---	0.40
	50	625	12,400	15	6	5.0	0	No	---	---

and materials of the pin and specimen results in different rates of expansion and, thus, friction forces are exerted at the interface and heat energy is released. However, only about 0.1 percent of the input energy appears at the interface, so the impact tester is inefficient.)

Tests were conducted using the rotary friction apparatus with the various materials of interest for this program. The variation in hardness of DN 301, again, was used to demonstrate the effects of mechanical properties on surface damage; the impurity level differences in air and vacuum melt stainless steel 304-L were incorporated to investigate how impurities could affect surface reaction ignition.

For the rotary friction tests, the initiation energy is reported herein as the zone between the lowest energy which caused a reaction and the highest energy which did not cause a reaction (Table 4-13). Figure 4-5 illustrates the relation between the initiation process and the hardness of the material; as the hardness increases, more energy is required to initiate reaction.

Table 4-13
ROTARY FRICTION INITIATION IN CPF

Material Condition	Vickers Hardness	Initiation Energy Range (ft-lb)	dU/dτ	
			Lower End (No Reaction) (ft-lb/in. ² sec)	Upper End (Reaction)
DN 301 Annealed	147	17.4-23.1	6.24×10^2	8.29×10^2
DN 301 3/4 H	326	20.4-28.3	7.33×10^2	1.02×10^3
DN 301 F H	355	23.7-38.8	8.50×10^2	1.67×10^3
SS-304-L Air Melt	89	2.7-4.7	9.70×10^1	1.68×10^2
SS-304-L Vacuum Melt	89	6.5-8.3	2.79×10^2	2.98×10^2
WC-Co Cermet	1,800	32.0-?	See discussion	
Ag Plated DN 301	50	?-3.5	False test	
Alumina	2,100		Fractured without reacting.	

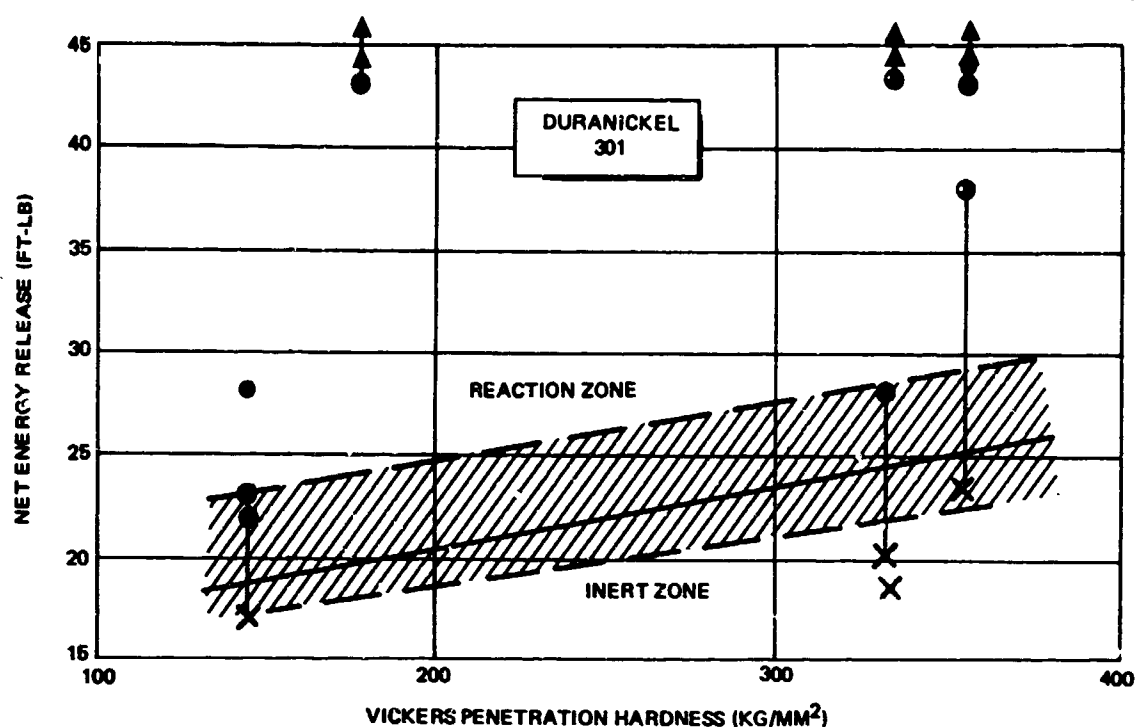


Figure 4-5. Rotary Friction Initiation of Duranickel 301 in CPF

There is a transition region between inert and reaction zones which probably indicates a region where other factors such as surface condition have noticeable effects.

In these tests, there is a definite difference in reactivity for different purities of stainless steel 304-L, with the purer material (vacuum melt) requiring an appreciably higher energy to initiate reaction.

To determine the energy release rate at the specimen interface, for comparison with the ABMA data, it is necessary to calculate the duration of the energy input and the contact area first. According to Ref 9, the duration of the energy input to the Rotary Friction Tester can be calculated from

$$\tau = \frac{\pi \alpha}{480 \sqrt{H}}, (\text{sec}) \quad (38)$$

where H is the total drop height of the pendulum (48 in.) and α is the angle of rotation of the upper specimen. Then, for the series of tests conducted for this study,

$$\tau = \frac{\pi}{480 \times 6.93} \alpha, \text{ (sec)}$$

$$\tau = 9.478 \times 10^{-3} \alpha, \text{ (sec)}$$

The contact area of the specimens (see Figure I-6) is

$$\begin{aligned} A &= \pi(R_o^2 - R_i^2) - 8 \times 0.125 \times 0.040 \\ A &= 0.492, \text{ (in.}^2\text{)} \end{aligned} \tag{39}$$

For an energy input of U ft-lb, the rate of energy input, $dU/d\tau$ can be calculated from the equation:

$$\begin{aligned} \frac{dU}{d\tau} &= \frac{U}{A\tau}, \text{ (ft-lb/in.}^2\text{ sec)} \\ &= \frac{U}{0.492 \times 9.47 \times 10^{-3} \alpha} \end{aligned} \tag{40}$$

$$\frac{dU}{d\tau} = 2.15 \times 10^3 \frac{U}{\alpha}, \text{ (ft-lb/in.}^2\text{ sec)} \tag{41}$$

Values of $dU/d\tau$ calculated in this fashion are listed in Table 4-13.

Calculation of interface temperatures for the rotary friction tests cannot be done by the same method used for the ABMA tests, (Equation D-14). The configuration of the upper specimens includes gaps in the bearing surface. (Figure I-6) Thus, during rotation, the upper specimen continually advances onto an area of the lower specimen metal which was not heated previously; this cool area is in contact with propellant which also was not heated. In addition, the rotation causes flow and convective heat transfer in the propellant fluid.

It is of interest to compare the $dU/d\tau$ trends obtained from the two different test methods, so comparable values are given in Table 4-14. It can be seen that generally, the initiation with rotary friction tester requires a smaller energy flux rate than with the ABMA tester. (The one case where it requires a higher flux corresponds to the overlarge range between stability and reaction which occurred with full hard Duranickel 301 (see Figure 4-6) and further testing would probably lower the upper value). Another difference is that the period of energy input is considerably longer in the rotary friction apparatus, roughly 10^{-1} sec compared with 10^{-3} sec for the ABMA tester.

The tests with the tungsten carbide cermet are anomalous when compared with previous results using the rotary friction tester. No flashes were seen for the specimens which reacted and shattered, and the energy apparently absorbed by the specimens was less than some tests without reaction. This behavior is interpreted to mean that the specimens reacted and failed during the very early stages of the rotation. When the specimen had shattered, there was no longer any friction load, and so the pendulum swung through freely. Making a rough extrapolation from the nonreactive tests, it would appear that the specimens failed before 30 percent of the test rotation was

Table 4 - 14
COMPARISON OF ABMA AND ROTARY FRICTION
INITIATION OF METALS IN CPF

Metal	Condition	ABMA $dU/d\tau$ for reaction	Rotary Friction $dU/d\tau$ for reaction
DN 301	Annealed	1.41×10^3	8.29×10^2
DN 301	3/4 H	1.59×10^3	1.02×10^3
DN 301	F H	1.62×10^3	1.67×10^3
SS-304	Air Melt	7.95×10^2	1.68×10^2
SS-304	Vacuum Melt	7.95×10^2	2.98×10^2

achieved. On this basis, even the minimum rotation of 15° would be too much, so tests of smaller rotations were not attempted. There is no way to calculate the energy actually used to initiate the reaction, but the lack of reaction at 32 ft-lbs indicates that the figure must be higher than this value.

The silver plated specimens again gave poor results because of included impurities. These reacted at a very low-energy level.

The alumina specimens fractured and failed at low-energy inputs, but they did not appear to have reacted. These tests were unsuccessful.

4.5 CONCLUSIONS

- A. The initiation tests demonstrate that there are linear relationships between certain material properties and the 50-percent reaction threshold energy (E₅₀). The material properties so correlated are yield stress and hardness. These correlations support, but do not prove, the equations derived which relate surface degradation rate (i. e., per operating cycle) to the same properties.
- B. The initiation tests demonstrate that the presence of impurities definitely catalyze reaction by reducing the minimum energy to cause reaction initiation. Absorbed water is shown to be an initiation catalyst.
- C. The initiation tests are too powerful to be accurate models of the processes in the ACS valve.
- D. The ABMA initiation tests can be used to determine the ignition temperature of metals immersed in oxidizers.

Section 5

MATERIALS PARAMETERS

5.1 VALVE WEAR THRESHOLD CONSIDERATIONS

The operating requirements for the ACS valve, a GHe leak rate upper limit of 30 SCC/hr after 10^5 operating cycles, entail valve design features which are consistent with these requirements. Leak rate is a function of several variables (Equation (1)) which can be grouped into classes. The classes are (1) the configuration of the sealing surfaces including contact area and surface finish, (2) the energetics of the valve, including its temperature and compressive stress, and (3) the properties and condition of the test fluid, including upstream and downstream pressures and viscosity. The properties and condition of the test fluid are fixed in the ACS valve system within certain operating limits, and are not further considered. Similar restrictions apply to the temperature of the system. However, temperatures developed in the valve because of its operation are of interest and are considered.

The sealing surface configuration factors can be subdivided into those aspects which are features of the valve design geometry (such as the closure surface area) and so should not change significantly during use, and those which are subject to change during valve operation, such as the surface finish of the closure.

The aspect of valve energetics which is important during leakage determination is the surface compressive stress. This factor, though, is a compound one, and for the ACS valve can be resolved into functions of the closure area, the fluid pressures, and the spring rate of the closure spring flexures. The latter term is the only one related to energy which can be manipulated, and it, like the geometry, is normally invariant during the service life of the valve.

Combining Equations (1) and (2), and substituting the normal values for the system and configuration parameters yields the equation

$$Q = 1500 \frac{H^3}{(1.25 \times 10^3 + \sigma_S)^{2/3}} \quad (42)$$

where σ_S is the stress due to the poppet spring.

By requirement, $Q_{\max} = 30$ scc/hr, and when this value is substituted in the equation, we can then define the relation between H_{\max} and σ_S which will give the required Q

$$H_{\max} = (5.07 + 4.06 \times 10^{-3} \sigma_S)^{2/9} \quad (43)$$

Due to the two-ninth power, H_{\max} is not very sensitive to σ_S ; $H = 1.43$ at $\sigma_S = 0$ and $H = 1.50$ and $\sigma_S = 300$ in the absence of additional loads caused by fluid pressure. This latter corresponds to the design maximum total contact stress. These results indicate that if for some reason connected with the operation of the valve it were expedient to alter the spring rate constant R , this change would not affect the surface finish requirements appreciably. The accuracy of this assertion is apparent in Figure VII-7 of Ref 1.

Since this maximum surface roughness for acceptable performance has been defined, if the surface finish resulting from operating the valve can be related to controllable parameters of the valve design, the result will be generation of design criteria and limits. These derivations are given in Appendix J.

The first and most conservative condition is the definition of the material parameters which will support an infinite life span. This is shown to be

$$\Omega = \frac{G_{AB}}{P_A} \bigg|_{n=\infty} \leq 0.23 \text{ } \overset{\circ}{A} \quad (44)$$

None of the values for G_{AB}/p_A given in Table 3-2 are this low--the lowest is 0.56 for zirconium carbide. Lubrication of the surfaces by the liquid propellant will raise this limit, but it would be unrealistic to expect an increase of greater than about ten fold when actual measurements are available. Thus materials with a dry G_{AB}/p_A ratio of 2 Å or less should be chosen.

The other very conservative condition is that plastic flow of the closure materials cannot be tolerated. As shown in Appendix J, this leads to the limiting material parameter

$$F_{I_{\text{no deform}}} \leq 53.6 E^{1/4}, \quad (1b) \quad (45)$$

which allows calculation of the maximum allowable impact force as a function of a material parameter, the bulk modulus.

This solution does not consider the reduction of the bulk modulus of the material caused by heating of the closure (Equation (25)). In addition, other undesired changes in the metal structure, caused by heating, may have to be avoided. Such occurrences as annealing, grain growth, and phase changes can alter properties sufficiently to speed up the failure rate.

If the maximum service temperature of the closure material in CPF is known, then Equations (24) and (25) can be solved jointly to give the maximum impact energy, $F_{I_{\text{max temp}}}$, corresponding to this temperature.

$$F_{I_{\text{max temp}}} \leq \frac{\Delta T (\Gamma_M W_M + \Gamma_P W_f) + 1.54 \times 10^{-8} (q_f + 3q_M)}{2.53 \times 10^{-8} \Lambda \mu E^{-1} (1 - \Lambda) \frac{dP}{d\tau} + 160 \Gamma_P W_f - 1_{-V} W_f} \quad (46)$$

Having discussed what may be considered to be the limiting cases, $n = \infty$, for F_I in terms of service constraints, (and related these to materials properties) it is now logical to consider the required operating cycle life $n = 10^5$.

It is shown that a definition of F_I relating to material properties and number of operating cycles is

$$F_{I, 100K} = 1.4 \times 10^{-4} \frac{P_A}{k_{AD}}, \quad (lb) \quad (47)$$

This can be solved to give values of F_I of 10^3 lb only if values k_{ad} for the closure materials are about 10^{-5} to 10^{-6} , corresponding to excellent lubrication (Table 3-3).

5.2 MATERIAL SELECTION PARAMETERS

The equations given above can be further combined to derive a set of relations between the properties of the closure materials, as demonstrated in Appendix J. This procedure yields the following set of material parameter equations:

$$\Omega = \left(\frac{G_{AB}}{P_A} \right)_{n = \infty} \leq 0.23 \text{ }^\circ \text{A} \quad (48)$$

$$\phi = \left(\frac{P_A}{k_{ad} E^{1/4}} \right)_{n = 100K} \leq 3.82 \times 10^5 \quad (49)$$

$$\Sigma = \left(\frac{y}{E^{3/4}} \right)_{n = 100K} = 9.35 \times 10^{-2} \quad (50)$$

$$\Psi = \left(\frac{k_{ad} G_{AB}^2}{P_A^2} \right)_{n = 100K} = 31.9 \text{ }^\circ \text{A}^2 \quad (51)$$

and (49) times (50) gives

$$\bar{E} = \frac{P_A \sigma_y}{k_{ad} E} \bigg)_{n=100K} = 3.57 \times 10^4 \text{ erg/cm}^2 \quad (52)$$

These equations define the relationships between the material properties when the valve configuration is unchanged from that currently used. There are insufficient equations to be solved simultaneously, three equations in five unknowns for $n = 100K$ cycles (52 is not a separate equation), one equation in two unknowns for $n = \infty$ cycles.

The grouped properties in the equations are treated as parameters for valve design (Table 5-1). These parameters actually are representations of the way the materials properties interact when the surfaces are subjected to adhesive wear, and define the resistance to wear. They are general terms, and are useful for any dynamic adhesive wear situation. The numerical values which they assume for maximum resistance to wear are specific for the particular valve configuration, and will be different in different systems.

In Table 5-1, the values of the individual material properties and of the adhesive impact wear parameters are given, where available, for K-96, the successful closure material, for K-84 and K-68, a pair of materials suggested during preparation of the proposal for this contract as of potentially even greater utility (the suggestion came from considerations of edge wear resistance and gall resistance, not from the adhesive impact wear parameters), for Duranickel 301, and for some other candidate materials suggested by AFML. The many columns which show unavailability of needed data illustrate the reason that the impact wear parameters are regarded as of tentative utility. It is at present impossible to conduct a valid check.

Table 5-1
MATERIAL SELECTION DATA CHECK SHEET

Material	Surface Energy (γ_{AB}) (erg/cm ²)		Penetration Hardness PA (kg/min ²)		Adhesive Wear Constant k _{ad}		Modulus E (psi)	Compression Yield σ_y (psi)	ν (\AA)		λ^2 (\AA^2)		χ_i^2 (erg/cm ²)
	Ordinary Condition	Test Fluid	Ordinary Condition	Test Fluid	Ordinary Condition	Test Fluid			Ordinary Condition	Test Fluid	Ordinary Condition	Test Fluid	
E-6	11,560 (est)	DNA	1,800	DNA	DNA	DNA	9.1×10^7	690×10^3	0.86	DNA	DNA	DNA	DNA
E-4 (copper)	11,580 (est)	DNA	1,890	DNA	DNA	DNA	7.2×10^7	650×10^3	0.83	DNA	DNA	DNA	DNA
E-6 (steel)	11,570 (est)	DNA	1,850	DNA	DNA	DNA	9.0×10^7	736×10^3	0.85	DNA	DNA	DNA	DNA
E-4 • K-64	1,575	DNA	1,850	DNA	DNA	DNA	See above pair	See above pair	0.85	DNA	DNA	DNA	DNA
Duranickel 301	170 (pure Ni)	DNA	480	DNA	DNA	DNA	3×10^7	49×10^3	7.1	DNA	DNA	DNA	DNA
Inconel 625	DNA	DNA	317	DNA	DNA	DNA	3.1×10^7	30×10^3	DNA	DNA	DNA	DNA	DNA
Hastelloy c	DNA	DNA	253	DNA	DNA	DNA	2.98×10^7	65.4×10^3	DNA	DNA	DNA	DNA	DNA
Silver Plate on Duranickel 301	920	DNA	80	DNA	DNA	DNA	3×10^7 (Dura- nickel)	49×10^3 (Dura- nickel)	11.5	DNA	DNA	DNA	DNA

Ordinary conditions refer to measurements made in ordinary ambient laboratory air.

DNA = Data not available

The effect of exposure to CPF on the properties is not known, and this is an important area for future studies. The properties of Kennametal K-96, where known, are entered into Table 5-1, since this material has exhibited the best performance to date in the ACS valve in CPF.

Consideration should be given to using two dissimilar materials, even though one of them may be significantly softer and have a higher surface energy than the other. The principal advantage of using dissimilar rather than identical materials is that the energy of adhesion G_{AB} may be reduced by as much as a factor of two. However, in order to avoid increasing the magnitude of the ratio G_{AB}/p_A the hardness p_A of the softer material must be significantly greater than one-half the hardness p_B of the harder material or

$$\frac{1}{2} * \frac{(\gamma_A + \gamma_B)}{p_A} > \frac{2\gamma_B}{p_B} \quad (53)$$

Candidate poppet and seat materials considered for resistance to corrosion wear program should be selected on the basis of certain critical physical characteristics of the oxide, fluoride, and chloride films which form on the materials. Table 5-2 is a check list which can be used to present these physical characteristics. No baseline comparison of known values of these characteristics can be presented at this time, since the needed data are not available.

Generally, candidate materials should form films in CPF that are thin, soft, ductile, tenacious, and have low permeability.

Table 5 -2
CORROSION WEAR MATERIAL SELECTION CHECK LIST

Physical Property	Film							
	Metal Oxide		Metal Fluoride		Metal Chloride		Candidate	Name
	Baseline	Candidate	Baseline	Candidate	Baseline	Candidate		
	Name	Name	Name	Name	Name	Name		
Thickness (Å)	100		10		10			
Adhesive strength (Kg/cm ²)								
Cohesive strength (Kg/cm ²)								
Permeability								
Compressive strength (Kg/cm ²)								
Ductility (% elongation)								

Section 6

RECOMMENDED FUTURE WORK

The complete application of the materials parameters and other factors discussed in the analysis requires collection of certain classes of materials properties data not readily available. These include:

A. For metals:

1. Surface energy, in ordinary condition and after fluorination.
2. Penetration hardness after fluorination.
3. Adhesion constant in ordinary condition and after fluorination.

B. For metal fluoride-chloride films:

1. Adhesive strength (to substrate).
2. Cohesive strength.
3. Permeability.
4. Compressive strength.
5. Ductility.

C. The reaction parameters for CPF and metals:

1. Activation energy.
2. Ignition temperature.
3. Reaction mechanism and order.
4. Temperature coefficients of reaction parameters.
5. Heat of reaction.

REFERENCES

1. G. T. Pond and H. Wichman. Advanced ACS Valve Development Program. The Marquardt Corp., Technical Report No. AFRPL-TR-69-250, December 1969.
2. C. D. Coulbert and P. Herr. Thrust Chambers for Space Storables. Marquardt Company, in "Visual Aid Prints and Abstracts, OART Space Storable Specialist Conferences," Miami Beach, September 1969.
3. R. Gray, NASA-LeRC. Telecon with D. L. Endicott, MDAC-West, March 1970.
4. Personal communication, telecon, Jim Maggean, TRW Systems, 15 April 1970.
5. Personal communication from R. Riddel, EAFB-RPL, January 1970.
6. G. F. Tellier and J. W. Lewellen. Poppet and Seat Design Criteria for Contaminant Particle Resistances. Rocketdyne Div, NARC, AFRPL-TR-70-1, April 1970.
7. Sgt. G. Gunderson, AFRPL. Personal Communication (telecon), January 1971.
8. W. D. English and H. D. Samuel. Failure Mechanism of ACS Valve in CPF Service. Interim Technical Report MDC G0688, August 1970.
9. S. M. Toy, L. E. Bell, W. D. English and N. A. Tiner. Tankage Materials in Liquid Propellants. AFML-TR-68-204, July 1968.
10. S. K. Asunmaa, W. A. Cannon, W. D. English, N. A. Tiner and S. M. Toy. Halogen Passivation Procedural Guide. AFRPL-TR-67-309, December 1967.
11. G. F. Tellier. Poppet and Seat Design Data for Aerospace Valves. Technical Report No. AFRPL-TR-66-147, July 1966.
12. Brush Instruments. Surface Measuring System - Operating Instructions. Manual No. 31381A, (no date).
13. E. Rabinowicz. Friction and Wear of Materials. John Wiley and Sons, New York, 1965.

14. R. E. Bolz and G. L. Lave. Handbook of Applied Engineering Science. Chemical Rubber Company, Cleveland, Ohio, 1970.
15. Materials Engineering. 1970 Materials Selector Issue. Reinhold Publishing Co. Vol. 70, No. 5, October 1969.
16. Chemical Rubber Co. Handbook of Chemistry and Physics. 46th ed, pages F-16 to F-22, 1965.
17. N. A. Lange, Handbook of Chemistry, 6th ed. Handbook Publishers, Sandusky, Ohio, 1946.
18. W. A. Cannon, W. D. English, S. K. Asunmaa, S. M. Toy, and N. A. Tiner. Halogen Passivation Studies. AFRPL-TR-66-330, January 1967.
19. N. A. Tiner, W. D. English, and S. M. Toy. Compatibility of Structural Materials with High Performance O-F Liquid Oxidizers. AFML-TR-65-414, November 1965.
20. NASA. Development and Demonstration of Criteria for Liquid Fluorine Feed System Components. CR 72063, DAC 60599, October 1967.
21. S. Kleinberg. The Compatibility of Various Metals with Liquid Fluorine. Air Products and Chemicals, Final Report, ASD-TDR-62-250, March 1962.
22. H. D. Samuel. Liquid Fluorine Shutoff Valve Development Program. DAC-61813, AFRPL-TR-69-41, April 1969.
23. W. Britsch. NASA LeRC. Telecon, 13 August 1970.
24. W. D. English and D. R. Spicer. Apparatus for Impact Testing in Fluorinating Agents, Materials Research and Standards. ASTM, 9, 30, 1969.
25. Kennametal, Inc. Properties of Kennametal Carbide Alloys. Bulletin B800C(10)B7 1967.
26. Anon. Bearings. Machine Design, No. 14, Page 34, 13 June 1968.
27. D. L. Endicott and L. H. Donahue. Development and Demonstration of Criteria for Liquid Fluorine Feed System Components. CR-72543, NAS-3-11195, DAC 53240, June 1969.
28. Huntington Alloy Products Division International Nickel Co. Engineering Properties of Duranickel Alloy 301 and Permanickel Alloy 300. Technical Bulletin T-32, 1963.

29. ASTM Method D-2512, Appendix B, Vol. 18, ASTM Book of Standards, 1970 Edition.
30. R. C. Juvinall. Engineering Considerations of Stress, Strain and Strength, McGraw Hill, 1967.
31. R. J. Roark. Formulas for Stress and Strain. McGraw Hill, 1954.
32. I. Dickens. Valve Seat Load Test Stress Analysis. Stress Memo 324, Marquardt Corp., 20 November 1970.
33. R. M. Joyce. Personal Communication, MDAC-West, March 1971.
34. G. Pfeifer. Results of Tests to Determine Poppet and Seat Closing Impact Forces in the Marquardt Advanced ACS Valve. MIR-388, Marquardt Corp., November 1970.
35. J. Stefan. On the Relation Between Theories of Capilarity and of Evaporation. Ann. Phys., 29, 655, 1886.
36. D. S. Clark and W. R. Varney. Physical Metallurgy for Engineers, Appendix G; Second Edition, D. Van Nostrand, New York, 1962.
37. McDonnell Douglas Astronautics Company-West. Fluorine Systems Handbook, DAC 59074, NASA CR-72064, July 1, 1967.
38. D. McLean, Grain Boundaries in Metals, Oxford University Press, New York. 1957, as reported in Ref 39.
39. P. Bauer, Investigations of Leakage and Sealing Parameters, IITRI, AFRPL-TR-65-153. August 1965.
40. J. B. Marriott and G. Rowden. The Erosion of a Cobalt-Chromium Alloy by Liquid Impact. Phil. Trans Royal Soc (London) Series A, Vol. 260, No. 1110, pp 144-149 (July 1966).

Appendix A

DYNAMIC AND STATIC CLOSURE LOADS

A.1 PARALLEL IMPACT FORCE

The flexure supports shown in Figures 2-1 and 2-2 exert a spring force on the poppet-armature assembly in the direction of the seat. This force decreases linearly (but not to zero) as the poppet moves from the open to the closed position. For the simplified case, with constant upstream pressure, if the pressure drop of the flowing fluid is assumed to increase linearly as the poppet moves from the open to the closed position (downstream line pressure decreases), then the sum of the spring force and the pressure difference can be assumed to remain essentially constant during poppet closing (See Figure A-1). Therefore, the poppet and armature have a constant acceleration during closing. This acceleration can be calculated from

$$a = \frac{(F_{\Delta P^o} + F_{S^o})g}{(W_p + W_a)} = \frac{F_T g}{W_T} = 32.2 \frac{F_T}{W_T}, \text{ (ft/sec}^2\text{)} \quad (\text{A-1})$$

where

a = acceleration, ft/sec²

$F_{\Delta P^o}$ = force caused by pressure drop across the poppet, lb

F_{S^o} = force resulting from the compression of the spring flexures in their open position, lb

W_p = weight of poppet, lb

W_a = weight of armature and flexures, lb

g = acceleration of gravity, ft/sec²

There is no hydrodynamic drag term necessary for gases in this particular ACS valve because the fluid flow tends to force the valve closed and not to oppose the poppet travel. A correction factor for liquids will be introduced

For the ACS valve suspension system, the effective impact weight $W_{I,e}$ is not the same as W_T , because (1) the kinetic energy of the armature, which is based on its weight, W_a , is absorbed in a different region of the valve; (2) a quantity of fluid behind the poppet must also be decelerated; and (3) the spring which drives the poppet remains in compression when the stroke is complete. The effective weight during the impacting process is

$$W_{I,e} = W_p + W_f + R \delta_c, \text{ (lb)} \quad (\text{A-5})$$

where

W_p = weight of poppet, lb

W_f = weight of fluid to be decelerated, lb

R = spring constant, in./lb

δ_c = spring deflection after closing, in.

The poppet force acting on the seat at impact (impact force) can be determined by converting the effective poppet kinetic energy to strain energy of the poppet and seat:

$$\frac{F_I \Delta}{12} = \frac{W_{I,e}}{2g} * v_I^2, \text{ (ft-lb)} \quad (\text{A-6})$$

or substituting for v_I from Equation (A-4) and rearranging

$$F_I \Delta = \frac{W_{I,e} h}{g \tau_c}, \text{ (in.-lb)} \quad (\text{A-7})$$

where

Δ = deflection, in.

If both the poppet and the seat are to be subjected to only one half their respective compressive* yield stresses, τ_y , a common design technique used to reduce fatigue failure, then the compressive deflection of each surface can be calculated from

$$\Delta = \frac{\sigma_y t}{2E}, \text{ (in.)} \quad (\text{A-8})$$

*Stress and strain will refer to compression loads in this report, unless otherwise noted.

The total compressive deflection of both the poppet and seat, Δ_T , is

$$\Delta_T = \left(\frac{\sigma_y t_p}{2E} \right)_p + \left(\frac{\sigma_y t_s}{2E} \right)_s, \text{ (in.)} \quad (\text{A-9})$$

If the poppet and seat are made of the same materials, which is the case for the ACS valves tested to date, Equation (A-9) reduces to

$$\Delta_T = \frac{\sigma_y t_T}{2E}, \text{ (in.)} \quad (\text{A-10})$$

where

$$t_T = \text{total thickness} = t_p + t_s, \text{ in.}$$

Combination of Equations (A-3), (A-7), and (A-10) to define F_I results in

$$F_I = 6.22 * 10^{-2} \left(\frac{E}{\sigma_y} \right) \left(\frac{h}{t_T} \right) \left(\frac{W_{I,e}}{\tau_c} \right), \text{ (lb)} \quad (\text{A-11})$$

As an example of the application of Equation (A-11), the impact force in the ACS valve with a tungsten carbide-cobalt cermet (K-96) seat and poppet is calculated

$$E = 9.1 * 10^7 \text{ psi}$$

$$\sigma_y = 6.9 * 10^7 \text{ psi}$$

$$h = 1.2 * 10^{-2} \text{ in.}$$

$$t_T = 1.9 * 10^{-1} \text{ in.}$$

$$W_p = 6 * 10^{-3} \text{ lb}$$

$$W_f = 3.6 * 10^{-4} \text{ lb}$$

$$\delta_c = 1 * 10^{-4} \text{ in.}$$

$$R = 1,300 \text{ lb/in.}$$

$$R\delta_c = 1.3 * 10^{-1} \text{ lb}$$

$$W_{I,e} = W_p + W_f + R\delta_c = 1.364 * 10^{-1} \text{ lb}$$

$$\tau_c = 1 * 10^{-3} \text{ sec}$$

Then

$$F_I = \frac{6.22 * 9.1 * 1.2 * 1.364}{6.9 * 1.9 * 1} * \frac{10^{-2} * 10^{-7} * 10^{-2} * 10^{-1}}{10^5 * 10^{-1} * 10^{-3}}$$

$$= 7.06 * 10 \text{ lb}$$

$$= 70.6 \text{ lb}$$

Some important points should be made here.

- A. It is realized that the above analysis is somewhat unconventional in approach. The method of Juvinall (Ref. 30), using conservation of momentum and equating kinetic energy with strain energy, in combination with Roark's analysis of the bending strain of the closure components (Ref 31), is a more exact model. However, in many cases, not all the data needed for this more exact model are available. The MDAC formulation is apparently a good approximation which is easier to apply and is less restricted by specific design features. Using the more exact formulation, the valve fabricator calculated an impact force of 101.0 lb (Ref 32). The measured impact force in GN_2 at 0 psig (15 psia) was 84 lb and at 300 psig was 76 lb (Ref 32).² If the bending strain is neglected, the equation for F_I (Ref 33) is

$$F_I = 0.862 v_I \sqrt{\frac{\pi}{2} \frac{E D_i M_p}{0.181}} \quad (\text{A-12})$$

which, when applied to the same valve design and test conditions, gives an impact force, F_I , of 294 lb.

- B. The introduction of σ_y in Equations A-8 through A-11 may draw some objections, but it is used (as $\sigma_y/2$) to indicate a design limit.
- C. Equation (A-11) is slightly modified from the earlier version published in Phase I Interim Report (Equation A-8, Ref 8). The major change is that of substituting for v_I a function of poppet stroke and closing time, instead of F_T and W_T , respectively, the force used to accelerate and the weight of the whole poppet and armature assembly. The substitution was made to use factors which are more readily determined for any valve.
- D. Values for F_I calculated by use of Equation (A-11) are several orders of magnitude smaller than those in the Phase I report. The earlier values were in error because of a misunderstanding by MDAC of the masses reported for closure components in Table A-2 of Ref 1.

- E. Analytical inclusion of hydrodynamic effects in Equation (A-11) has not been achieved. Empirical data reported in Ref 34 indicate a divisor for F_I ranging from 1.5 to 3.0 for water at room temperature. In the same reference it is suggested that the factor for other liquids is

$$F_{I, \text{ liquid}} = F_{I, \text{ water}} * \frac{\text{liquid density}}{\text{water density}} * \frac{\text{liquid viscosity}}{\text{water viscosity}}$$

A.2 SURFACE STRESSES

The surface stresses at impact are

$$s_I = \frac{F_I}{A}, \text{ (lb/in.}^2\text{)} \quad (\text{A-13})$$

Note that if the poppet impacts the seat while they are parallel, the apparent contact area, A , may be assumed to be equal to the real contact area in the case of the ACS valve because the finish of the poppet and seat surfaces is very smooth.

A.3 NONPARALLEL IMPACT

When the poppet contacts the seat at an angle, additional factors must be considered. The first of these is the force which must be exerted to rotate the poppet so that it is parallel to the seat for final closure. The moment of inertia of the poppet about its center of gravity is

$$I_p = 1/3 \frac{W_p r_N^2}{g} \quad (\text{A-14})$$

where

I_p = moment of inertia of poppet assembly

r_N = radius of poppet nut, in.

It can be shown, then, that the force on impact is decreased by a factor which is a function of the radial distance of B, the contact point (Figure 3 - 8) from the center of the poppet.

The equation is

$$F_{I, \alpha} = \frac{0.5}{\sqrt{1 + 3\left(\frac{B}{r_N}\right)^2}} F_I, \text{ (lb)} \quad (\text{A-15})$$

where

B = radial location of contact point B, in.

α = contact angle, degrees

Note that B is not a function of the angle for the small angles ($\alpha_{\max} = 0.5^\circ$ originally, now held to less than 1 minute of arc) in the ACS valve. The displacement B changes by no more than $1 * 10^{-6}$ inches due to cocking, while the allowed slack in the flexures is $1 * 10^{-4}$ in. Note too that r_N must be the radius of the total assembly that rotates, i.e., it includes the poppet retainer and ring nut if these are used. For such an assembly ($r_N = 0.375$, $B = 0.1$, $\alpha = 0.5$), the factor is equal to 0.88; i.e., the impact force is reduced to 88 percent of the value for parallel impact.

Following the analysis given by Roark (Ref 31), it is possible to derive a formula for the surface stress for angled impact (Figure A-2). The formula is

$$\sigma_{I, \alpha} = \frac{0.395}{\alpha \beta} \sqrt[3]{\frac{E^2 F_I}{d_d^2}}, \text{ (lb/in}^2\text{)} \quad (\text{A-16})$$

for small angles.

where

α = the angle between the poppet and seat, degrees

β = the angular displacement from the vertical of the contact point along the duboff, degrees

d_d = duboff diameter, in.

This formula yields relatively large stresses — for an $\alpha\beta$ product of 2, the calculated value of $\sigma_{I,\alpha}$ may surpass 10^6 psi for some hard materials; in such cases yielding will occur.

By simple geometry (Figure A-3), assuming a sharp-edged seat (no duboff), one can derive the contact area due to yeilding of the material at angled impact, $A_{I,\alpha}$:

since

$$\alpha_{I,\alpha} > \alpha_y, \text{ assume } \sigma_y$$

$$F_{I,\alpha} = \sigma_y A_{I,\alpha}, \text{ (lb)} \quad (\text{A-17})$$

$$= \sigma_y \pi \left(\frac{D_o}{2} \right)^2 (e_A - \sin \theta_A) \quad (\text{A-18})$$

$$X_{I,\alpha} = \frac{D_o}{2} \left(1 - \cos \left[\frac{6 F_{I,\alpha}}{\pi \sigma_y \left(\frac{D_o}{2} \right)^2} \right]^{1/3} \right), \text{ (in.)} \quad (\text{A-19})$$

A typical value of $X_{I,\alpha}$ for K-96 is 2×10^{-5} in.

R87

R87

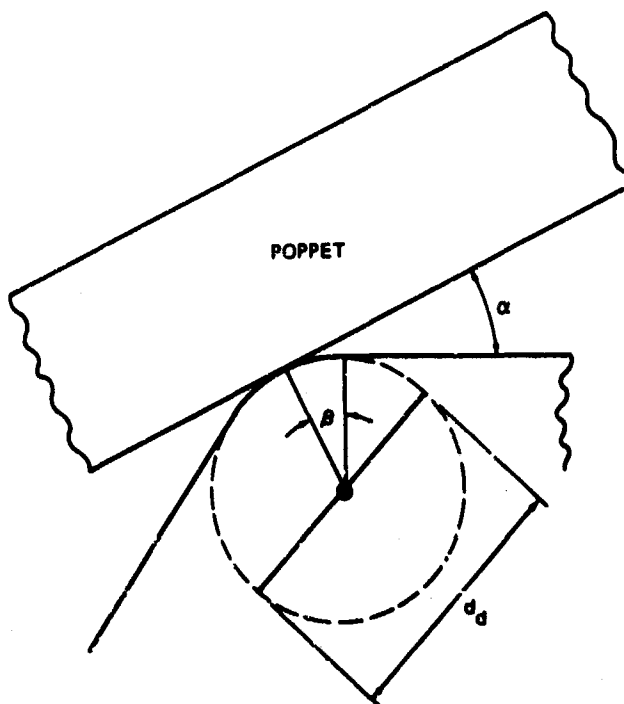


Figure A-2. Angled Configuration

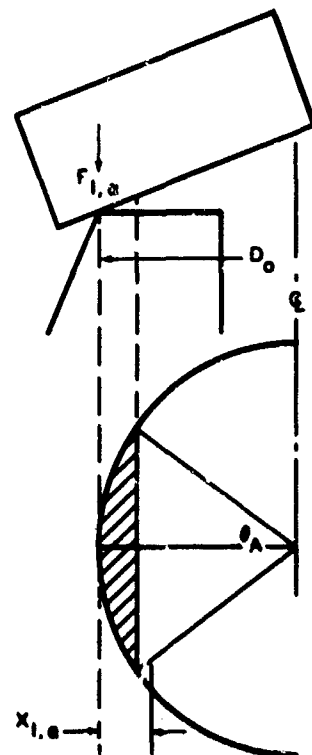


Figure A-3. Angled Impact Contact Area

Appendix B

ADHESIVE WEAR

Most of the material in this appendix was abstracted from Rabinowicz (Ref 13).

B.1 SURFACE ENERGY

The surface energy of a material is most easily measured when the material is in its liquid state, hence theoretical correlations for calculating this energy have been developed for this condition. The surface energy* of a liquid is about one-sixth of the latent heat of vaporization of the molecules that constitute the surface layer of the liquid (Ref 35).

$$\gamma_m = \frac{L_v \rho_m}{6}, (\text{ergs/cm}^2) \quad (\text{B-1})$$

where ρ is in g/cm^3

The surface energy* of a pure solid material at its melting temperature is equal to its surface energy in the liquid state, since melting affects the bulk intermolecular energy balance, not the surface energies.

This relation is not strictly true for mixtures and alloys in which the surface condition and energy can be changed by mechanical working, heat treating, etc. For such cases, the Young-Dupre relation

$$\gamma_m = \gamma_f (\cos \alpha + 1), (\text{erg/cm}^2) \quad (\text{B-2})$$

between surface energy and liquid contact angle, α , is more suitable, but measurements are not available in the systems of interest for the present program.

*Metric units are used here for surface tension and surface energy because most available data are reported in metric units. In all equations which use γ , a conversion factor has been included so that the results are in consistent English units.

The surface energy of the solid increases as its temperature decreases below its melting temperature, and can be calculated from the relationship

$$\gamma_{\theta} = \gamma_m + K_{\theta}(\theta_m - \theta_x), \text{ (ergs/cm}^2\text{)} \quad (\text{B-3})$$

where

$$K_{\theta} = 0.5, \text{ (erg/cm}^2 \text{ } ^\circ\text{K)}$$

For those materials for which γ is not available from the literature or from the parameters needed for Equation (B-3), an approximate value can be calculated by means of the relationships plotted as the lines in Figure 2-9;

$$\gamma_A = k_{\gamma} \sqrt[3]{P_A}, \text{ (erg/cm}^2\text{)} \quad (\text{B-4})$$

where

$$k_{\gamma} = 280 \text{ for metals}$$

$$k_{\gamma} = 64 \text{ for inorganics and ceramics}$$

B.2 ENERGY OF ADHESION

The energy of adhesion between 1 cm² plates of two materials, a and b, is given by the relationship

$$G_{AB} = \gamma_A + \gamma_B - \gamma_{AB}, \text{ (erg/cm}^2\text{)} \quad (\text{B-5})$$

The value of G_{AB} is dependent on the similarity of the materials. For example, if the materials are identical, γ_{AB} reduces to zero and Equation (B-5) can be approximated by

$$G_A = 2 \gamma_A, \text{ (erg/cm}^2\text{)} \quad (\text{B-6})$$

If the materials in contact are sufficiently similar or interact, as evidenced by mutual solubility or the formation of intermetallic compounds, Equation (B-5) can be approximated by

$$G_{AB} = 3/4 (\gamma_A + \gamma_B), \text{ (erg/cm}^2\text{)} \quad (\text{B-7})$$

If the contacting materials are very insoluble and do not form intermetallic compounds, the value of γ_{AB} is quite low, and the Equation (E-5) approximation becomes

$$G_{AB} \approx 1/2 (\gamma_A + \gamma_B)' \text{ (erg/cm}^2\text{)} \quad (\text{B-8})$$

B.3 WEAR PARTICLE DIAMETER

Two groups of adhesive wear particles can be distinguished by their behavior and their size. The larger particles fall free after being generated from the substrate, and in a moving fluid are quickly swept from the wearing interface. The smaller size particles at first adhere to the surface that pulled them from their original matrix. Later they transfer back and forth between the two surfaces, growing by agglomeration of other adherent particles which they encounter. Finally they become large enough and are released by the wearing surface.

In practice, each group of wear particles has a spread in size of approximately a factor of ± 3 on either side of the average. For loose particles, the average diameter is given by

$$c_l = 2.60 * 10^2 \frac{G_{AB}}{p_A} \text{ , (}\mu\text{in.)} \quad (\text{B-9})$$

Therefore, the minimum size loose particle generated can be calculated from

$$c_{\min} = 87 \frac{G_{AB}}{p_A} \text{ , (}\mu\text{in.)} \quad (\text{B-10})$$

If the minimum loose particle diameter is equal to the size of the minimum adhesive junction diameter, the load which would produce a contact area whose diameter is the same as that of the minimum wear particle can be calculated from

$$F_{l, \min d} = 7.32 * 10^{-6} \frac{G_{AB}^2}{p_A} \text{ , (lb)} \quad (\text{B-11})$$

The diameter of the average particle of material which is adherent on material B can be calculated from

$$c_u = 52 \frac{\gamma_A}{p_A}, \text{ (}\mu\text{in.)} \quad (\text{B-12})$$

Note the use of γ_A instead of G_{AB} in this and subsequent equations (following Rabinowicz).

The diameter of the smallest adherent particle can be found from

$$c_t = 17 \frac{\gamma_A}{p_A}, \text{ (}\mu\text{in.)} \quad (\text{B-13})$$

Since c_t is approximately 10 percent of c_{\min} and allowing for statistical spread, it follows that if the applied load is less than 5 percent of $F_{I, \min}$, no particles will be formed and no adhesive wear will occur. This corresponds to

$$F_{I, \text{ no wear}} \leq 3.76 * 10^{-7} \frac{\gamma_A^2}{p_A}, \text{ (lb)} \quad (\text{B-14})$$

These impact force limits are calculated to be: copper, $5.5 * 10^{-3}$ lb; steel, $7.5 * 10^{-5}$ lb; tungsten carbide, $2.3 * 10^{-5}$ lb; and nickel, $6.6 * 10^{-2}$ lb. Such low values of the force are not practical for use in low-leak valve design, so of necessity, some adhesive wear must occur.

Appendix C

RATE OF WEAR OF CLOSURE SURFACES

C.1 LOOSE PARTICLE WEAR

It is assumed that loose particles have a hemispherical shape, as is done in Ref 13, we define, from Equation (14),

$V_{t,h}$ = Volume of average loose particle (hemispherical shape), in.³

$$V_{t,h} = 1/2 * 4/3 \pi \left(\frac{c_l * 10^{-6}}{2} \right)^3, (\text{in.}^3) \quad (\text{C-1})$$

or

$$V_{t,h} = 4.60 * 10^{-12} \left(\frac{G_{AB}}{P_A} \right)^3, (\text{in.}^3) \quad (\text{C-2})$$

The observed shape of the adhesive wear pits and particles approaches sphere segments (see Section 3.1.2), which indicates that a modified formula should be used for calculation of particle volumes. The equation for the volume of a segment of a sphere is

$$V = 2 \frac{1}{6} \pi h (h^2 + 3r^2) \quad (\text{C-3})$$

where

h = segment height (= pit depth)

r = radius across segment

In the present case, $h=r/4$, so Equation (C-3) reduces to

$$V_F = 0.127 \pi r^3 \quad (\text{C-4})$$

where

subscript F = flat particle

(The equivalent formula for hemispherical particles is

$$V_h = 0.67 \pi r^3, (\text{in.}^3) \quad (\text{C-5})$$

These equations yield particle volumes of 8.58×10^{-11} and $4.48 \times 10^{-10} \text{ in.}^3$, respectively, for the observed pit diameters. The segment-shaped particles are about one-fifth the volume of hemispherical ones of the same radius. For particles of this shape, the equation relating loose particle volume to G_{AB}/p_A is then

$$V_{l,F} = 8.7 * 10^{-13} \left(\frac{G_{AB}}{F_A} \right)^3, (\text{in.}^3) \quad (\text{C-6})$$

If $N_{l,F}$ is the number of loose, flat particles generated per stroke, and $V_{w,l}$ (Equation 17) is the total volume of free particles formed, since

$$V_{w,l} = 7.04 * 10^{-4} \left(\frac{k_{ad} F_I s}{P_A} \right), (\text{in.}^3) \quad (\text{C-7})$$

then

$$N_{l,F} = V_{w,l} \div V_{l,F}, (\text{particles}) \quad (\text{C-8})$$

Substituting F_I from Equation (A-11) into Equation (C-7), then combining with Equations (C-6) and (C-8) we obtain

$$N_{l,F} = 5.04 * 10^7 \left[\frac{k_{ad} E}{P_A \sigma_y} \left(\frac{p_A}{G_{AB}} \right)^3 \right] \left[\frac{h_s}{t_T} \right] \left[\frac{W_{I,e}}{\tau_c} \right] \quad (\text{C-9})$$

Using the data in Appendix F and in the tables in Section 3.3.3.1, the sizes and numbers of loose wear particles for a few materials were calculated. The data are presented in Table C-1.

Table C-1

PARAMETERS OF LOOSE WEAR PARTICLE GENERATION

Term	Copper	Steel	Tungsten Carbide	Duranickel
C_{ℓ} , $\mu\text{in.}^3$ (Equation B-9)	$7.2 * 10^3$	$9.36 * 10^3$	$2.08 * 10^2$	$4.16 * 10^3$
$V_{w,\ell}$ (F_I from Equation A-11)	$4.71 * 10^{-9}$	$7.1 * 10^{-1}$	$9.2 * 10^{-15(a)}$	$4.3 * 10^{-12(b)}$
$V_{\ell,F}$ (Equation C-6)	$1.91 * 10^{-8}$	$4.06 * 10^{-8}$	$4.43 * 10^{-13}$	$3.57 * 10^{-9}$
$N_{\ell,F}$ (per stroke)	$2.47 * 10^{-1}$	$1.74 * 10^{-4}$	$2.08 * 10^{-2}$	$8.42 * 10^{-3}$
<div> <div>(a) k_{ad} for WC estimated = $4 * 10^{-5}$</div> <div>(b) k_{ad} for Ni estimated = $7 * 10^{-3}$</div> </div>				

These low values for the number of particles formed suggest that the primary wear mechanism cannot be caused by formation of loose particles, but that formation of adherent particles must also be considered.

C.2 COMBINED WEAR

In analogy to the above derivation, note that the volume of the average adherent flat particle is, after setting $G_{AB} = 2 \gamma_A$,

$$V_{u,F} = 6.98 * 10^{-15} \left(\frac{G_{AB}}{P_A} \right)^3, (\text{in.}^3) \quad (\text{C-10})$$

There is no test information available on the total volume of adherent particles formed, but according to Rabinowicz (Ref 13), the number of particles generated is a function of the reciprocal of the cube of the particle diameter.

$$N = f\left(\frac{1}{c}\right) \quad (\text{C-11})$$

Hence the number of particles of diameter c_2 can be calculated from the known number with diameter c_1 by means of the equation

$$N_2 = N_1 \left(\frac{c_1}{c_2} \right)^3 \quad (\text{C-12})$$

or, in the particular case at point

$$N_{u,F} = N_{l,F} \left(\frac{c_l}{c_u} \right)^3 \quad (\text{C-13})$$

Since

$$c_l = 2.60 * 10^2 G_{AB}/P_A \quad (\text{Equation B-9})$$

$$c_u = 52 \gamma_A/P_A \quad (\text{Equation B-12})$$

and

$$G_{AB} = 2 \gamma_A \quad (\text{Equation B-6})$$

Then

$$c_l / c_u = 10$$

and

$$N_{u,F} = 10^3 N_{l,F} \quad (\text{C-14})$$

An appreciable number of particles are predicted to be generated per closure stroke of the ACS valve, ranging from 250 for copper to 0.1 for steel (data from Table C-1).

The process occurring on the closure surfaces then consists of

- A. Generation of loose wear particles of some average size (depending on the closure material), and causing roughening by the pits formed when the particles are generated.
- B. Generation of adherent wear particles which cause surface roughening by two modes - pit formation and also peak formation where the particles adhere.

In order to properly calculate surface damage, all these processes must be included. Hence the equations must be bimodal to account for the effects of both size ranges of particles.

Define A_j as the circular cross section of the particle j , where $j = l$ or u . Then (dropping the subscript F),

$$A_j = \frac{\pi}{4} (c_j * 10^{-6})^2, \text{ (in.}^2\text{)} \quad (\text{C-15})$$

Let A_Σ be the total equivalent area of all particles generated per stroke

$$A_\Sigma = \sum_j N_j A_j, \text{ (in.}^2\text{)} \quad (\text{C-16})$$

A_c has been previously defined as the total contact area between seat and poppet

i. e.

$$A_c = \frac{\pi}{4} (D_o^2 - D_i^2), (\text{in.}^2) \quad (\text{C-17})$$

Then let Z_w be the fraction of the surface area worn by a single stroke;

$$Z_w = A_j \div A_c \quad (\text{C-18})$$

and the fraction unworn

$$Z^o = 1 - Z_w$$

By substitution

$$Z_w = 6.95 * 10^3 \left(\frac{k_{ad} E}{G_{AB} \sigma_y} \right) \left(\frac{hs}{t_T} \right) \left(\frac{W_{I,e}}{\tau_c} \right) \quad (\text{C-19})$$

The depth of pits from either loose or adherent particles are 1/4 the particle radius or 1/8 of the diameter, c_j (Section 3.3.2.2). The AA surface finish in the immediate neighborhood of and including the pit is 1/4 of the pit depth. Similarly, the asperity heights due to adherent particles are equal to 1/8 of the particle diameters (assuming that they lie with their longer dimensions along the surface), and the finish in the neighborhood of the particle is 1/4 of the height.

Then the surface roughness y_j , for each process is found by means of

$$y_j = 1/4 * 1/8 c_j, (\mu \text{ in.}) \quad (\text{C-20})$$

and the average roughness in the worn area will be

$$\bar{y}_j = \frac{\sum_j A_j y_j}{A \sum_j}, (\mu \text{ in.}) \quad (\text{C-21})$$

which, by substitution, is equal to

$$\bar{y}_j = 1.18 * 10^{-8} \left(\frac{G_{AB}}{P_A} \right)^3 \left(\frac{\sigma_y G_{AB}}{k_{ad} E} \right) \left(\frac{t_T}{sh} \right) \left(\frac{\tau_c}{W_{I,e}} \right), (\mu \text{ in.}) \quad (\text{C-22})$$

In order to calculate the effect of wear on the surface finish, the following assumptions are made:

- A. The probability of wear in any location on any stroke is numerically equal to Z_w , the fraction of the surface worn in one stroke.
- B. The probabilities of wear at any location on successive strokes are independent.
- C. Multiple wear strokes at any location do not cause degradation any greater than the first wear strokes.
- D. Impact is parallel.

The fraction unworn after n strokes is then

$$Z_n^o = (Z^o)^n = (1 - Z_w)^n \quad (C-23)$$

The fraction worn after n strokes

$$Z_{w,n} = 1 - (Z^o)^n = 1 - (1 - Z_w)^n \quad (C-24)$$

Then $\bar{y}_{n,j}$ = overall average surface finish after n strokes

$$\bar{y}_{n,j} = y^o Z_n^o + \bar{y}_j Z_{w,n} \quad (\mu \text{ in.}) \quad (C-25)$$

$$\bar{y}_{n,j} = y^o (1 - Z_w)^n + \bar{y}_j (1 - [1 - Z_w]^n) \quad (\mu \text{ in.}) \quad (C-26)$$

$$\bar{y}_{n,j} = (y^o - \bar{y}_j) (1 - Z_w)^n + \bar{y}_j \quad (\mu \text{ in.}) \quad (C-27)$$

By expansion and substitution of actual values, it is easily shown that most terms are of second or higher order, and that Equation (C-27) is equivalent to

$$\bar{y}_{n,j} = y^o + n\bar{y}_j Z_w - ny^o Z_w \quad (\mu \text{ in.}) \quad (C-28)$$

Solutions to this equation for several materials are presented in Table 3-5

C.3 'WET' VALVE WEAR RATES

When the valve is operated with a liquid propellant flowing through it, the rate of wear is changed by a considerable amount. The exact correction factors which apply to CPF are not known, but it is possible to make some estimates which should at least indicate the direction that will be taken.

- A. From valve manufacturer's data, the presence of a fluid will reduce F_I in the 'floating' piston model by a factor of 3 (Ref 32).
- B. The data in Table 3-4 for k_{ad} in the presence of liquid propellants show a change in k_{ad} for steel of about 10^{-2} , which is equivalent to good lubrication. This factor will be applied to all closure materials.
- C. The data in Table 3-3 for wear particle size indicate that a good lubricant changes the particle size of copper by a factor of 10^{-1} . This factor will be applied for all closure materials.

When these new factors are introduced into the equations for calculation of surface finish, the increased life spans are dramatic (see Table 3-5).

Appendix D IMPACT HEATING

D.1 ENERGY RELEASE AT REACTION INTERFACE

According to Toy et al. (Ref 9), impact energy available for reaction initiation appears as friction resulting from radial expansion of the vertically compressed surfaces. The maximum rate of energy release occurs at the perimeter of the member with the smaller diameter—the pin in ABMA tests and the seat land in the ACS valve. In the same reference it is pointed out that only that portion of the energy released in the upper 0.002 in. of the material is usable for reaction initiation. At greater depths, the metal is too far from the liquid propellant to undergo reaction. The following equation is derived in Ref 9 for calculating the energy release rate at material interfaces to a depth of 0.002 in.

$$\begin{aligned} \frac{dU_{fij}(r, \tau)}{d\tau} = & \frac{\mu_{ij}}{12} \frac{rP(\tau)}{d\tau} \left[\frac{\Lambda_i}{E_i} \left(1 - \frac{1 - \Lambda_i}{2} \right) \left(\frac{r_i^2 - r_{pn}^2}{r_i^2} \right) \right. \\ & \left. - \frac{\Lambda_j}{E_j} \left(1 - \frac{1 - \Lambda_j}{2} \right) \left(\frac{r_j^2 - r_{pn}^2}{r_j^2} \right) \right], \text{ (ft-lb/sec)} \end{aligned} \quad (D-1)$$

where

$\frac{dU_{fij}(r, \tau)}{d\tau}$ = rate of energy release at distance r from center of striker pin, at time τ after impact, between materials i and j

μ_{ij} = coefficient of friction between surfaces of materials in test

$P(\tau)$ = pressure at time, τ due to compression, lb/in.²

Λ = Poisson's ratio

E = Bulk modulus, lb/in.²

r_{pn} = Radius of first member (= striker pin radius for ABMA tester), in.

r_i = radius of i'th member, in.

r_j = radius of j'th member, in.

Because the pin-specimen interface on the ABMA tester is of primary interest in the current program, we reduce $i = pn$ or $r_i = r_{pn}$ and Equation (D-1) becomes:

$$\frac{dU}{d\tau} = \frac{\mu r_{pn} P(\tau)}{12} \frac{dP(t)}{d\tau} \left[\frac{\Lambda_{pn}}{E_{pn}} - \frac{\Lambda_{sp}}{E_{sp}} \left(1 - \frac{1 - \Lambda_{sp}}{2} \right) \left(\frac{r_{sp}^2 - r_{pn}^2}{r_{sp}^2} \right) \right] \quad (D-2)$$

where subscript sp = specimen

For the ACS valve, in which the seat has the smaller radius and the same material is used for both seat and poppet, the equation is transformed to:

$$\frac{dU}{d\tau} = 4.17 \times 10^{-2} \frac{\Lambda_{\mu} P D_o}{E} \left(\frac{1 - \Lambda}{2} \right) \left(\frac{r_p^2 - (D_o/2)^2}{r_p^2} \right) \frac{dP}{d\tau}, \text{ (ft-lb/sec)} \quad (D-3)$$

D.2 SAMPLE CALCULATION-ABMA PROCESS

In order to apply Equation (D-2) or (D-3), the sequence of events during compression loading and releasing must be understood. In the tests reported in Ref 9, it was demonstrated that the behavior of the ABMA system was remarkably constant for a wide variation in test parameters. The pressure-time history at the striker pin-specimen interface was determined by placing a strain gage at that location. It was determined that the duration of the process from initial contact to final rest was a constant that did not vary for different loads. At constant impact energy, the pressure-time curves were superimposable even with a variety of materials used for different members. For different impact energies, the $P(\tau)$ curves were of similar shape and could be superimposed simply by changing the scale or gain used to record the pressure.

The above points are emphasized, because this constancy of behavior is the basis for solution of Equation D-2 for impact energies different than those for which strain gauge traces are available.

The calculation of $P(\tau)$ starts with defining its maximum value. Then, the relation of $P(\tau)$ to time is developed. From this relation, $dP(\tau)/d\tau$ is calculated at various times.

The relation between the peak pressure, $P(\tau)_{\max}$, at various impact energies Z , and that at 72 ft-lb is given in Ref 9 as

$$P(Z, \tau)_{\max} = \sqrt{\frac{Z}{72}} P(72, \tau)_{\max}, \text{ (lb/in.}^2\text{)} \quad (\text{D-4})$$

and the value for $P(72, \tau)_{\max}$ was found to be 159,000 lb/in.² at $\tau = 0.234$ sec in the same reference. Hence $P(\tau)_{\max}$ can be calculated simply for any impact energy. As stated earlier, the $P(\tau)$ curves all have the same shape, only the height of the peak varies. Because of this, a single curve can be used to represent all the data, if the curve is normalized by plotting $P(\tau)/P(\tau)_{\max}$ (i. e. percent of $P(\tau)_{\max}$) versus time. This curve is presented as Figure D-1.

In order to determine $dP/d\tau$, the inflection points were found at 0.023 and 0.417 ms.

The first derivative of the curve was taken as equal to zero at time zero, at 0.234 ms. and at 0.6 ms. The slope of the $P(\tau)$ curve was measured at the two inflection points to calculate the maximum values for $dP(\tau)/d\tau$. The absolute values of the maxima and the zero values are also plotted on Figure D-1 to give the bare outline shape of the $dP(\tau)/d\tau$ curve. This curve has also been normalized, $(dP/d\tau)_{\max} = 2.05 \times 10^9$ psi/sec for $P(\tau)_{\max} = 3 \times 10^5$ psi.

Note that energy flows in the reverse direction after the maximum stress is reached, from the compression of the interface materials back to the plumbet. This energy flow is also responsible for frictional heating at the interface, so that absolute values of $|dP/d\tau|$ (and $|dU/d\tau|$) are of interest, rather than their signs.

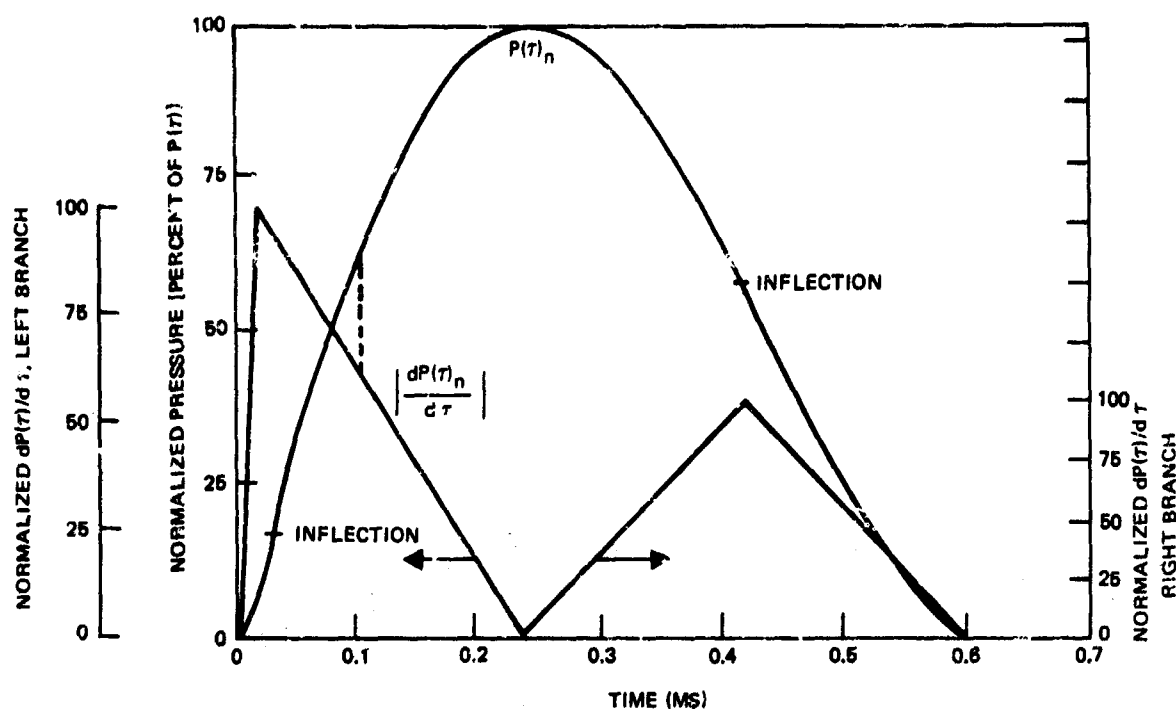


Figure D-1. Normalized Pressure Curves for Various Impact Energies

The solution of Equation (17) for a maximum value of the energy release rate requires that the product of $P(\tau)$ and $dP(\tau)/d\tau$ taken at the same instant of time be a maximum. A trial-and-error evaluation of the product was performed by reading appropriate points from Figure 4-4. The maximum value for the product was found to occur at 0.1 ms after impact and is equal to $0.632 [P(\tau)]_{\max}$ times $0.632 [dP(\tau)/d\tau]_{\max}$. A typical value for this product is 2.43×10^{14} psi²/sec for a 252 ft-lb impact.

In order to calculate the temperature reached at the interface during impact, it is necessary to find the average values for $dU/d\tau$ over the impact time interval. Equation (D-2) can be used for this purpose by performing the calculation using average values of $P(\tau)$ and $dP(\tau)/d\tau$. Average $P(\tau)$ is taken as 0.55 times the maximum value (the factor 0.55 was obtained by inspection of Figure D-1). Average $dP(\tau)/d\tau$ was taken as one half of the total area under the $dP(\tau)/d\tau$ curve.

Table D-1 has some values for P and $dP/d\tau$ calculated for several impact energies.

TABLE D-1
INTERFACE PRESSURES AT VARIOUS IMPACT ENERGIES

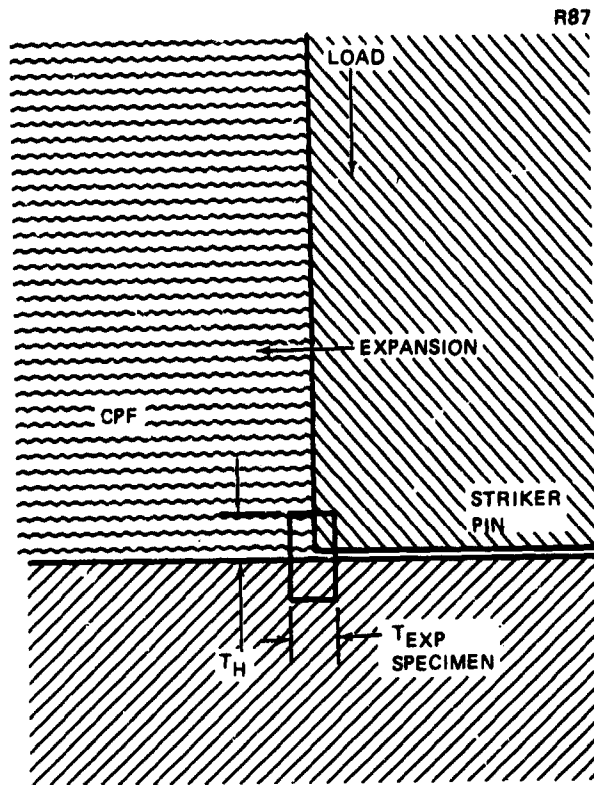
Impact Energy (ft-lb)	Peak Pressure P_{max} (lb/in. ²)	Peak Pressure Rate (lb/in. ² -sec)	Average Pressure P_{av} (lb/in. ²)	Average Pressure Rate (lb/in. ² -sec)
50	133,000	9.10×10^8	73,200	5.01×10^8
100	187,000	1.27×10^9	103,000	7.05×10^8
200	265,000	1.82×10^9	146,000	1.00×10^9
300	324,000	2.22×10^9	178,000	1.22×10^9

D.3 TEMPERATURE INCREASE DUE TO IMPACT

When the radial expansion occurs due to the vertical compression, the energy calculated by means of equation D-2 (or D-3) appears as friction heat at the periphery of the smaller member.

Using some straightforward assumptions about the processes occurring, it is possible to derive an equation which can be used to calculate a predicted interface temperature. The assumptions used are the following:

- A. The heat is released over the 'length' of the radial expansion of the member of smaller diameter. For the ABMA tester, this amounts to 7.5×10^{-4} in.
- B. The material heated corresponds to the above length, to a depth of 2×10^{-3} in., the value earlier suggested (Ref 9) as the maximum depth to which reaction can occur.
- C. The energy input is partitioned between the two members and the fluid in accordance with their locations, as shown in the sketch.
- D. The energy is used solely to heat the materials. A correction term can be introduced to account for loss of energy by thermal conductivity, radiation, etc. However, when this was done, it was found that such heat losses amount to a maximum of 0.1 percent of the energy input because the process occurs in such a short time interval.
- E. The fluid boils and vaporizes because of the heat input. The temperature for this change of phase is not defined, so for convenience in relating to the operating conditions of the ACS valve, the boiling point at the maximum valve operating pressure is selected (160°F at 450 psia).
- F. Because the impact process is so rapid, it is considered that negligible PV expansion of the vapor will occur, and no term is included for this work.
- G. Although the heat capacities of materials are known to change with temperature, for current purposes it is sufficient to use constant values.



The equation as derived below has actually been generalized beyond Point C above to include the conditions where the lower member is smaller than the upper, and also for where they have the same diameter.

The derivation is as follows:

Let subscript UP indicate upper member, LO indicate lower member, and f indicate fluid.

If:

$$r_{UP} < r_{LO}, K_{UP} = 1, K_{LO} = 2, K_f = 1$$

$$r_{UP} > r_{LO}, K_{UP} = 2, K_{LO} = 1, K_f = 1$$

$$r_{UP} = r_{LO}, K_{UP} = 1, K_{LO} = K_f = 2$$

The cross-section area of the heated region was defined above as the radial expansion times the reactive depth

$$A_H = r_{\text{exp}} * r_H, (\text{in.}^2) \quad (\text{D-5})$$

Then the volume heated is equal to this area times the circumferences of the smaller member.

$$V_H = r_{\text{exp}} * r_H * \pi * d_{\text{min}}, (\text{in.}^3) \quad (\text{D-6})$$

($d_{\text{min}} = D_o$ for ACS valve, $= d_{\text{pn}}$ for ABMA tester)

The volume is partitioned into 3 portions—upper member, lower member, and fluid. These volumes are then, for the i 'th component

$$V_i = 2K_i r_{\text{exp}} r_H \pi d_{\text{min}}, (\text{in.}^3) \quad (\text{D-7})$$

and the weights are

$$W_i = 2K_i \rho_i r_{\text{exp}} r_H \pi d_{\text{min}}, (\text{lb}) \quad (\text{D-8})$$

There are four separate processes which absorb heat as the reaction zone is heated: (1) heating of metal, (2) heating of liquid to the boiling point, (3) evaporation of the liquid, and (4) heating of vapor to the final temperature.

Let heat capacities be symbolized by Γ .

If U_T is the energy input, then

$$\begin{aligned} U_T = & \Gamma_{\text{UP}} W_{\text{UP}} \Delta T + \Gamma_{\text{LO}} W_{\text{LO}} \Delta T + \Gamma_f W_f (T_B - T_{\text{INIT}}) \\ & + L_V W_f + \Gamma_P W_f (T_{\text{FIN}} - T_B) \end{aligned} \quad (\text{D-9})$$

but

$$\Delta T = (T_{\text{FIN}} - T_B) + (T_B - T_{\text{INIT}}) \quad (\text{D-10})$$

$$\therefore T_{\text{FIN}} - T_B = \Delta T - (T_B - T_{\text{INIT}}) \quad (\text{D-11})$$

$$\begin{aligned} U_T = & \Gamma_{\text{UP}} W_{\text{UP}} \Delta T + \Gamma_{\text{LO}} W_{\text{LO}} \Delta T + \Gamma_f W_f (T_B - T_{\text{INIT}}) \\ & + L_V W_f + \Gamma_P W_f (\Delta T - (T_B - T_{\text{INIT}})) \end{aligned} \quad (\text{D-12})$$

This rearranges to

$$\begin{aligned} U_T = & \Delta T (\Gamma_{\text{UP}} W_{\text{UP}} + \Gamma_{\text{LO}} W_{\text{LO}} + \Gamma_P W_f) \\ & + (T_B - T_{\text{INIT}}) (W_f (\Gamma_f - \Gamma_P)) + W_f L_V \end{aligned} \quad (\text{D-13})$$

substituting $1.288 * 10^{-3} \tau_c dU/d\tau$ for U_T (the constant serves to change the units of $dU/d\tau$ from ft lb to Btu) and equation D-8 for W_i , and rearranging

$$\Delta T = \frac{1.288 * 10^{-3} \tau_c dU/d\tau - (2\pi/K_f \rho_f r_{\text{exp}} r_H d_{\text{min}}) \{L_V - (T_B - T^0) (\Gamma_f - \Gamma_P)\}}{2\pi r_{\text{exp}} r_H d_{\text{min}} (K_{\text{UP}} \rho_{\text{UP}} \Gamma_{\text{UP}} + K_{\text{LO}} \rho_{\text{LO}} \Gamma_{\text{LO}} + K_f \rho_f \Gamma_P)}, \quad (^\circ\text{F}) \quad (\text{D-14})$$

This equation is more accurate than the version given in the interim report. When it is used, the ignition temperature for Duranickel 301 in CPF, calculated from ABMA tests, is 1,950°F (calculation with the earlier equation gave a temperature of 2,280°F).

Appendix E

ROTARY SLIDING FRICTION AND PLASTIC DEFORMATION INITIATION

E. 1 INTRODUCTION

Friction and local plastic deformation can be involved in the initiation of reactions between structural materials and high-energy liquid propellants. Pure friction generates local hot spots which may be enough to initiate the reaction. When local plastic deformation is also involved, fresh material surfaces are exposed to the propellant while they are still hot.

An apparatus to study initiation under conditions which cause friction and/or local plastic deformation is described below.

E. 2 TEST SYSTEM

The apparatus consists of a pendulum, impact arm and latch mechanism, pneumatic cylinder, calibrated dial, and test section (Figure 4-8). A lower test specimen fits in the specimen holder, and an upper specimen is attached to the test rod (Figure 4-1). The two specimens can be made of the same or of different materials. The specimen faces are placed in contact, then a pneumatic cylinder is used to apply a vertical compression load to the specimens. The specimens are located in a double moat; the first contains the liquid propellant test fluid, and the second contains a refrigerant (e.g., LN_2 for operation at -320°F). A transparent shield surrounds the entire test section to allow visual observation of the system during the test while controlling the atmosphere around the test section. A self-aligning hydraulic mount underlies the lower specimen and moat assembly.

Energy is supplied to the mechanism by a swinging pendulum which strikes the arm and latch mechanism. The pendulum motion is translated into horizontal rotational movement of the upper test specimen. When the pendulum contacts the arm, the test rod, arm, latch and bearings are accelerated to a speed independent of the load and the angle of rotation. The angle of rotation is controlled by the position of the latch release.

The final height that the pendulum reaches after striking the arm and latch mechanism is measured by a pointer on the calibrated dial. In addition to the pointer position, irregularities such as excessive vibration, safety hazards, and noises, or any sign of wear, are noted.

From its usual start position, 48 in. above the impact arm, the pendulum is capable of delivering 50 ft-lb of energy; of this, 9 ft-lb are dissipated in the apparatus other than at the specimen interface, and 41 ft-lb are available for tests. The standard deviation was determined to be ± 0.03 ft-lb.

The apparatus connects to a gas oxidizer supply manifold, liquid oxidizer supply, purge, vacuum, and LN_2 supply. The plumbing system is very similar to that of the ABMA Impact Tester.

E. 3 SPECIMEN DETAILS

The upper specimen has a diameter of $3/8$ in. on its lower bearing face and $1/2$ in. on its upper portion. The test rod is also of $1/2$ -in. diameter. The lower specimen is a square, 1 in. on edge, with rounded corners, and $1/16$ -in. thick.

E. 4 TEST PROCEDURE

- A. Sample Preparations--The test faces of the rotating upper specimen and square lower-sheet specimen are machined to a 32 microinch finish, and then polished with 400 grit silicon carbide paper using a machine oil lubricant. They are cleaned in acetone, air dried, dipped in Oakite cleaner for 2 minutes, flushed with distilled water, and dried with gaseous nitrogen. Before the specimens are tested, they are degassed in trichloroethylene, dried in GN_2 , cleaned in Freon, dried in GN_2 , and packaged in polyethylene bags. Porous and plastic specimens are vacuum baked at 105°C , 1 torr, 18 hours after cleaning.
- B. Apparatus Cleaning--The test chamber components are cleaned in the same pretest manner as the pin and sheet specimens.
- C. Test Preparations--The GN_2 pneumatic cylinder supply is placed in an operating condition by opening supply valves and checking out remote valve controls.

The specimen holder and pin and sheet specimens are placed in position. The pendulum is raised and locked in position. The arm and latch is set to proper

angle of rotation, $\theta \leq 30$ degrees. The pointer for the calibrated disk is set at a position where the swing of the pendulum will engage and move it to a point of maximum follow through of the pendulum. The glass viewing shield for the test chamber is closed and a GN_2 sweep line connected to the test chamber. The compartment is purged sufficiently to remove all moisture and a positive pressure is maintained. The oxidizer supply is connected.

Further operations are carried out remotely from the control room. The mechanical safety catch is released so that the solenoid switch will release the pendulum. The pneumatic cylinder is pressurized to the predetermined value required to load the specimen in compression and the pressure recorded. The room ventilator is turned on. The oxidizer control valve to test chamber is opened and approximately 5 ml of liquid oxidizer is flowed into the test fluid cup. The test cell is darkened and the solenoid switch is actuated to release the pendulum. The system is observed carefully to detect possible reaction flashes.

The pressure in the pneumatic cylinder is released to remove the load from the specimens. The GN_2 sweep is turned on to purge propellant residues.

After waiting until all propellant has dissipated as determined by a monitoring system, the test cell is reentered. The positions of the pointer on the calibrated disk and the indicating arm are recorded. The specimens are removed, decontaminated, and examined visually and with a microscope for signs of reactions. If no reaction sites are observed, the test procedure is repeated four more times at the same test setting. Zero reactions in five tests are taken to indicate that the particular conditions are not hazardous.

Test data are recorded on the Test Report Form (Figure E-1).

E.5 CALCULATIONS

The energy imparted to the system is computed by calculating the difference between the pendulum's initial and final height (from the calibrated disk reading). This gives the total energy released during its swing. From this is subtracted the energy dissipated in the apparatus itself, 9 ft-lb, determined in calibration tests. The remainder is the energy imparted to the specimens.

PROPELLANT _____ TEMPERATURE _____

SPECIMEN PARAMETERS	UPPER	LOWER
Shape and Dimensions		
Material		
Surface Finish		

[illegible]

148

Appendix F

DATA FOR CALCULATIONS

The numerical data tabulated in this appendix have been collected in one place for convenience when performing calculations using the various equations presented in the report. There are four categories of data presented.

- Material properties (Table F-1)
- CPF properties (Table F-2)
- Valve configuration parameters (Table F-3)
- Equation constants $K_0 = 0.5 \text{ erg/cm}^2\text{°K}$

Table F-1
MATERIAL PROPERTIES

	17-4 PH	Copper	Steel	Zinc	WC	WC in Co
$M_p, ^\circ F$	2,800 (Iron)	1,980	2,800 (Iron)	787	5,200	--
$C_{AB}/F, \text{\AA}$	--	28	36	42	1.1	0.8
$L_V, \text{erg/gm}$	6.81×10^{10} (Iron)	7.36×10^{10}	6.81×10^{10} (Iron)	1.52×10^{10}	--	--
$\rho_M, \text{lb/in.}^3$	0.281	3.21×10^{-1}	2.8×10^{-1}	2.6×10^{-1}	5.63×10^{-1}	5.38×10^{-1}
$q_M, \text{Btu/in. sec } ^\circ F$	2.41×10^{-4}	5.15×10^{-3}	8.1×10^{-4}	1.51×10^{-3}	--	9.26×10^{-4}
E, psi	2.9×10^7	1.7×10^7	3.1×10^7	1.3×10^7	8.56×10^7	9.1×10^7
α_Y, psi	1.80×10^5	4.5×10^3	5.6×10^5	1.8×10^3	9×10^5	6.9×10^5
$P_A, \text{kg/mm}^2$	--	80	1,000	38	1,950	1,800
$f_m, \text{Btu/lb}$	0.12	1.0×10^1	1.2×10^{-1}	1.0×10^{-1}	--	5×10^{-2}
N (dimensionless)	0.305	0.355	0.30	0.25	--	0.21
		<u>Dry</u> <u>Lubed</u>	<u>Dry</u> <u>Lubed</u>	<u>Dry</u> <u>Lubed</u>		<u>Dry</u> <u>Lubed</u>
k_{ad} (dimensionless)	--	3.2×10^{-2} 1×10^{-5}	4.5×10^{-2} 2×10^{-5}	1.6×10^{-1} --	--	--
μ_f (static) (dimensionless)	--	1.6 0.08	0.58 0.1	0.85 0.04	--	0.58 0.1

Table F-2
CPF PROPERTIES

$$\rho_f = 6.47 * 10^{-2} \text{ lb/in.}^3 : \Gamma_f = 3.3 * 10^{-1} \text{ Btu/lb}^\circ\text{F}$$

$$\Gamma_P = 0.198 \text{ Btu/lb } ^\circ\text{F} : q_f = 1.39 * 10^{-6} \text{ Btu in. /in.}^2 \text{ sec } ^\circ\text{F}$$

$$\text{Bp}_{1 \text{ atm}} = 8.4^\circ\text{F} : L_v = 74.7 \text{ Btu/lb} : \text{Bp}_{450} = 160^\circ\text{F}$$

$$\eta = 3.38 * 10^{-4} \text{ lb/ft-sec}$$

Table F-3
VALVE CONFIGURATION PARAMETERS

$H^0 = 1 \text{ } \mu\text{in.}$	$r_p = 5 * 10^{-1} \text{ in.}$	$W_T = W_a + W_p = 1.63 * 10^{-1} \text{ lb}$
$D_i = 1 * 10^{-1} \text{ in.}$	$s = 1 * 10^{-5} \text{ in.}$	$\sigma_s = 300 \text{ psi}$
$D_o = 1.24 * 10^{-1} \text{ in.}$	$\tau_c = 1 * 10^{-4} \text{ sec}$	$W_{i,e} = W_p + W_f + R\delta_c = 1.364 * 10^{-1}$
$F_{\Delta P \bullet}(\text{CPF}) = 0.12 \text{ lb (est)}$	$t_T = 1.9 * 10^{-1} \text{ in.}$	$d_d = 5 * 10^{-3}$
$F_{s \bullet} = 6.6 \text{ lb}$		$\alpha = 0.5 \text{ degrees}$
$h = 1.2 * 10^{-2} \text{ in.}$	$W_f = (\text{CPF}) = 3.6 * 10^{-4} \text{ lb}$	$\omega = 1.2 * 10^{-2} \text{ in.}$
$R = 1,300 \text{ lb/in.}$	$W_p = 6 * 10^{-3} \text{ lb}$	$r_d = 2.5 * 10^{-3} \text{ in.}$
$R * \delta_c = 1.3 * 10^{-1} \text{ lb}$	$r_H = 2 * 10^{-3} \text{ in.}$	$F_T = 6.72 \text{ lb}$
$\delta_c = 8.4 * 10^{-3} \text{ in.}$	$r_{pn} = 2.5 * 10^{-1} \text{ in.}$	$r_{sp} = 3.12 * 10^{-1} \text{ in.}$
$r_N = 1.33 * 10^{-1} \text{ in.}$	$B = 6.2 * 10^{-2} \text{ in.}$	$r_{exp} = 7.5 * 10^{-4} \text{ in.}$

APPENDIX G

GLOSSARY OF SYMBOLS

Main Symbols

A	area; contact area, in. ²
Å	Angstrom unit
Al	aluminum
a	acceleration, ft/sec ²
B	initial contact position on poppet, radial location, in.
C	diameter of wear particle, microns (micrometers)
Cl	chlorine
c	diameter of wear particle, microinch (μ in. or in. $\times 10^{-6}$)
D	seat diameter, in.
d	diameter, in.
E	bulk modulus (Young's modulus), lb/in. ² — impact energy, ft-lb
EDH	equivalent drop height, in.
E ₅₀	50-percent reaction threshold energy, ft-lb
F	force, lb — fluorine — Fahrenheit, deg
F ₂	molecular fluorine
G	energy of adhesion, erg/cm ² or dyne/cm
g	acceleration of gravity, ft/sec ²
H	surface finish, μ in. or in. $\times 10^{-6}$ — hydrogen
H ₂	molecular hydrogen
h	poppet stroke, in. -- drop height (friction tester), in.

Main
Symbols (Continued)

I	chemical element, unspecified
J	chemical element, unspecified
j	reaction constant — psuedo concentration
K	equation constant
k	process constant
L	latent heat of phase change, Btu/lb — liquid
l	applied load, lb
\dot{M}	rate of formation of fluoride film, mass/time
m	molecular diameter, cm
N	number of particles -- nitrogen
n	number of valve cycles
P	pressure, lb/in. ² (absolute)
p	Vickers penetration hardness, kg/mm ²
Q	gas leakage rate, s. c. c. He/hr
q	thermal conductivity, in.-Btu/sec-in. ² -°F
R	poppet spring rate, lb/in. — Raakine temperature — Rockwell hardness
r	radius, in.
S	circumference of seat land, in.
s	horizontal sliding distance of poppet, in.
T	absolute temperature, °R
TIE	threshold initiation energy, ft-lb
t	material thickness, in.
U	energy, Btu
u	undetermined exponent
V	volume, in. ³

Main
Symbols (Continued)

v	velocity, ft/sec
W	weight, lb
w	width of seat land, in.
X	chemical element, unspecified
x	incremental distance, seat circumference, in.
Y	chemical element, unspecified
y	peak-to-valley height, μ in. or in. $\times 10^{-6}$
Z	fraction of surface area; probability
α	contact angle, deg - specimen rotation, deg
β	angular location of contact on duboff
Γ	heat capacity, Btu/lb
γ	surface energy, erg/cm ² or dyne/cm
Δ	compressive deflection of surface, in.
ΔT	temperature change, deg
δ	poppet spring deflection, in.
η	gas viscosity, at T °R, lb-sec/ft ²
θ	absolute temperature, °K
Λ	Poisson's ratio
μ	coefficient of static friction
Ξ	material parameter, erg/cm ²
ρ	density, lb/in. ³
Σ	material parameter - summation
σ	compressive stress, lb/in. ²
τ	time constant
Φ	material parameter

Main
Symbols (Continued)

Ψ	material parameter A^2
Ω	material parameter A

Superscripts

o	Initial conditions
'	modified value
n	number of valve cycles
u	undetermined exponent
-	mean value

Subscripts

A	property of material A (the softer material if two are considered)
a	armature
B	property of material B, the harder of the two – Rockwell B scale
C	Rockwell C scale
c	closed, or for time interval, period from initial contact to full closure
d	seat land exterior duboff
E	local area affected by wear
e	effective
F	flattened
f	fluid
H	heated zone
h	hemispherical
I	at impact
i	inside

Subscripts (Continued)

j	arbitrary location or parameter
K	kinetic
LO	lower member
l	average size loose particle
M	metal
m	melting point
N	poppet nut
n	number of strokes or cycles
o	outside
P	pressure
p	poppet
pl	plastic flow
R	reaction rate
S	spring
s	seat
sp	specimen
T	total
t	smallest size adherent particle
UP	upper member
u	average size adherent particle
V	vapor
v	vaporization
w	worn away
x	selected system condition
y	yield

Subscripts (Continued)

α	angle relative to major diameter, degrees – contact angle, degrees
γ	surface energy
Δ	difference
θ	thermal – final pendulum position, deg
Σ	sum of all processes per stroke
1	upstream
2	downstream
1, 2, 3, , j	arbitrary integral numbers for sequential positions
50	value causing reaction in 50 percent of tests
ab	abrasion
ad	adhesion
aver	average
exp	expansion
max	maximum
max temp	energy equal to maximum temperature
measured	measured
min	minimum
MST	maximum service temperature, °F
n ∞	indefinite lifespan
no deform	no plastic deformation due to impact loads
100K	1×10^5 operating cycles

Appendix H

SURFACE FLUORINATION REACTIONS

H.1 CHEMICAL PROCESS OF FLUORINATION

In a chemical reaction between two species, it is necessary to break one old chemical bond and form at least one new bond;



Since chemical bonds represent a condition of lower energy than the free atoms,



it is necessary to supply energy to the molecule to reverse the procedure and cause bond rupture. This energy can be measured using common laboratory methods. As the reaction proceeds and new bonds are formed, heat is released. In many reactions, bond formation occurs simultaneously with bond fracture.



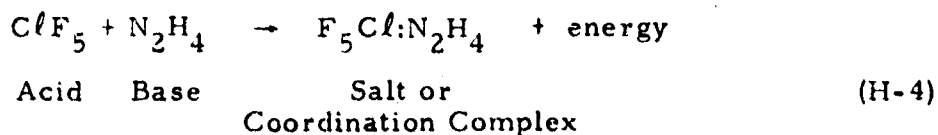
This type of reaction may require less energy input than a similar one in which the bonds break completely before new ones are formed.

The energy needed to start the reaction can be determined in a reversible isothermal system which has no other energy sinks. The energy determined in this fashion is called the "activation energy" or "heat of activation." The value so determined is the minimum energy to start the reaction. Generally, the term activation is applied to the reversible isothermal process. At any other condition, the process is called initiation.

Initiation energies are invariably greater than the activation energy. In an initiation process occurring under nonisothermal conditions, the reaction starts in the region of highest temperature. But this hot region tends to lose energy continuously to cooler regions. Hence, a larger total is required to start the reaction. In addition, the reaction heat released may be dissipated fast enough so that a self-sustaining reaction cannot occur even then initiation is successful.

In the reactions of fluorinating agents and materials, three loose classes can be defined. The first class consists of those reactions which occur spontaneously at room or colder temperatures, i. e., hypergolic reactions. When these are studied carefully, in many cases it is found that there is some extraneous factor operating to introduce an alternative reaction path. The factor may be a chemical catalyst, an impurity, or some other reaction occurring which supplies energy. In most cases, removal or suppression of the stray factor raises the spontaneous reaction temperature above room temperature. The hydrogen-fluorine reaction is of this type.

The second class of reactions is that which occurs in self-igniting fashion from slightly above room temperature to about 350° F. These systems are also easily initiated by shock or impact. Study of the mechanisms of thermally initiated reactions reveals that most of them start by thermal cleavage of the fluorinating agent to give free fluorine atoms which then react vigorously with the other reagent. In those reactions occurring in the lower part of the temperature region, there is usually a preliminary reaction of the type known as a Lewis acid-base or coordination reaction, releasing heat, which is then used to initiate fluorine bond rupture.



The bond rupture and subsequent reaction generally, but not always, occur in the already complexed fluorinating agent, mainly because the energy is locally available. If the energy released by complex formation is great enough the fluorinating reaction will be spontaneous at and below room temperature, and we have a class I hypergolic reaction.

Most reactions of fluorinating agents with hydrogen compounds, including organic compounds, occur in the class II temperature range.

The third class of reactions requires temperatures greater than 350°F for initiation. Most (but not all) reactions of metals with fluorinating agents are found in this class. Two inhibitory factors place substances in this class.

One factor is the necessity of breaking some fairly stable bond to cause the reaction to start. This bond has to be cleaved even though the fluorinating bonds already have been cleaved. The other inhibition can be the pre-existence of a protective film or passivated condition, due to another reaction path which does not yield sufficient energy to cause a self-sustaining reaction. Both these inhibitory factors may act at once to result in a very high ignition temperature requirement.

Structural alloys which are compatible with fluorinating agents obviously have relatively high ignition temperatures. Their purely thermal ignition processes generally require rupture of bonds between the metal atoms. In many cases, the metal-metal bonds become weak enough to react with the fluorinating agent at the temperature at which the interatomic bonds become so weak that the solid metallic crystalline lattice collapses, i. e., at the melting point. This has been noted for many metals in GF_2 .

If the postulate is true that the reaction of some metals at or above their melting points is due to weakened intermetallic bonding, which opens the metal atoms to interaction with fluorine atoms, then mechanical processes which weaken or break these same metallic bonds should aid initiation. The addition of sufficient mechanical energy to cause yielding or failure of the metal is a situation of this type. Obviously, some bonds must be broken if the metal atoms move relative to each other. These atoms are open to fluorine attack until new bonds form. This concept does not contradict the observations that metals fractured in LF_2 do not ignite, because there are no free F atoms at the temperature of LF_2 .

The amount of reaction which will take place must be a function of the total heat available. This leads to the commonly observed temperature dependence for reaction rates, many of which double for each 20°F increase in temperature. The heat available can have two sources. First is the system or other heat which activates the first atoms. Second, there is the heat of reaction

obtained from the first-reacting atoms. In a short duration initiation situation, this reaction heat is the only energy available to sustain the reaction after the initiation process is complete. If the reaction is to continue, there must be sufficient heat released to initiate an equal number of molecules after the normal energy losses to the surroundings and other energy sinks. The analysis in Appendix D, developed for analysis of the heat flow originating from friction, can also be applied to analyze the partition of the heat of reaction. However, a term for work of expansion of CPF vapor must be added, since over the longer time period this effect is no longer negligible.

The above discussion has centered on the energetics of reactions. There are some other factors of equal importance. The concentration of reactant species is one of these. Most reactions between molecules of different species show considerable dependence on both relative and absolute concentrations. The relative concentration dependence can be exemplified by the combustion limits shown by combustible gases. If one component is at too low or too great a concentration, it is impossible to cause a self-sustaining reaction. This is usually because the species at the very high concentration has so many molecular collisions with its own kind that any activated molecules become deactivated before they contact a molecule of the low concentration type with which they can react.

The absolute concentration dependence has its strongest effect on the rate of a reaction, and not as much on the initiation process. The rate is usually directly proportional to some power of the concentration. The exact value of the exponent varies from reaction to reaction, and may change in a single reaction as a function of other parameters. For most common reactions, the exponent lies between one-third and three. Heterogeneous reactions of solids and fluids usually have fractional exponents.

This concentration dependence is perhaps the chief reason that room temperature reactions of halogen fluorides are so much more vigorous than those of fluorine; at pressures near atmospheric the liquid halogen fluorides are about 10^3 more concentrated than is CF_2 at the same pressure and temperature.

Another important factor is the condition and behavior of the reaction products. Products which are volatile at the reaction zone conditions quickly diffuse

away and do not exert much effect on the system energetics, except for thermal energy which they carry. Even this energy may be transferred back to reactant molecules by means of intermolecular collisions. However, if the reaction is diffusion-rate controlled, the presence of the products can hinder the course of the reaction.

If the reaction products are not volatile they will tend to condense and interfere seriously with the contact between the reactants, especially if one of the reactants is a solid. The product tends to coat the solid. The only way to prevent this manner of snuffing out is to supply the product with enough energy so that it is volatile in the reaction zone and leaves the zone with high enough speed that it is beyond the range of interference before it cools sufficiently to condense. If this process occurs, the removal of considerable reaction energy by the product reduces the amount available for activation of reactants, because when the heat of condensation finally becomes available to activate unreacted atoms, these atoms are too far from the reaction zone to become involved in the reaction before they lose their energy by collisions.

The configuration of the ACS valve also plays an important part in the extent of any reaction after it is initiated. The small volume of CPF that has access to the heated region, and the limited direction of access tend to restrict a continually propagating reaction. Reaction heat transmitted to the propellant will vaporize the propellant; reaction products are also initially in the vapor state. The expansion of these vapors will tend to push a considerable fraction of the unreacted CPF away from the reaction zone. This reduction in concentration can slow the reaction sufficiently so that there is not enough heat generated to sustain the necessary continuing initiation. Add this to the fact that the deformation due to closure impact is quickly over, and so greater heating of the metal is needed to maintain initiation, and it is easy to see how the reaction can die out rapidly.

It is impossible to carry the analysis of chemical corrosive wear of metals in CPF further at this time because significant numerical data are lacking for the bulk chemical reactions of CPF with metals. The following types

of data are needed to carry the analyses far enough to develop predictive equations:

- A. Activation energy as a function of temperature.
- B. Reaction rate as function of temperature, concentration, pressure, and other parameters.
- C. Heat of reaction.
- D. Reaction order.
- E. Isothermal ignition temperature of metal in CPF.
 - 1. Oxide film on metal.
 - 2. Fluoro-chloride film on metal.
 - 3. Bare metal.
- F. Hot wire ignition temperature in CPF.

Until such relations can be developed and analyzed, it will be impossible to predict from theoretical considerations the rate of wear, cratering, and surface roughening caused by local hot-spot initiation of bulk fluorination reactions; however, empirical correlation of test data can be used to define operating limits.

H.2 REACTIVE IMPURITIES

The effect of impurities as they relate to corrosive wear must be mentioned. Two general cases can be distinguished.

The first case is that of impurities which react spontaneously upon contact with CPF. The heat of reaction or corrosive reaction products, or both, can cause degradation of the surface finish. However, except for very improbable circumstances, such degradation will be general throughout the system and not confined to the closures.

The second case is due to impurities which react in accord with the second general class of fluorination reactions; thermal initiation up to 350°F or impact initiation. Typical materials would include Teflon particles, ice crystals, carbon particles, fluorocarbon oils, water of hydration in the passive film, silica gel particles from Kel-F grease, and partially fluorinated hydrocarbons and organics. These are discussed in Section 3.5.

TEST MATERIAL

Material	Configuration	Supplier	Source	Heat or Lot	Specification
Duranickel 301	1.5 in. sq by 36 in.	Inco Dist Sales	Huntington Alloy Products, International Nickel	N3754F	Hot Fin. sq Hot Fin.
Stainless Steel 304-L(A)					
Air Melt	5/8 in. rod for ABMA specimens	Allen Fry Steel	Crucible Steel	139969	AMS 5647 QQS 763D
Air Melt	3/4 in. rod for Upper Rotary Specimens	Allen Fry Steel	Universal Cyclops	G-5154	AMS 5647B QQS 763D
Air Melt	1-1/4 in. sq for Lower Rotary Specimens	Allen Fry Steel	Universal Cyclops	L-1111	AMS 5647B QQS 763D
Vacuum Melt	3/4 in. rod for ABMA and Upper Rotary Specimens	Allen Fry Steel	Universal Cyclops	C-9147-K4	AMS 5647B QQS 763D MBO 160-02 (no ultrason

N. A. : Not Applicable

Table I-1

TEST MATERIAL PROPERTIES AND COMPOSITIONS

Lot	Specifications	Properties as Reported by Supplier					% Composition
		Yield (KSI)	Tensile (KSI)	Elong (%) (in.)	Reduction Area (%)	Brinnell Hardness	
	Hot Fin. sq Hot Fin.	N. A.	N. A.	N. A.	N. A.	N. A.	C, 0.10; Mn, 0.27; Fe, 0.05; S, 0.005; Cu, 0.02, Al, 4.37; Ti, 0.45; Ni, 94.21; Co, trace, included in Ni
	AMS 5647 QQS 763D	68.0	93.4	46.7	73.7	229-235	C, 0.03; Mn, 1.53; P, 0.021; S, 0.030; Si, 0.45; Cr, 18.60; Ni, 9.25; Mo, 0.07; Cu, 0.10; Co, 0.08; Fe, rem
	AMS 5647B QQS 763D	66.5	95.0	48.6	73.4	212-217	C, 0.023; Mn, 1.54; P, 0.023; S, 0.014; Si, 0.73; Cr, 18.37; Ni, 9.61 Mo, 0.04; Ti, 0.01; Cu, 0.06; Cb, 0.01; Co, 0.02; Fe, rem
	AMS 5647B QQS 763D	60.0	96.0	45.0	75.7	207-217	C, 0.013; Mn, 1.28; P, 0.015; S, 0.017; Si, 0.66; Cr, 18.02; Ni, 9.49, Mo, 0.08; Cu, 0.08; Co, 0.09; Fe, rem
	AMS 5647B QQS 763D MBO 160-020F (no ultrasonic)	66.2	97.9	49.0	82.3	196-223	C, 0.028; Mn, 1.72; P, 0.030; S, 0.014; Si, 0.56; Cr, 18.86; Ni, 9.33; Mo, 0.03; Cu, 0.05; Co, 0.07; Fe, rem

1 C

Cell #	% Composition	JK Inclusions			
		A	B	C	D
	C, 0.18; Mn, 0.27; Fe, 0.05; S, 0.005; Cu, 0.02, Al, 4.37; Ti, 0.45; Ni, 94.21; Co, trace, included in Ni				
35	C, 0.03; Mn, 1.53; P, 0.021; S, 0.030; Si, 0.45; Cr, 18.60; Ni, 9.25; Mo, 0.07; Cu, 0.10; Co, 0.08; Fe, rem				
17	C, 0.023; Mn, 1.54; P, 0.023; S, 0.014; Si, 0.73; Cr, 18.37; Ni, 9.61 Mo, 0.04; Ti, 0.01; Cu, 0.06; Cb, 0.01; Co, 0.02; Fe, rem				
17	C, 0.013; Mn, 1.28; P, 0.015; S, 0.017; Si, 0.66; Cr, 18.02; Ni, 9.49, Mo, 0.08; Cu, 0.08; Co, 0.09; Fe, rem				
23	C, 0.028; Mn, 1.72; P, 0.030; S, 0.014; Si, 0.56; Cr, 18.86; Ni, 9.33; Mo, 0.03; Cu, 0.05; Co, 0.07; Fe, rem	Thick	1	1	0 1.5
		Thin	0	0	0 1

Appendix I TEST PROGRAM

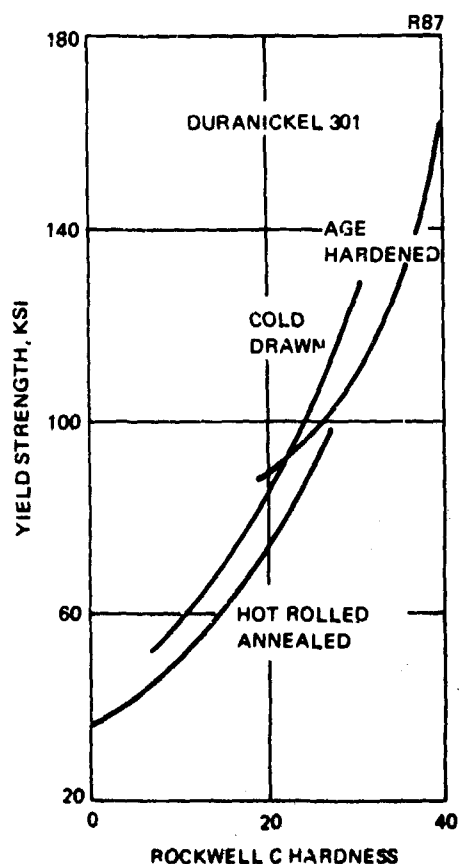
I.1 MATERIALS

I.1.1 Test Closure Materials

Materials used in the various tests are presented in the following subsection. Their selection was approved by the AFML Project Engineer.

I.1.1.1 Phase I, Part 2

Duranickel 301 - WH (work hardened) was the only material tested in this part. Its analysis and properties are listed in Tables I-1 and I-2. The Rockwell hardness was measured on random samples of test specimens after fabrication (See Subsection I.3 for details of specimens).



I.1.1.2 Phase II, Part 1

The alloys first selected for testing were Berylco nickel 440 and Duranickel 301. The Berylco nickel was to be obtained from air-cast and vacuum-cast lots to allow a comparison between the effects of contaminants. However, labor problems at the manufacturing plant prevented the acquisition of vacuum-cast material. After consultation with the AFML Project Engineer, Stainless Steel 304-L from air-melt and vacuum-melt batches was substituted.

TEST MATERIAL PROPERTIES

Material	Configuration	Supplier	Source	Heat or Lot	Specifications	Yi (K
Stainless Steel 304-L (A) (Continued)						
Vacuum Melt	1-1/4 in. sq for Lower Rotary Specimens	Allen Fry Steel	Universal Cyclops	C-8167-K3	AMS 5647A QQS 763C&D MBO 160-020 (no ultrasonic)	57
Berylco Nickel 440	1-1/4 in. dia by 24 in.	E. Jordan Brooks Co.	Kawecki Berylco Industries	A-10	None	N.
Polycrystalline Aluminum Oxide	Preformed to specimen shapes	R. D. Yrossman & Assoc.	ManLabs, Inc.	---	None	De 99
Carmet Alloy CA-4	Preformed to specimen shapes	Carmet Corp.	Carmet Corp.			De 15
Silver Plated DN-301	Preformed to speci- men shapes, 0.001 in. Ag plated	Anodyne, Inc.	Anodyne, Inc.	51636 51509		N.

N. A. = Not Available

TEST MATERIAL PROPERTIES AND COMPOSITIONS (Continued)

Heat or Lot	Specifications	Properties as Reported by Supplier					% Com
		Yield (KSI)	Tensile (KSI)	Elong (%) (in.)	Reduction Area (%)	Brinell Hardness	
C-8167-K3	AMS 5647A QQS 763C&D MBO 160-020 (no ultrasonic)	57.0	88.0	55.0	79.9	187-170	C, 0.023; Mn, S, 0.007; Si, Ni, 9.67; Mo, Co, 0.12; Fe,
A-10	None	N. A.	N. A.	N. A.	N. A.	R _B 84-86	C, 0.21; B, < Be 1.81; Fe, < Al, 0.037; Pb, Ti, 0.41, Cr, Mg, 0.003; Ni
---	None	<u>Density</u> 99 + %	N. A.	N. A.	N. A.		99 + % pure
		<u>Density</u> 15.00	N. A.	N. A.	N. A.	R _A 91.9- 92.2	WC, 94.0; Co,
51636 51509		N. A.	N. A.	N. A.	N. A.	N. A.	Process steps Vapor degreas 100% HCl dip; strike; Ag stri plate; rinse in

continued)

ported by Supplier

Reduction Area (%)	Brinell Hardness	% Composition	JK Inclusions			
			A	B	C	D
79.9	187-170	C, 0.023; Mn, 1.62; P, 0.025; S, 0.007; Si, 0.67; Cr, 18.64; Ni, 9.67; Mo, 0.03; Cu, 0.04; Co, 0.12; Fe, rem	Thick	0	0	0 1.5
			Thin	0	0	0 1
N.A.	R _B 84-86	C, 0.21; B, < 0.001, Be 1.81; Fe, 0.35; Si, 0.14; Al, 0.037; Pb, 0.002, Ti, 0.41, Cr, 0.072; Mg, 0.003; Ni, rem				
N.A.		99 + % pure				
N.A.	R _A 91.9- 92.2	WC, 94.0; Co, 6.0				
			Microporosity 9.250 x Normal well sintered.			
N.A.	N.A.	Process steps Vapor degrease; alkaline clean; 100% HCl dip; Nickel chloride strike; Ag strike; Ag electro- plate; rinse in deionized water				

Table I-2

MECHANICAL PROPERTIES OF CERTAIN SPECIMENS

Material	Measured Rockwell Hardness	Equivalent Vickers Hardness (Ref 5)	Approx Yield Strength (ksi) (Ref 4)
Stainless Steel 304-L, Air Cast, (work hardened)	R _B 44	89	Not applicable for Stainless Steel
Stainless Steel 304-L, Vacuum Cast (work hardened)	R _B 44	89	Not applicable for Stainless Steel
Duranickel 301 Vac Annealed; 1800° 5 min, LN ₂ Quench	R _B 77	147	30
Duranickel 301 (work hardened)	R _B 87	179	45
Duranickel 301 (annealed after full hard)	R _C 22	247	75
Duranickel 301 (aged 1100° 4 hr; cooled to 900° at 15° per hr; (3/4 hard))	R _C 32	326	119
Duranickel 301 (aged to 1080° 16 hrs; cooled to 900° at 15° per hr; (full hard)	R _C 36	360	138
Berylco Nickel 440	R _B 86	176	Not applicable

Duranickel 301 was to be used in three heat-treat conditions of selected hardnesses to supply data on the relationship between hardness and reactivity.

The properties and analyses of the alloys as received are listed in Table I-1.

Test specimens were machined from the alloys (see Subsection I.2). The Duranickel specimens were heat treated to several hardness conditions. The hardness of representative random samples of all test specimens was determined by means of a Rockwell tester. The equivalent yield strengths of the Duranickel 301 were read from the graphs presented in Ref 28. These are tensile yield, but from the data in Ref 28 it was noted that compressive yield strength is generally within 5 percent of tensile yield, and the direction of the difference cannot be predicted. The various property data are presented in Table I-2.

When the test program was planned, the three hardness levels of the Duranickel were to be (1) annealed with $R_B \sim 75$; (2) half hard (HH) with $R_C \sim 28$ and (3) full hard (FH) with $R_C \sim 42$. When the specimens were received from the vendor, they were found to have hardness of $R_B 77$, $R_C 32$ and $R_C 36$. It was decided to continue with the tests with these specimens. However, during the ABMA tests, it was found that while the $R_B 77$ material gave positive results (local ignition spots or burn craters), $R_C 32$ did not react at the maximum impact energy available. The $R_C 36$ discs were not tested because it was assumed that they, too, would not react. To get sufficient data for correlation purposes, it was necessary to obtain and test specimens of lesser hardness; two sources were found. The $R_C 36$ impact discs, which had not been used, were returned to heat treat for overaging; this process gave a set of specimens with a $R_C = 22$. In addition, some extra sets of the specimens used in a work-hardened condition for Phase I tests were available ($R_B 87$) and these were added to the test program.

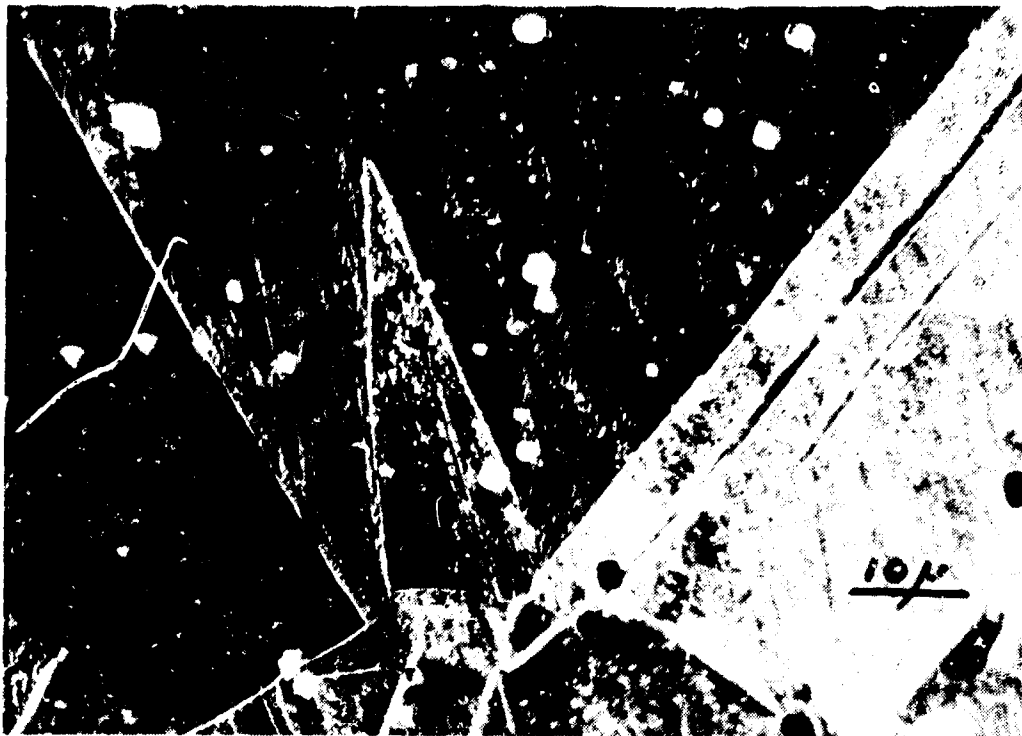
The rotary friction specimens were used in the conditions as received from the initial heat treatments because the test apparatus is capable of inducing reactions in material of very great hardness.

The two types of stainless steel 304-L (air melt and vacuum melt) have the following relative characteristics: the elemental analyses are very similar, with the vacuum-melt lots being slightly high in manganese, phosphorus, and chromium, and lower in sulfur, molybdenum, and copper. The other minor elements fall in the same ranges for the five lots from the two processes. Electron micrographs of discs prepared from Air Melt heat 139969 and Vacuum Melt heat C-9147-K4 were prepared. The grain sizes differed appreciably; surprisingly the air melt grains were much larger than those of the vacuum melt, and the air melt grains showed considerable twinning. The difference in sizes was quite noticeable, as shown in Figure I-1. Also detectable in these photographs is the much greater frequency of local impurity inclusions in the air melt material. This difference is emphasized in Figure I-2. Here the specimens were prepared by polishing only, with no etching, so that the inclusions stand out from the background. Some regions of the air melt found by cross sectioning have inclusion frequencies of 10 to 100 greater than those shown in Figure I-2, whereas the concentration in the vacuum melt seemed to be at a fairly uniform level throughout. The face surfaces are presented in the photographs as representative of the location on specimens subject to CPF attack during tests. The impurities are found in different locations in the two materials. There is a random distribution in the air-melt material, but segregation at grain boundaries in the vacuum melt, see Figures I-3 and I-4.

I. 1. 1. 3 Phase II, Part 2

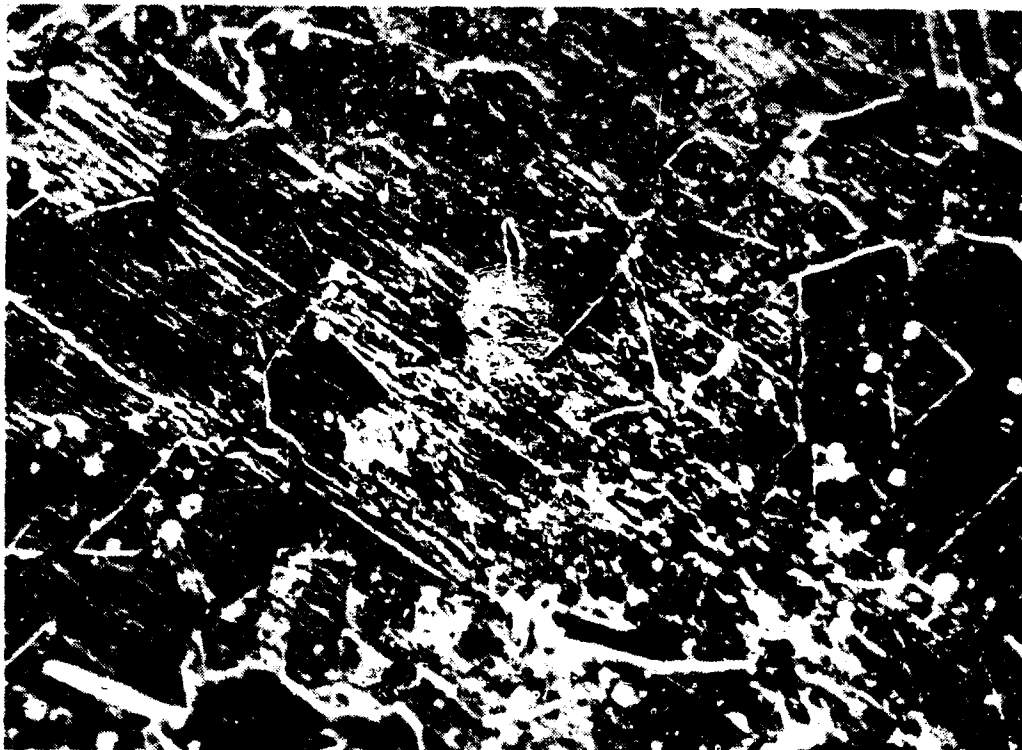
The materials selected as representative candidate closure materials, with the agreement of the AFML Project Engineer, were polycrystalline aluminum oxide (hot pressed), silver plated Duranickel 301, and tungsten carbide cermet dispersion in cobalt. Details of the materials may be found in Table I-1.

Aluminum oxide was selected because it is well known to be a hard, long-wearing material with a very great resistance to corrosive attack in fluorine media. The batch used to prepare specimens was identical to that used for preparation of special closures to be used in the ACS valve by the valve fabricator.



SS-304-L AIR MELT X1350

(MDAC-EMP-HM-94)



SS-304-L VACUUM MELT X1350

(MDAC-EMP-HM-98)

Figure I-1. Microstructure of Stainless Steel 304-L

50µ

B. PHOTOMICROGRAPH OF POLISHED FACE SURFACE OF SPECIMEN
(MDAC)
VACUUM-MELT 304-L.

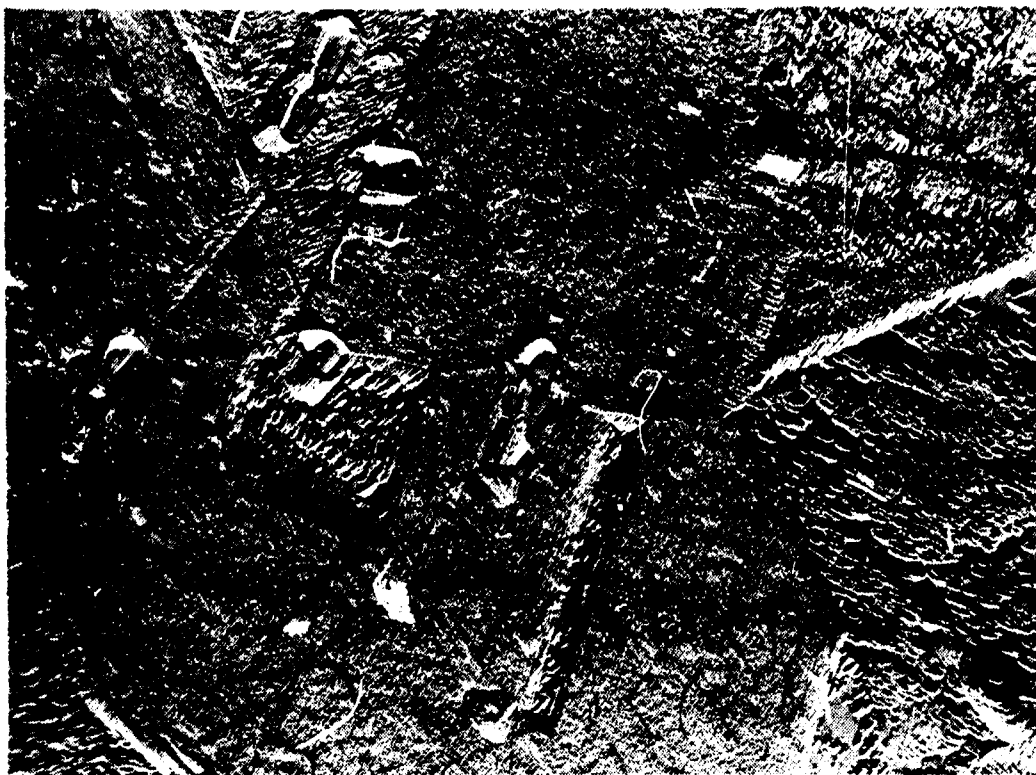
ORIGINAL MAGNIFICATION 470X

50µ

A. PHOTOMICROGRAPH OF POLISHED FACE SURFACE OF AIR-MELT
SPECIMEN 304-L. IMPURITIES OF TWO DIFFERENT SIZE
CATEGORIES ARE NOTED.
(MDAC)

ORIGINAL MAGNIFICATION 470X

Figure 12. Inclusions in Stainless Steel 304-L



(MDAC-EMP-HT-192)

Figure 1-3. Replica Electron Micrograph of 304-L Vacuum-Melt Surface
(Note distribution of etch pits as indication of segregated (impurity-rich) phase along grain boundaries. Original magnification 5100X)

The tungsten carbide-cobalt cermet was selected as representative of the material currently known to function in the best fashion in the ACS valve in CPF. Kennametal alloy K-96 was first selected, but it could not be supplied within the time limits of the contract. Carmet Corporation alloy CA-4 of the same nominal composition was substituted.

Silver plated Duranickel 301 was included to test the effect of a soft non-corrodable metal in the system. Unfortunately, the process of electroplating introduced impurity inclusions into the silver. These were not visible at the 20X magnification used to examine the specimens upon receipt. They were detected by the anomalous behavior of the silver plated material during test. Examination at higher magnifications disclosed the presence of the inclusions. Electron microprobe analysis of the inclusions indicated the presence of sulfur and carbon. Figure I-5 is a microphotograph showing the distribution and sizes of the inclusions in a typical specimen. However, not all specimens contain appreciable concentrations of the inclusions.



(MDAC-EMP-HT-197)



(MDAC-EMP-HT-199)

Figure 1-4. Specimen Replica Electron Micrographs of 304-L Air-Melt Surface Electropolished for 1 Min in 10-Percent Oxalic-Acid
(Note Etch Pit Distribution in a Random Fashion and Impurity-Free Grain Boundaries. Original Magnification 4850X)



* C + 5

(MDAC)

UPPER SILVER SURFACE, SHOWING INCLUSIONS. THESE SPECIFIC SPECIMENS WERE FOUND TO CONTAIN CARBON AND SULPHUR. (ORIGINAL X 100)



SURFACE

SILVER

INTERFACE

NICKEL

(MDAC)

CROSS-SECTION SHOWING POOR BOND BETWEEN SILVER AND DURANICKEL AND INCLUSIONS IN INTERIOR OF SILVER. (ORIGINAL X 240)

Figure I-5. Photomicrographs of Silver-Plated Duranickel

I.1.2 Test Fluids

I.1.2.1 Chlorine Pentafluoride

Approximately 15 pounds of chlorine pentafluoride were on hand from a previous NASA contract and had been furnished from AFRPL. Vapor pressure measurements indicated a high degree of purity. The only impurities which could be detected by mass spectrographic analysis were N_2 , CO_2 , and CF_4 ; the total quantity of these impurities was estimated to be less than 0.5 percent by weight. Purity is unknown, but probably greater than 99 percent by weight.

I.1.2.2 Hydrofluoric Acid

Reagent grade hydrofluoric acid (50 percent aqueous) was used. It was manufactured by J. T. Baker Chemical Co. It was supplied in 1-pound capacity polyethylene bottles.

Chemical Analysis - Lot 33969

(Supplied by Manufacturer)	<u>Percent</u>
Assay (HF)	49.5
Fluosilicic Acid (H_2SiF_6)	0.001
Residue after ignition	0.0001
Chloride (Cl)	0.0001
Phosphate (PO_4)	0.00005
Sulfate and Sulfite (as SO_4)	0.0001
Heavy Metals (as Pb)	0.00001
Iron (Fe)	0.00002
Copper (Cu)	0.00001
Arsenic (As)	0.000002

I.2 SPECIMENS

Test specimens were machined from the alloys to the following configurations.

- A. ABMA discs 5/8 in. diameter by 1/16-in. thickness.
- B. Rotary friction lower specimens = 1-in. square by 1/16-in. thickness.
- C. Rotary friction upper specimens = See Figure I-6.

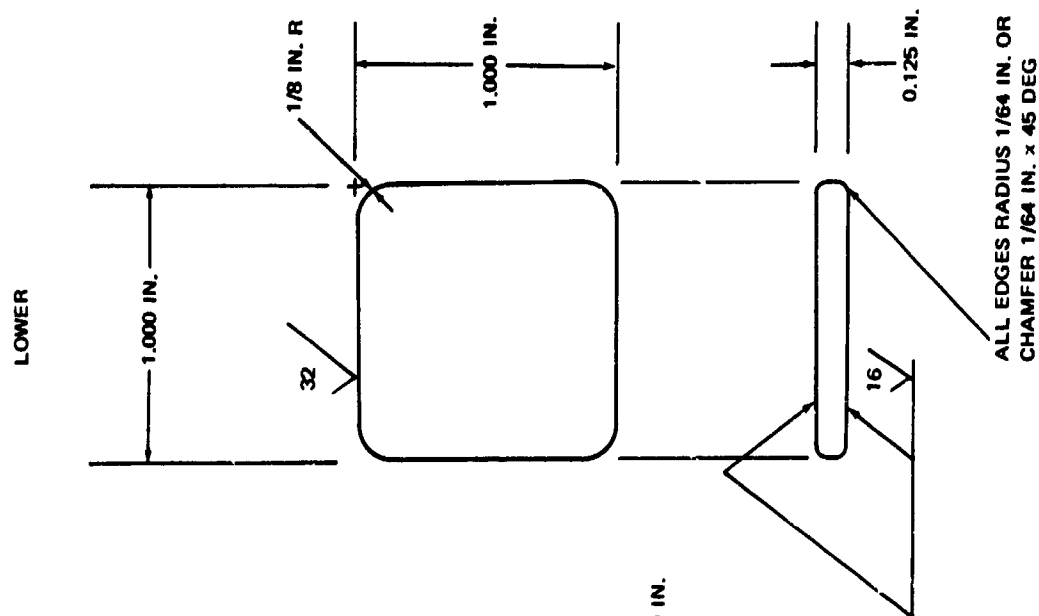
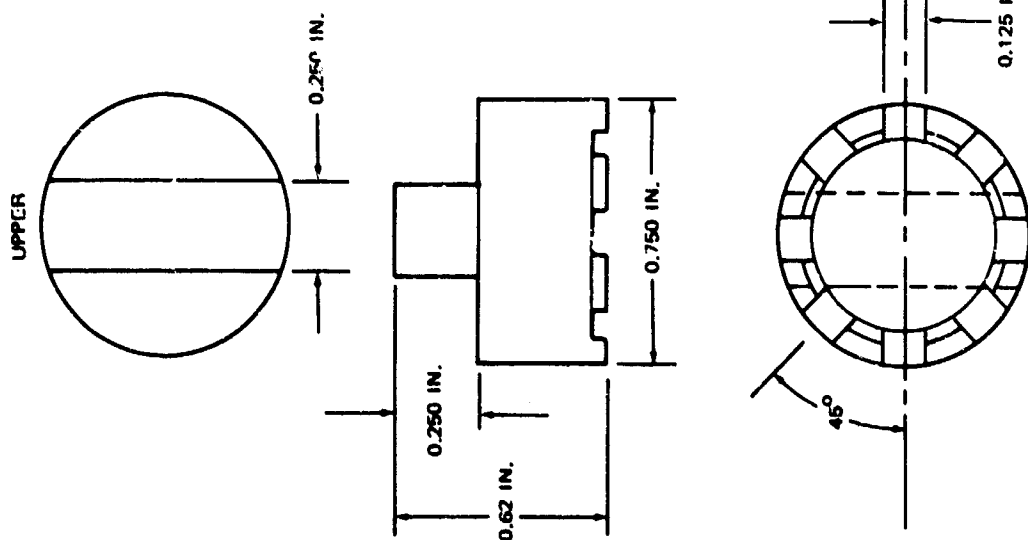


Figure I-6. Rotary Friction Test Specimens

The surface finish on test surfaces was at least as smooth as 10 rms. Other surfaces were not controlled, but were about 32 rms.

Corrosion coupons were made in a variety of shapes, depending on the material available. All were 1/16-in. thick, however.

I. 3 APPARATUS

I. 3.1 Surface Finish

The surface finish of random samples of the various materials specimens was measured by means of a Brush Surfindicator, Model MS-1000-01, together with a Brush Electro-Hydraulic Drive, Model MS-1400. The apparatus was calibrated using a standard 125AA microinch finish block before each measurement. The surface finishes are listed in Table 4-2.

I. 3.2 Microscopes

Specimens were routinely examined before and after tests, using a Bausch and Lomb Stereozoom metallurgical microscope, 10X to 20X.

Electron micrographs were taken with a Hitachi research model HU-11 electron microscope.

I. 3.3 Corrosion Test Apparatus

The usual test method was modified to model to some extent exposure of materials to contaminant HF generated in a valve closure. Hence, the apparatus was not standard.

The immersion test container consisted of a 1-quart polyethylene bottle with a screw lid. A "nest" of 1/4 by 3-in. pieces of polyethylene tubing was placed in the bottle.

The container and tubing was thoroughly washed, rinsed, and wiped dry. The tubing was then placed in the container to form a fairly level surface that was mostly open. The surface was about 3/4 in. from the bottom of the container. (Figure I-7).

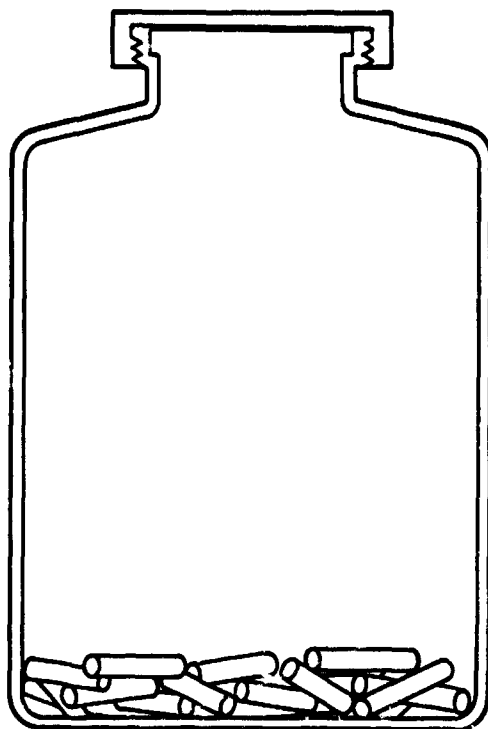


Figure I-7. Corrosion Test Container

Reagent grade HF was poured into the container to a depth of 1/2 in. The pouring was performed in a manner so that all pieces of tubing were under some of the incoming stream.

I. 3. 4 ABMA Impact Test Apparatus

These tests were conducted using the ABMA drop-weight open cup impact tester that was modified for the tests with high-energy propellants (Ref 24). For most of the tests on the current program, impact energy inputs greater than the usual 72 ft-lb were required. For these tests, the apparatus was modified by increasing the mass of the plummet from 20 pounds to 60.25 pounds by the addition of lead weights. This additional mass required the substitution of a huskier hold and release mechanism and a stronger lift cable.

With the modifications noted, the maximum impact energy was raised to 293 ft-lb. Although the test data indicated that an even larger impact energy would be desirable for some specimens, this could not be achieved because

other portions of the test system were at the maximum load they could withstand. For example, the hardened 17-4 PH striker pins occasionally buckled slightly in the 293 ft-lb tests.

I. 3. 5 Rotary Friction Test Apparatus

The Rotary Friction apparatus described in Ref 9 was used. (See Appendix E) (Figure I-8); two modifications were made. The first was the installation of a Nupro model SS-4-UW double-acting, pneumatically-operated, welded bellows valve in the line between the hand valve at the lower end of the CPF supply cylinder and the mechanically operated, propellant-control valve. The second was the provision of a shield that completely enclosed the test chamber to reduce access of air.

I. 4 CORROSION TESTS IN AQUEOUS HF

I. 4. 1 Test Objective

The objective of this test series was to determine the corrosion rate in 50-percent aqueous HF of materials suggested for use as the closures of the ACS valve. All the materials selected are known to be quite resistant to CPF in static exposure. However, due to its ubiquity, it is difficult to avoid occasional contamination by water, and water reacts with CPF to form hydrofluoric acid (HF), which is very corrosive. Considering the fine surface finish needed to ensure low leak rates for the ACS valve, a comparison of the resistance to corrosion of the closure materials aided in the selection of the best closure materials.

The test method was modified somewhat from the usual immersion test to model to some extent the conditions expected in the valve closure. Details are given below. (See Subsection I.4.4).

I. 4. 2 Fluid Characterization

I. 4. 2. 1 Pretest

Identity and Source

Hydrofluoric Acid, ACS Reagent Grade; J. T. Baker Chemical Co. Lot 33696. Transported and stored in 1-pound polyethylene containers.

Analysis

(See Subsection I. 1. 2. 2)

I. 4. 2. 2 Post Test

No post-test characterizations were conducted. It was noted that the HF appeared unchanged except for tests with WC in Co. In this one case, the HF developed a pink color, probably due to dissolved cobalt.

I. 4. 2. 3 Control Test for Fluid

None conducted.

I. 4. 3 Material Characterization

I. 4. 3. 1 Pre-test

See Table I-1 for manufacturer and source.

I. 4. 3. 2 Specific Processing

Corrosion specimens of metals were prepared from rod stock. Blanks were milled to final size and then ground and polished.

Corrosion specimens of silver plated Daranickel 301 were prepared by electroplating specimens fabricated in the above manner.

Corrosion specimens of aluminum oxide were prepared by hot pressing the oxide powder directly to the coupon dimensions.

Corrosion specimens of tungsten carbide in cobalt were prepared by hot pressing the "green" powder to the desired size. The coupons were then ground and polished.

I. 4. 3. 3 Preparation For Test

Specimens were cleaned for testing by washing in distilled water, rinsing dry with isopropyl alcohol, and then vapor degreasing in Gensolv A (trichlorofluoromethane) for 20 minutes. Porous materials (Al_2O_3 and WC in Co) were then baked in a vacuum (1 torr, 105°C, 18 hr) to remove absorbed solvent. The dried specimens were weighed on an analytical balance.

I. 4. 3. 4 Properties

See Table I-1 for pretest properties and Table 4-2 for post-test properties.

The specimens were removed from the test medium, washed in running distilled water, wiped dry, and then vacuum baked dry at 105°C, 1 torr, 18 hours.

I. 4. 3. 5 Material Control Test

None conducted

I. 4. 4 Test Procedures

I. 4. 4. 1 Test Description

Tests were conducted with a single material at a time.

The specimens, after weighing, were immersed in Reagent HF in a plastic beaker for 5 minutes, with frequent agitation and stirring. The specimens were then removed, blotted dry with soft absorbent paper. (Specimen C of Berylco nickel did not undergo this pretest immersion).

The blotted specimens were immediately placed on the upper surface of the nest of plastic tubing in the test container (subsection I. 4. 2), in a manner that the two specimens were in mutual contact at some point, and the specimens were tipped so that part, but not all, of each was immersed in the liquid HF. The test container was then closed and put in a constant-temperature environment.

Test specimen C of Berylco nickel 440 was not placed on the nest, but was suspended from the top of the container so that it was in the vapor only, and not in contact with other specimens. Flexible plastic tubing was used to suspend it.

The tests were left undisturbed for a period of time, noted in Table 4-1.

Test termination consisted of removing the test container from the environment, opening the container, and flooding the interior with running distilled water to wash away the HF. The specimens were removed, dried, examined, and weighed

I. 5 OPEN CUP IMPACT INITIATION TESTS

I. 5. 1 Test Procedure

The tests were conducted in the normal fashion (Ref 29) using the MDAC-West modified ABMA Impact Tester. Specimens, Monel sample cups, striker pins, and guide bars were cleaned for fluorine service and then packaged,

but they were not passivated for CPF service. The tungsten carbide-cobalt cermet test discs were baked overnight in a vacuum oven at 1 torr (continuously pumped), 105°C, 18 hours, and then protected from atmospheric moisture until tested. To demonstrate the effect of moisture, three of the discs were exposed to air at a relative humidity of 100 percent at 70°F for 18 hours after they had been baked dry. These discs were tested with the absorbed moisture present.

The remainder of the test apparatus was cleaned thoroughly in place. Specimens were placed in sample cups and the assemblies were placed in stainless steel trays. The trays of specimens, striker pins, and guide bars were placed in the test cell; then, this cell was sealed and purged with dry GN_2 . When the cell atmosphere was dry, LH_2 was flowed into the anvil moat to maintain a temperature of 10°F.

The specimens in the cups and striker pins were mounted individually in the anvil, about 4 ml of liquid CPF was flowed into the cup, the lights were extinguished, and the plummet was released from a selected height. After 4 to 5 tests at various drop heights, the specimens were removed from the cell through a small airlock; they were examined immediately using a 20X stereozoom metallurgical microscope. Then the specimens were engraved to indicate the test number and placed in a vacuum oven at 105°C and 1 torr for at least 18 hours; this technique was used to bake out oxidizer residues to prevent corrosion. From the observations during the tests and from examination of the specimens, appropriate energy levels for the next short series of tests were selected and the testing was continued.

The test drops were conducted at a variety of impact energies to find the energy at which 50 percent of the specimens would react (E_{50}). The method of picking the drop energies was slightly modified from the standard up-and-down process to allow a group of 4 or 5 specimens to be tested before selecting the next energy levels. The threshold initiation energy (TIE) was also determined. The TIE is the greatest test energy at which no reaction is detected.

In the tests, the energy output from the reactions was very low, and very few flashes were observed. However, reaction sites and burn craters were detected easily when the specimens were examined. In many cases, the interface between the specimen and the soft Monel sample cup showed more

reaction sites than the hardened striker pin-specimen interface, but these former reaction sites appeared to be initiated in the Monel and hence were not considered in evaluation of whether a reaction had occurred. Figure I-9 is a reproduction of a typical drop-test series.

The results of the tests, calculations, and conclusions will be found in Subsection 4.3.

I.6 ROTARY-SLIDING FRICTION INITIATION TESTS

I.6.1 Test Method

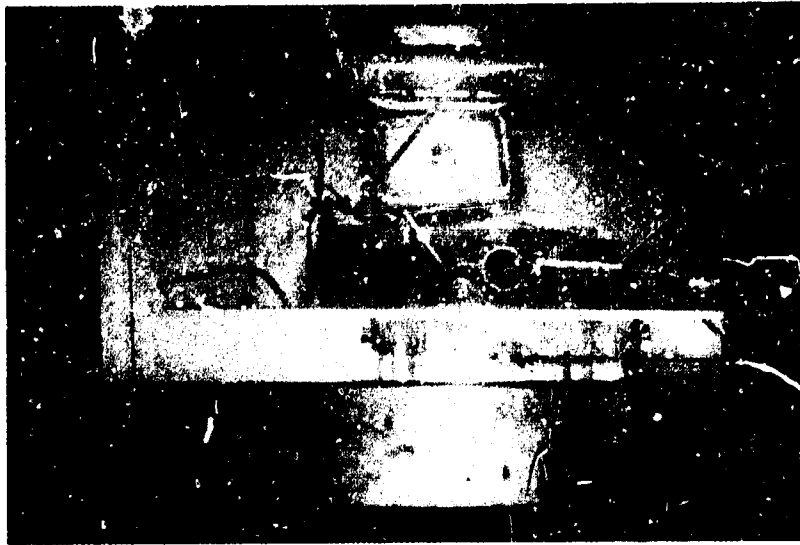
This unique instrument (Figure I-8) developed by MDAC-West on a previous contract with AFML (Ref 9). An outline description of its function and the procedure for its use is appropriate. This outline may be found in Appendix E.

I.6.2 Test Procedure

The procedure described in Ref 9 was followed. Upper and lower specimens were cleaned for fluorine service and then packaged until required. Porous material specimens (alumina and tungsten carbide cermet) were vacuum baked at 105°C, 1 torr, for 18 hours. The specimens were not prepassivated. The test apparatus was cleaned thoroughly in place.

The pendulum was raised and locked for each test. The specimens were mounted, the shield was locked in place, and the GN_2 purge was turned on. (In a few instances, the purge caused displacement of the lower specimen; if this displacement was not detected before the test, the results were invalid.) The post-impact pendulum height recorder was placed in a vertical position, the pendulum was shifted to the magnetic latch, and the test cell was closed. Then, gas at a regulated pressure was supplied to the pneumatic cylinder to load the specimens in compression. LN_2 was turned on to chill the specimens and the propellant moat to 10°F.

When the test temperature was reached, the purge was turned off, liquid CPF (10 ml) was flowed onto the specimens, the lights were extinguished, and the pendulum was released. Flashes or other occurrences were noted.

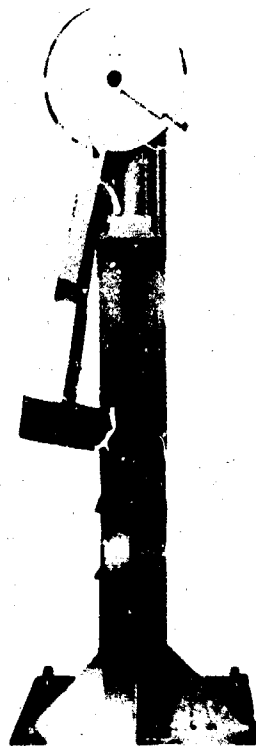


VIEW IN 45-DEG
MIRROR OF
IMPACT AREA

LOWER END
OF PLUMMET

MDAC

A. OPERATOR'S VIEW OF ABMA IMPACT TESTER



MDAC

B. ROTARY FRICTION TESTER

Figure I-8. Initiation Test Apparatus

IMPACT SENSITIVITY TEST

Oxidizer CPFSample DN 301-AApparatus Open CupDate 24 Nov. '76Operator F. FAHEYAmbient Temp. 70 °FHumidity 45 %Pressure 28.3 in. HgPlummet Weight 60 1/2 lbsStriker Pin ^{Diam 1/8"}
Area 0.0314 in²Spring Modulus NA lbs/inSample Thickness 1/16 in.Sample Volume ~ 4 mlTest Temp. 19 °F

Drop Number	Drop Height Scale Position	Calc Impact (ft lbs)	Type of Reaction (Visible)					Remarks
			Extreme	Moderate	Faint	Char	None	
1	MAX (16)	293					✓	Burn craters
2	MAX	293					✓	Burn spots
3	9	165					✓	No rxn. spots
4	9	165					✓	None
5	13	238					✓	None
6	13	238		✓ (splash)			✓	None
7	11	201					✓	None
8	11	201					✓	None
9	15	275			✓ splash		✓	Small craters
10	15	275					✓	CONTAM. - No rxn
11	16 - Max	293		✓			✓	Burn craters
12	15	275			✓		✓	no burns
13	15	275					✓	Burn craters
14	14	256					✓	Burn craters
15	13	238					✓	Burn craters only
16	13	238					✓	No burns
17	14	256			✓ splash		✓	Burns
18	13	238					✓	Rebound burns only
19	13	238					✓	None
20	13	238					✓	Very small burns
21	13	238					✓	None
22	13	238					✓	Rebound burn
23	13	238					✓	Burns
24	13	238					✓	No burn
25	13	238					✓	Rebound burn
26	13	238					✓	Rebound burn
Total Number of Reactions:			9 (Rebound not counted)					at least 9

Estimated initial rebound height of plummet during blank test: NA in.

Note # 18-20 in Aluminum cups - no tests

Figure I-9. Typical Data Record

The purge was then turned on again and the LN_2 was turned off. After all CPF had been exhausted, the test cell was opened and the final height of the pendulum noted. The tested specimens were removed and new ones were mounted. The specimens were examined immediately under the 20-power microscope for signs of reaction and were then baked for at least 18 hours in a vacuum oven at 105°C and 1 torr.

Data collected from tests of Duranickel 301 Annealed are given in Table I-3 as a sample of the information collected in the tests.

The results of the tests, calculations, discussion and conclusion will be found in Section 4.4.

Table I-3
ROTARY FRICTION TEST OF DURANICKEL 301-A IN CPF

Cylinder Pressure (psi)	Final Pendulum Position (deg)	Reaction	
		Visible (Light)	Burns
300	Not Available	Yes	Yes
225	42	Not Observed	Yes
200	35	Yes	Yes
150	36	No	Yes
100	19	No	No

NOTE: Test Temperature = 10°F
Specimen rotation angle = 60°

Appendix J

MATERIAL PARAMETERS

For an infinite life cycle span, the adhesive wear processes must not result in wear roughening which is greater than the value $H = 1.5$. Adopting the conservative position that the most severe conditions of wear must be the basis for the calculations, equation (B-14) defines the material properties needed —

$$H_{\max} = 1.5 = 6.5 \frac{G_{AB}}{P_A} \quad (J-1)$$

Then

$$\frac{G_{AB}}{P_A} \leq 0.23 \text{ } \overset{\circ}{A} \quad (J-2)$$

$n = \infty$

In addition to increases of surface roughness, there is one other major damage which the valve can suffer under purely mechanical loads. This damage is plastic flow or rupture of the closures when the impact loads are too high. This process will remove material from one location and pile it up in another which can result in a permanent cocking of the poppet and greatly increased leakage. The edges of the seat land are the location most liable to be affected by this process. Since very minor damage in this location not only increases H rapidly, but also causes a decrease in the sealing area width (w in equation (1)) with resultant increase in leak rate, such damage must be prevented.

To avoid deformation in the area of initial sharp edge contact, $\sigma_{1, \alpha}$, defined in equation (6), must not exceed the yield stress of the seat material, σ_y .

Substituting equation (6) for σ_y of equation (4) allows definition of $F_{I \text{ no deform}}$

$$F_{I \text{ no deform}} = 1.72 E^{1/4} \left[d_d (D_o - d_d \cos \alpha) \right]^{1/4} \left(\frac{h F_T W_{I,e}}{t_T W_t} \right)^{3/4} \quad (J-3)$$

If the nominal design values for configuration and energy terms are substituted into this equation, the result,

$$F_{I \text{ no deform}} \leq 53.6 E^{1/4}, \quad (J-4)$$

allows calculation of the maximum allowable impact force as a function of a material parameter, the bulk modulus.

Having discussed what may be considered to be the limiting cases for F_I in terms of service constraints, (and related these to materials properties) it is now logical to consider the required operating cycle life, $n = 10^5$ cycles.

A definition of F_I can be developed by combining and rearranging equations (4), (14), (15) and (16) with simplifying assumptions. This result relates F_I to material properties and number of cycles;

$$F_{I,n} = 14 \frac{P_A}{n k_{ad}} \quad (J-5)$$

or for 10^5 cycles

$$F_{I,100K} \leq 1.4 \times 10^{-4} \frac{P_A}{k_{ad}} \quad (J-6)$$

The impact energy determined by equation (J-6) relating to leak rate development should be the same as that determined by Equation (J-4) relating to plastic deformation.

Then

$$53.6 E^{1/4} = 1.4 \times 10^{-4} \frac{P_A}{k_{ad}} \quad (J-7)$$

or

$$\left(\frac{P_A}{k_{ad} E^{1/4}} \right)_{n=100K} \leq 3.82 \times 10^5 \quad (J-8)$$

In similar fashion, if F_I (equation 4) is equated to $F_{I \text{ no deform}}$ (equation (J-4)), and the normal design values for configurations and forces are substituted, the relation

$$\left(\frac{\sigma_y}{E^{3/4}} \right)_{n=100K} \leq 9.35 \times 10^{-2} \quad (J-9)$$

is obtained.

The above calculations are based primarily on the formation of adherent particles of average size.

$$c_u = 52 \frac{G_{AB}}{P_A} \quad (J-10)$$

The load to generate a contact area equal to this size of particle is

$$F_{I, u} = 4.39 \times 10^{-6} \frac{G_{AB}^2}{P_A} \quad (J-11)$$

Equating (E-5) to (32), we obtain

$$\left(\frac{k_{ad} G_{AB}^2}{P_A^2} \right)_{n=100K} \leq 3.19 \text{ \AA}^2 \quad (J-12)$$